

# The Jurassic Petroleum System in the Danish Central Graben (PETSYS)

Technical notes

Nina Skaarup, Peter Alsen, Claus Andersen, Karen Dybkjær,  
Morten Gausby, Tjerk Heijboer, Jussi Hovikoski, Finn Jakobsen,  
Peter Johannessen, Christian Knudsen, Lars Kristensen,  
Anders Mathiesen, Margrethe Thorup Nielsen,  
Hans Peter Nytoft, Henrik Ingermann Petersen,  
Anders Pilgaard, Jens Therkelsen,  
Erik Thomsen & Rikke Weibel



# The Jurassic Petroleum System in the Danish Central Graben (PETSYS)

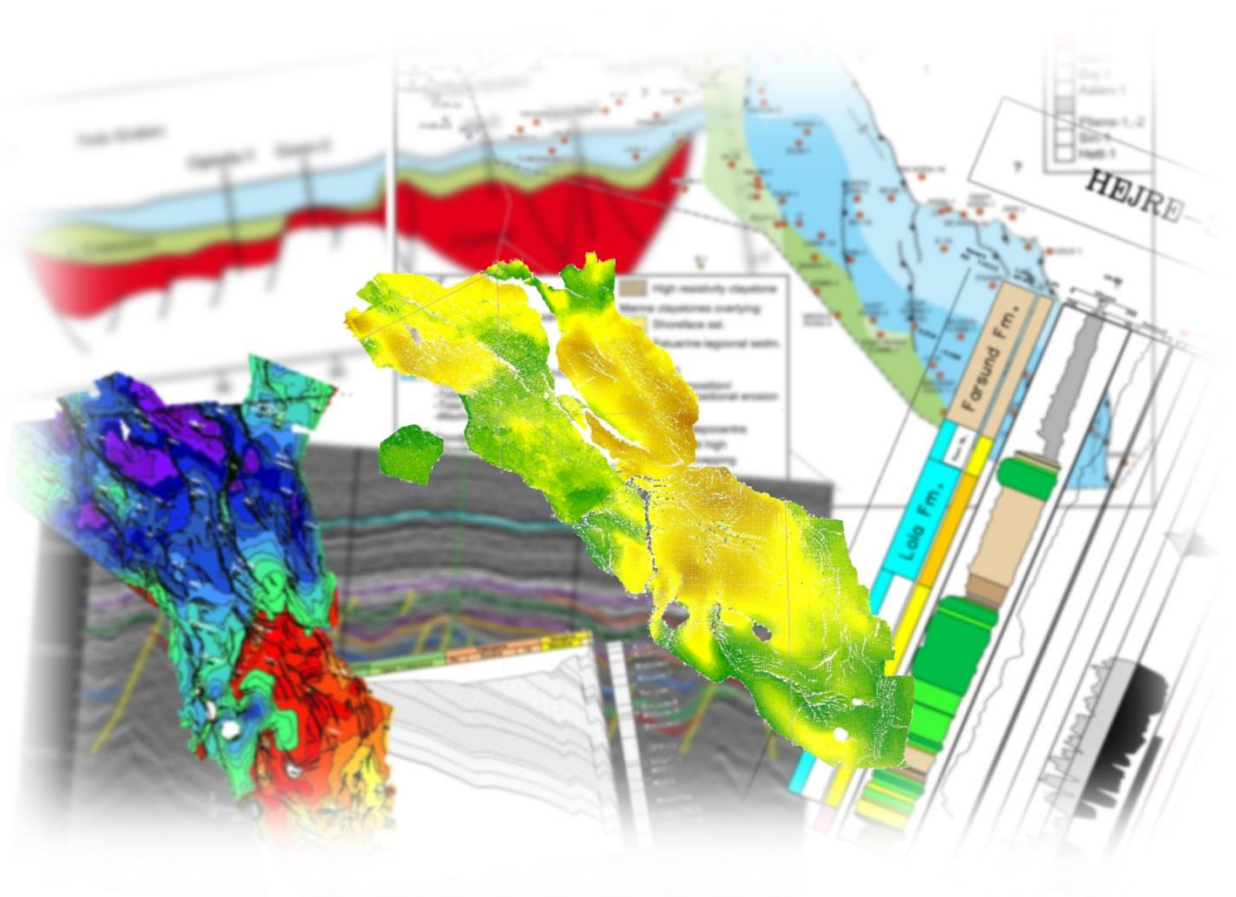
Technical notes

Nina Skaarup, Peter Alsen, Claus Andersen, Karen Dybkjær, Morten Gausby, Tjerk Heijboer,  
Jussi Hovikoski, Finn Jakobsen, Peter Johannessen, Christian Knudsen, Lars Kristensen,  
Anders Mathiesen, Margrethe Thorup Nielsen, Hans Peter Nytoft,  
Henrik Ingermann Petersen, Anders Pilgaard, Jens Therkelsen,  
Erik Thomsen, Rikke Weibel,

Released 01.01.2018

# The Jurassic Petroleum System in the Danish Central Graben

## Technical notes





# The Jurassic Petroleum System in the Danish Central Graben

## Technical notes

### 1 Regional seismic interpretation and mapping

- 1.1 Database
- 1.2 Interpretation approach
- 1.3 Merged horizon files
- 1.4 Synthetic seismograms
- 1.5 Structural profiles
- 1.6 Seismic time-structure maps
- 1.7 Time-isochore maps
- 1.8 Well velocities
- 1.9 Depth structure maps
- 1.10 Schematic spatio-temporal structural activity maps
- 1.11 Jurassic subcrop and supercrop maps
- 1.12 Rock physics templates
- 1.13 References

### 2 Results of log interpretation, including the methodology used for the screening procedure, preparing CPI plots, calculation of reservoir parameters and the GR/DT log facies analysis of the Jurassic succession

- 2.1 Petrophysical evaluation (screening procedure)
- 2.2 CPI plots
- 2.3 LAS files
- 2.4 Reservoir parameters
- 2.5 GR/DT log facies
- 2.6 Quantification of GR/DT log facies
- 2.7 Porosity considerations
- 2.8 Porosity-permeability plots
- 2.9 Database with core analysis data
- 2.10 References

### 3 Stratigraphy and depositional environments

- 3.1 Lithostratigraphy
- 3.2 Bio- and chronostratigraphy
- 3.3 Sequence stratigraphy
- 3.4 Chemostratigraphy
- 3.5 Depositional environments
- 3.6 Core descriptions
- 3.7 Palaeogeographic maps
- 3.8 References

### 4 Petrography and diagenesis

- 4.1 Database
- 4.2 Approach
- 4.3 Microscopy
- 4.4 Qemscan
- 4.5 X-ray diffraction (XRD)
- 4.6 Porosity and permeability
- 4.7 Data quality
- 4.8 References

## **5 Hydrocarbon shows/discoveries database**

5.1 Access at map level

5.2 Access at well level

## **6 Source rock analysis**

6.1 Rock-Eval data

6.2 Vitrinite reflectance measurements

6.3 References

## **7 Basin Modelling**

7.1 Event-splitting using sequence stratigraphy

7.2 Boundary conditions

7.3 Calibration

7.4 Event-split using seismic data

7.5 Kinetics

7.6 Available data for basin modelling

7.7 2D basin modelling

7.8 References

## **8 Analysis of oils and source rock extracts using GC-MS and GC-MS-MS**

8.1 Extraction

8.2 Separation

8.3 Gas chromatography-mass spectrometry (GC-MS and GC-MS-MS)

8.4 References

## **9 Provenance of Upper Jurassic sandstones in the Danish North Sea**

9.1 Introduction

9.2 Zircon provenance

9.3 Rutile chemistry

9.4 Quartz chemistry

9.5 References

## **10 Variation in chemical composition, Ar/Ar ages and Pb/Pb isotope signature of K-feldspar in Heno Formation sandstones in selected wells**

10.1 Summary

10.2 Introduction

10.3 Microprobe analysis

10.4 Ar/Ar dating

10.5 Pb/Pb isotopes in the K-feldspar

10.6 References

# 1 Regional seismic interpretation and mapping

The following note gives a brief description of the regional structural interpretation of the Jurassic in the Danish Central Graben carried out in the PETSYS project with the aim to facilitate the use of the horizon files of selected seismic markers uploaded to the Website system. The note summarises information on the 3D seismic database, interpretation methodology, selection and definition of regionally mapable markers. In addition the methodology to construct synthetic seismograms, key seismic structural profiles, time-structure and time-isochore maps are described. Separate chapters deal with analyses of well derived acoustic velocities and used velocity functions to depth-convert selected horizons critical for maturity modelling.

A series of so-called spatio-temporal activity maps have been produced from time-isochore maps to describe the structural styles and tectonostratigraphic evolution through Jurassic times in DCG. They are supplemented by Jurassic subcrop and supercrop maps. The nomenclature of structural units we use in the text follows Japsen et al. (2003).

Finally rock physics templates showing  $V_p/V_s$  ratios versus acoustic impedance (AI) plots for different lithostratigraphic units and depth ranges are described for wells with both P- and S- sonic logs.

## 1.1 Database

Final migration versions from seven (7) separate 3D surveys in public domain of various vintages have been used. They are from north to south: PAG95, NACS, MC3D-Angelina2007, PAM-99 South, DUC2005, Kraka-Extension-2000 and ES2002, the latter and part of Angelina being a multi-client survey (Fig. 1.1). The line orientations are SW-NE parallel to the general structural dips apart from the southern surveys in the salt-structure dominated area, DUC2005 and ES2002, where the in-line direction is E-W. Pertinent details on the individual surveys can be found on the GEUS Website ([www.geus.dk](http://www.geus.dk)).

The data quality of the surveys in the Jurassic section is generally fair to good; however, it is rather variable in the NACS survey in the north. The data coverage of this survey extends into Norwegian waters and is actually a merge by Mærsk Oil and Gas of several older surveys, which was designed to focus on the Cretaceous section.

A major problem exists when a thick high-velocity chalk section directly overlies low-velocity Upper Jurassic shales at Base Cretaceous Unconformity (BCU). This gives rise to severe ringing and interbed multiples that mask the imaging of the uppermost Jurassic section. In order to overcome the multiple problem a F-K filter was applied post-stack on flattened volumes at BCU to remove parallel events immediately below on parts of the DUC2005 and the Angelina data. This improved the ability to pick dipping events although this robust treatment was on the expense of removing some of the subsurface data.

Apart from ES2002 data where a constant shift of 32 msec was applied during loading to tie to the DUC2005 data to the north, no shifting has taken place. The misfit between the remaining individual datasets was either 0 or below 12 msec, which was considered acceptable for regional interpretation.

All the used data-sets have an areal overlap of varying size (Fig. 1.1). A critical area for ties of high confidence between the DUC05 and PAM-99-South is in the northern part of block 5504/07 north of the Valdemar Field, where only a minor overlap exists.

There is almost full 3D coverage of the entire DCG. A minor triangular data gap exists in block 5603/26 in the Feda Graben. More crucial for the structural interpretation is a small data gap along the so-called Lulu Cross-Fault at the boundary between the Søgne Basin and the northern Tail End Graben in block 5604/22 and in blocks 5504/3 & -4, where the Coffee Soil Fault Zone changes direction from NNW-SSE to WNW-ESE north of the NW Adda-1 location. A small data gap also exists along the fault zone further south in block 5505/18.

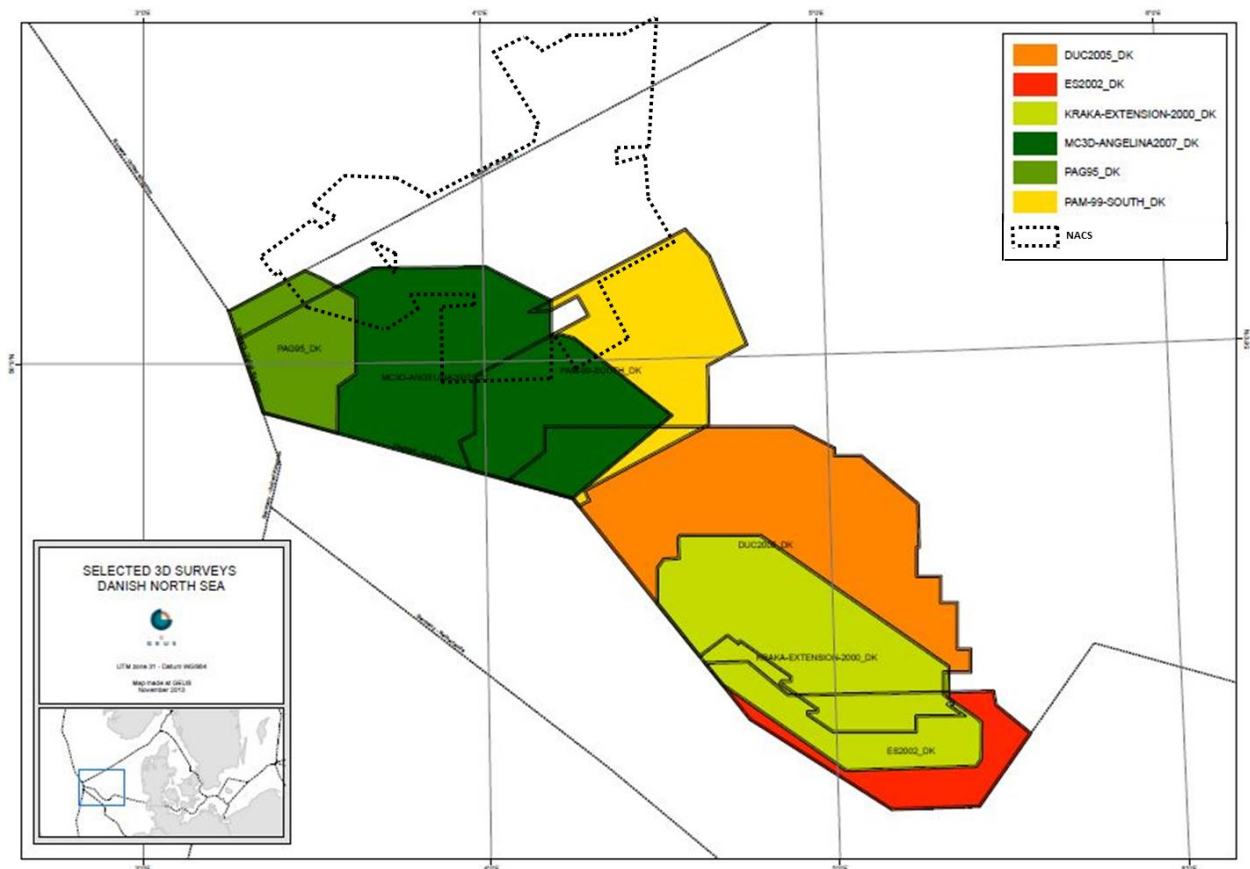


Fig. 1.1: 3D seismic database

## 1.2 Interpretation approach

The seismic interpretation was carried out in SeisWorks. As a starting point a large number of reflectors which can be traced over a larger area were tied to well-sections using the Landmark Syntool software (Figs. 1.2 & 1.4). The marker horizons have been annotated with pre-fix PSS and a number from below. In total 10 horizons of structural and stratigraphic relevance was selected for regional mapping where possible, either in the entire study area or in parts. It is noted that the Jurassic is split structurally in two major areas: 1) an eastern part with a thick Jurassic succession and 2) a western more structural complex and generally thinner succession separated by the Jens Inversion Ridge and The Arne-Elin Graben characterized by post-Jurassic movements. This complicates the confidentiality of direct ties across this

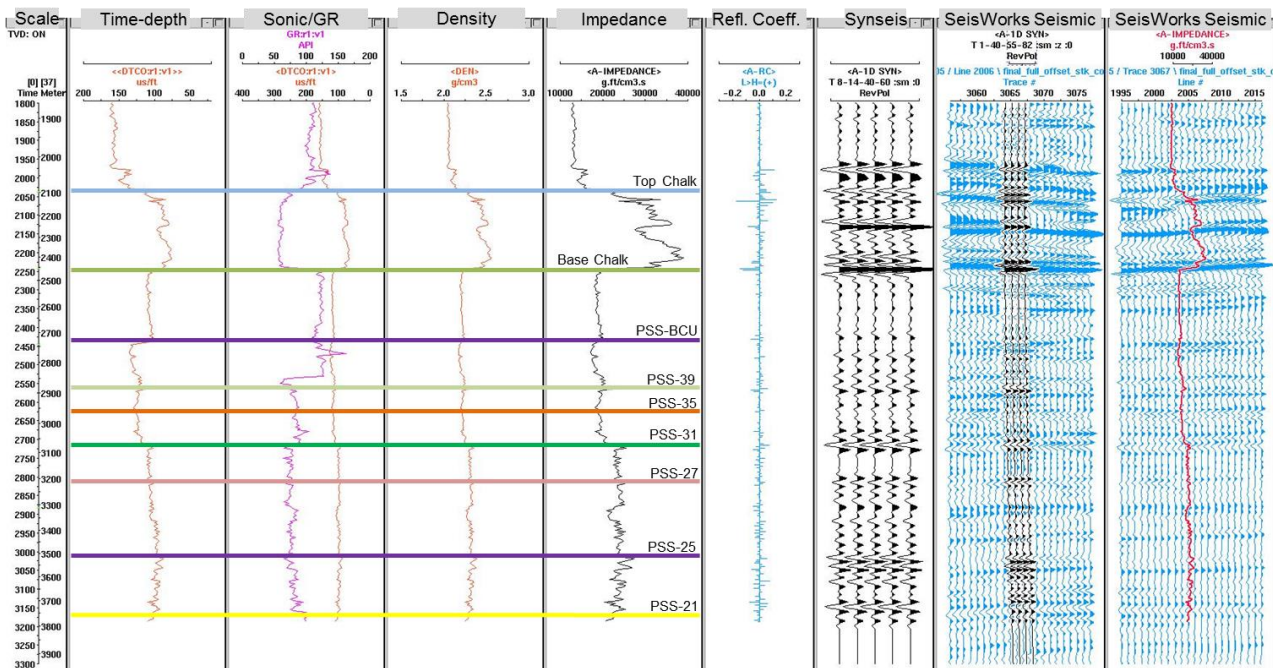


zone; therefore the interpretation has been guided by stratigraphic data from wells. Due to the structural complexity and poor imaging the Arne-Elin Graben area has not been interpreted apart from the upper shallow horizons.

The interpretation is carried out with a distance between lines and traces not exceeding 125 m. The density is locally higher in areas with surveys overlaps. Horizontal faults heaves have been left open in the horizon interpretation. An example of interpretation density and fault trace pattern is shown on the SeisWorks screen-dump in Fig. 1.3.

## Well: Fasan-1

Seismic survey: DUC05



Time-depth table:  
Curve loader

Wavelet extraction (3400-4000ms): 1-40-55-82

Fig. 1.2: Example of seismic synthetic seismogramme (Syntool) with seismic ties

## Time structure Map Area South

PSS 31  
(near base M. Volg)

Seismic surveys:  
duc05, ES02, Kraka ext

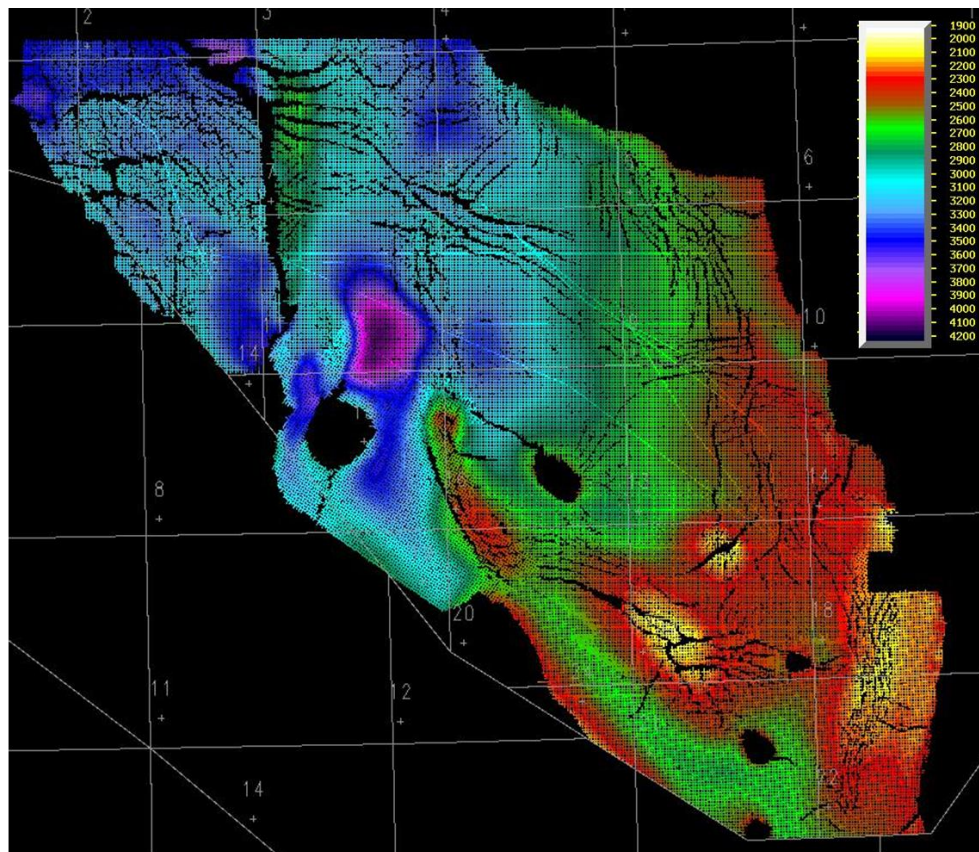


Fig. 1.3: Screen dump from SeisWorks showing interpretation density and fault traces

### 1.3 Merged horizon files

The horizon interpretations on the individual surveys have been merged into final horizon files and are available as ASCII-XYZ files on the PETSYS Website (see menu seismic data). They are annotated with sur-fix .final.dat.

A brief characterisation in stratigraphic order of the interpreted horizons is given below:

*PSS\_Rotl*: The horizon has been interpreted in the north-western part of DCG where Pre-Zechstein strata in places directly underlie the Jurassic succession.

*PSS\_1*: The horizon picked in a rather strong amplitude trough marks the Near Top Triassic tied to wells in all areas where Triassic is present.

*PSS\_Base\_Jura*: This is a merge of *PSS\_Rotl* and *PSS\_1* and the top Zechstein reflector on the salt ridges in the Søgne Basin. The distinction between the three horizons allows construction of a regional Base Jurassic subcrop map.

*PSS\_9*: The reflector is picked on top of a generally high amplitude reflector zone and marks the Near Top Middle Jurassic level. It is noted that the interpreted extension of the marker in the north-west in the Eg Basin and northern Danish Feda Graben is without well control.

*PSS\_13*: It is picked in a strong trough tying to the top of the Lola Formation as defined in the well U-1x. In the south-east it tops a thick, uniform and rather transparent interval; in the west it marks the lithological boundary at the base of the Ravn member of the Heno Formation.

*PSS\_15\_TopRavn*: This is a merge of three different horizons marking the top of intervals of roughly the same stratigraphic age. In most of the area the merge represents the *PSS\_15\_A* marker, which ties to the top of the sands encountered in the Svane-1 well located in the northern Tail End Graben. In the Søgne Basin north of the Lulu Cross Fault the *PSS\_15\_B* ties to the top of turbiditic sands drilled in N3/7-6. To the northwest in the Angelina and part of the NACS survey area the marker (a distinct trough) ties to the top of the Ravn member of the Heno Formation.

*PSS\_25*: This is picked in the lower of a characteristic double reflection, which can be traced with high confidence in the thick eastern depocentres. It is an intra-Farsund Formation horizon stratigraphically close to Volgian-Kimmeridgian boundary. The marker is not identified in the north-west.

*PSS\_29*: This marker has only been interpreted in the north-west on the Angelina and NACS surveys. It ties to the top of an interval in the Farsund Formation characterised by increased GR and Resistivity levels in a number of northern wells (Fig. 1.4).

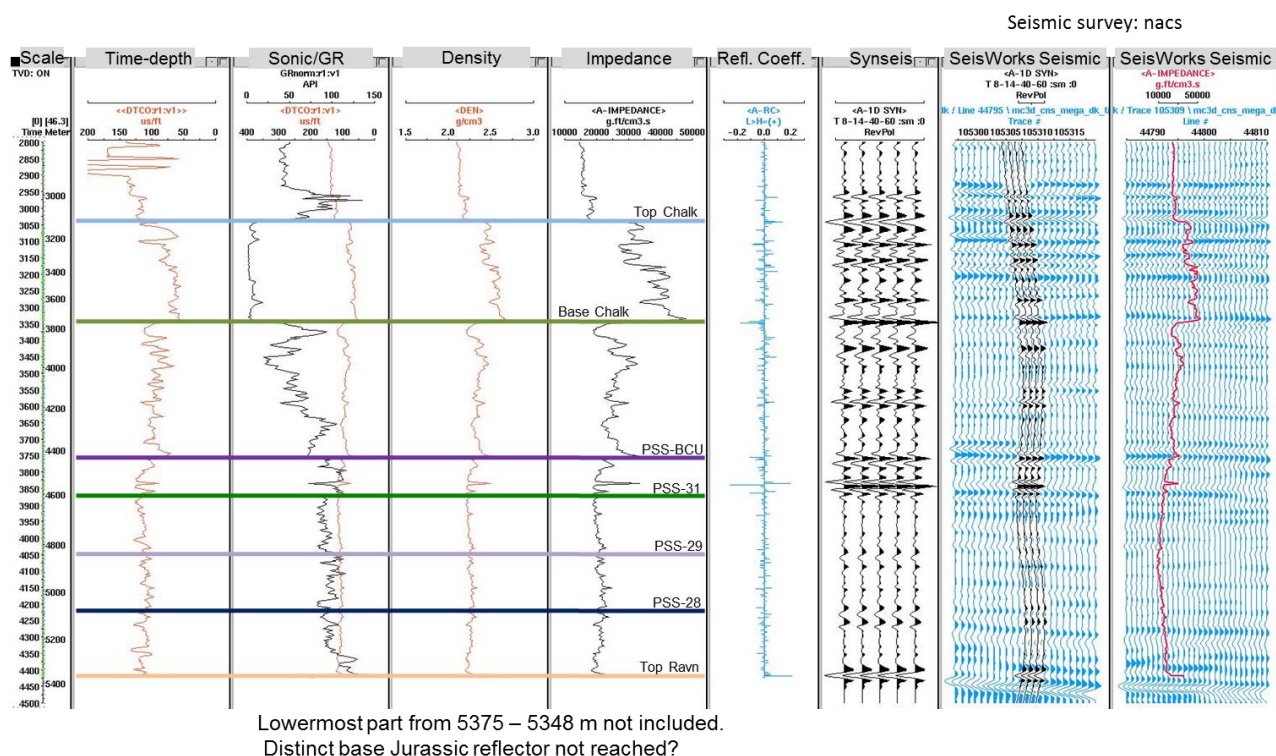
*PSS\_31*: The reflector is interpreted throughout the study area. It is a distinct marker in the east corresponding to a marked downward increase in acoustic impedance in the Farsund Formation close to the Lower-Middle Volgian boundary (Fig. 1.3). In the northwest it represents a structural unconformity truncating underlying strata. *PSS\_29* is often truncated in the greater Heno Plateau area.

*PSS\_35*: This reflector is an intra Middle Volgian marker tied into the TD-level in the Iris-1 well in the north-east. It has not been identified and interpreted in the north-west due to poor ties across the Heno Plateau, where poor imaging originates from BCU multiples.

*PSS\_BCU*: The Base Cretaceous Unconformity has been interpreted over the entire area. It is an easily recognised seismic event (strong peak) marking the top of the low impedance Farsund Formation.

The seismic markers are shown on the *Chronostratigraphic Chart* (Fig. 3.1) within the Stratigraphy menu on the PETSYS Website as well as in the technical note on stratigraphy (Fig. 3.1) giving the relationships to chronostratigraphy and sequence-stratigraphic framework.

# Well: Hejre-2



Time-depth table:  
Curve loader

Wavelet extraction (3400-4000ms): 5-14-40-60

Fig. 1.4: Example of seismic synthetic seismogramme (Syntool) with seismic ties

## 1.4 Synthetic seismograms

Synthetic seismograms of 86 wells are displayed using the *wells* menu on the Website. They have been generated by the Landmark *Syntool* software. This allows display (Figs. 1.2 and 1.3) of time-depth relationships based on well velocity surveys and VSP's, GR-Sonic and Density log traces with location of interpreted seismic markers and calculated acoustic impedance and reflectivity coefficients, respectively. The location of check shots is shown with small green dots on time-depth scale to the left. The log-based synthetic trace is further shown on a line section and the AI-log on a trace section through the well location. A wavelet extraction over a relevant time window was carried out prior to calculate the synthetic traces. The applied trapezoid frequency spectrum is indicated.

Adjustments to the time-depth curves were necessary in some wells in order to establish a good match to the most distinct reflectors (e.g. Base Chalk and BCU) and the log breaks.

Comments to the quality of the synthetics are offered when necessary. This is relevant in the case of e.g. deviated wells, strong structural dips, poor seismic reflectivity, structural complexity and log quality.

## 1.5 Structural profiles

24 interpreted seismic sections are displayed by activating the map menu under the heading *Structural Profiles* on the Website system. The sections are screen dumps of arbitrary line segments from the individual surveys crossing one or several well locations. The seismic markers are all annotated with their PSS-number and the same colour code as for the synthetic seismograms has been applied. In addition to the regionally mapped reflectors described above more reflectors, which can be traced locally, have been shown especially in areas to the south and east, where the Jurassic is thick.

The sections have been chosen with the intention to illustrate the structural style in all sub-basins of DCG and to provide well ties. The profiles show the ties to 57 wells in total.

It is noted that both vertical and horizontal scales may differ from section to section.

## 1.6 Seismic time-structure maps

Time-structure maps of the nine regionally interpreted horizons described in chapter 1.2 have been generated from the merged horizon files and can be displayed on the Website in the map menu. The data have been gridded using the Landmark Z-MAP Plus software. Fault polygons were generated followed by gridding with a search radius of 150 m and a grid increment of 200 m. For each horizon the grids, fault polygons and contours are placed in separate folders. The predefined contour interval varies from horizon to horizon in order to obtain the best graphic solution.

## 1.7 Time-isochore maps

In order to illustrate the Jurassic basin fill history through time simple time-isochore maps of all intervals bounded by the regionally interpreted horizons are generated by subtraction in SeisWorks of the merged horizon files and are displayed on the Website in the map menu without gridding performed. This simple approach limits the map to areas, where both top and base of the interval is defined. This applies to intervals bounded by horizons PSS\_25, PSS\_35 and PSS\_29, which only have been interpreted in the eastern and western area, respectively.

Some of the intervals have been combined when the horizons have been interpreted basin-wide. Time-isochore PSS\_BCU – PSS\_Base Jura (Fig 1.5) shows the combined time thickness of the Jurassic. It demonstrates the overall half-graben geometry of the DCG with thin to absent Jurassic in the Outer Rough Basin on the flanks of the Mid North Sea High in the west to more than 3500 ms in the Tail End Graben adjacent to the Coffee Soil Fault Zone.

A split of the Jurassic into two parts: a lower interval defined by the time-isochore PSS\_15\_TopRavn – PSS\_Base Jura and an upper interval defined by time-isochore PSS\_BCU – PSS\_15\_TopRavn show distinct differences in the fill history. In the lower part narrow depocentres are located in the east with only a thin cover on the plateaus to the west of the Arne-Elin Graben and the Jens Inversion Zone. This differs in the upper part where eastern depocentre becomes wider and with only a thin succession in the Salt Dome Province to the south and the Søgne Basin in the north. To the west the Feda Graben and Gertrud Graben

show the shape of two opposite dipping half-grabens separated by the NW-SE trending Gert Ridge and a fault zone extending to the Gwen wells.

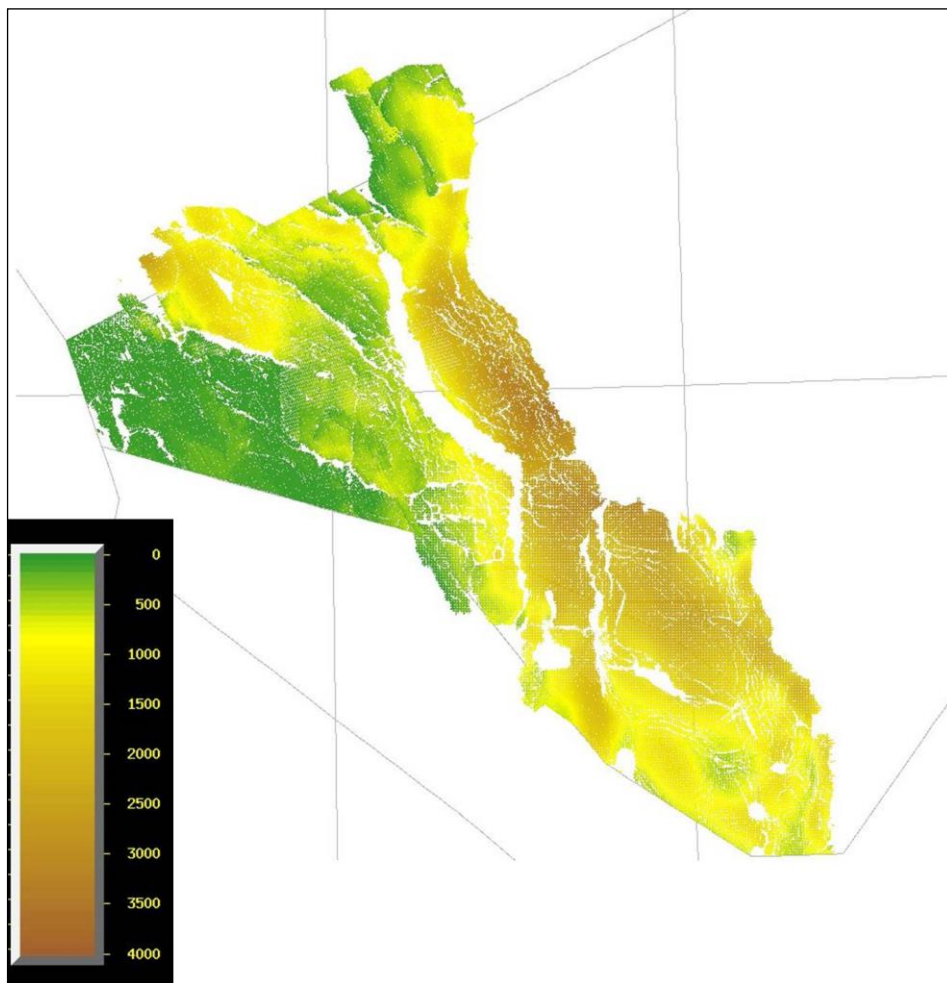


Fig. 1.5: Time Isochore PSS\_BCU-PSS\_Base Jura

A further split of the upper interval is made at PSS\_31 (the intra Volgian Unconformity). The interval below (PSS\_31 – PSS\_15\_TopRavn) reaches a maximum time-thickness of 1200 ms (eqv to about 1700 m) in the Tail End Graben deposited over a time span of less than 4 ma. The overlying interval bounded by PSS\_31 and PSS\_BCU shows more gentle thickness variations with the main eastern depocentre divided into smaller separate basins. The development of the Feda and Gertrud Grabens took place during this time period. Similarly the southern Arne-Elin Graben started to subside and is characterised by a thick fill. Only a thin cover mostly below seismic resolution exists in the Outer Rough Basin.

## 1.8 Well velocities

The Jurassic velocity structure derived from well sections is analysed both with respect to average velocity to regionally interpreted horizons and interval velocities between bounding reflectors. The results are

tabulated in a spread-sheet found on both the map and seismic data menu based on the time-depth curves from each well presented on the synthetic seismograms (chapter 1.3).

The velocity field is highly variable in the Jurassic, which makes it a challenge to establish velocity functions to depth-convert time-maps into reliable depth-maps. A few observations are commented upon:

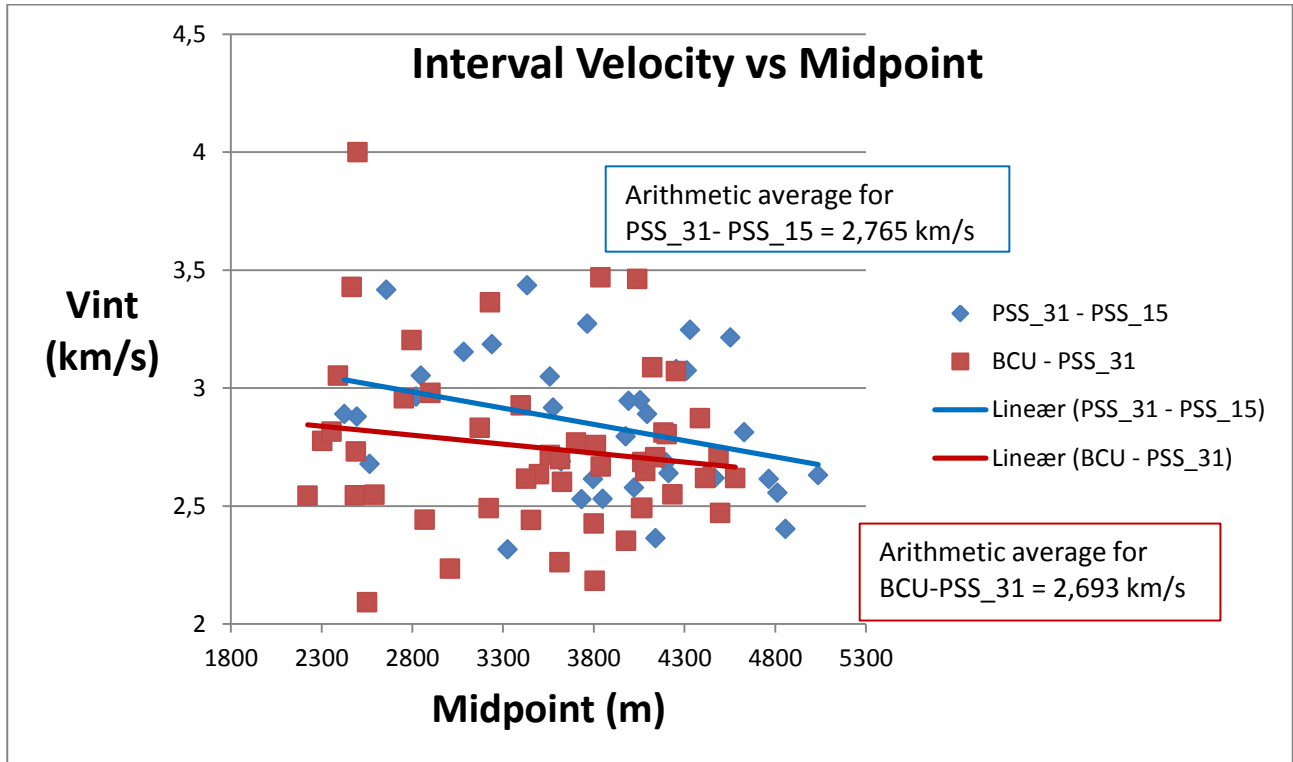


Fig. 1.6: Interval velocity vs Midpoint crossplot for intervals: PSS\_31-PSS\_15 and PSS\_BCU-PSS\_31

The interval velocities for the upper intervals PSS\_BCU – PSS\_31 (Ryazanian - Middle Volgian) and PSS\_31 - PSS\_15\_TopRavn (Lower Volgian - intra Upper Kimmeridgian) are plotted versus midpoint depth in Fig 1.6. There is a considerable scatter and no obvious depth relationships exist in the two intervals. The two outliers in the upper interval are the Ugle-1 well with very high  $V_{int}$  (4.0 km/s) in spite of shallow burial depth and the North Jens-1 well with low  $V_{int}$  (2.1 km/s).

The interval velocities of the drilled intervals below PSS\_15\_TopRavn and the entire Jurassic (PSS\_BCU – PSS\_1) are plotted versus interval thickness in Fig 1.7. It is noted that  $V_{int}$  for the entire Jurassic succession cluster around a value of 3.0 km/s in the drilled thickness range up to 1500 m. In contrast  $V_{int}$  of the Jurassic below PSS\_15\_Top Ravn show an inverse relationship with thickness with highest velocity values at small thicknesses. This is in part a result of biased sampling. Most of the data represent wells drilled in the Heno Plateau area and represent intervals with a high proportion of high velocity sandstones of the Heno Formation compared to well sections with a higher proportion of claystones (e.g. thick Lola Formation). The two outliers in the plot represent the Cleo-1 and Amalie-1 wells, both wells located in the north-east adjacent to the Coffee Soil Fault Zone.

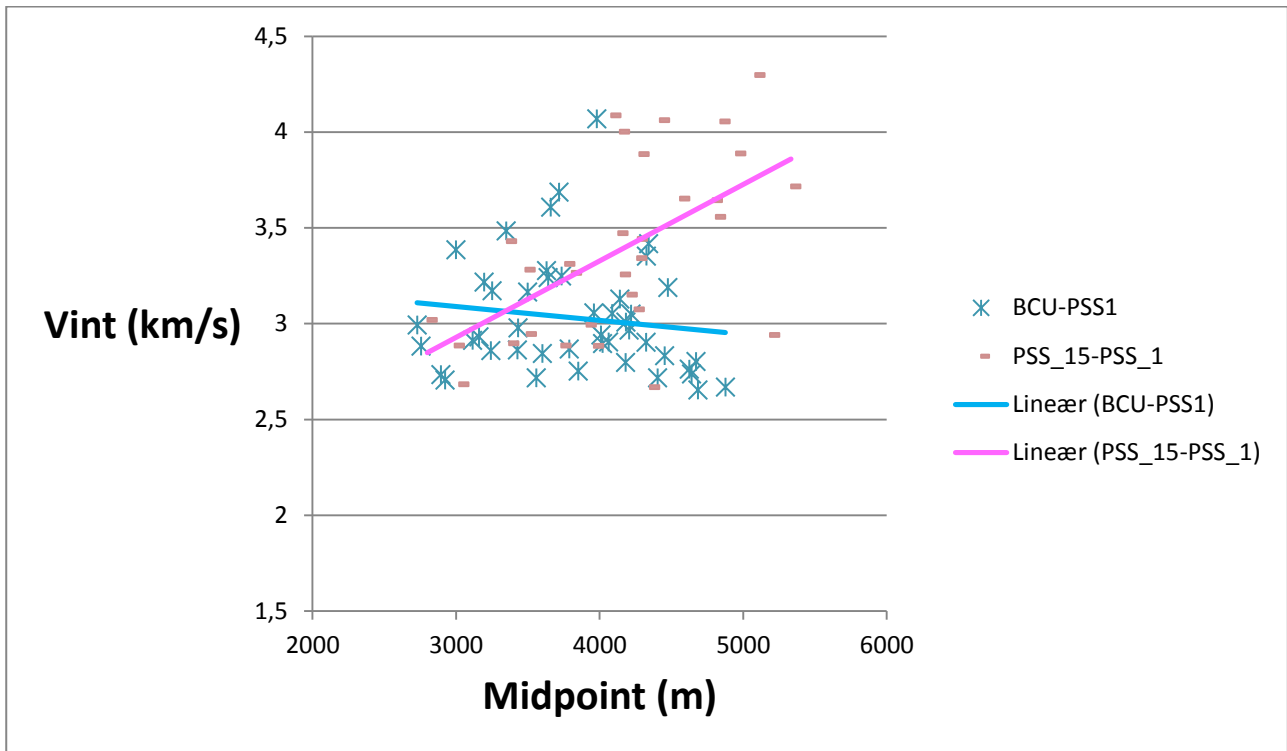


Fig. 1.7: Interval velocity vs Midpoint crossplot for intervals: PSS\_BCU-PSS\_1 and PSS\_15\_TopRavn-PSS\_1

Recorded average velocities to the seismic markers are highly dependant on the nature of the post-Jurassic overburden. This is illustrated in Fig 1.8 where  $V_{avg}$  to horizon PSS\_31 in each well is plotted on a Chalk Group isochore map from Britze et al. (1995a). High  $V_{avg}$  corresponds to a thick overlying, high velocity Chalk Group.



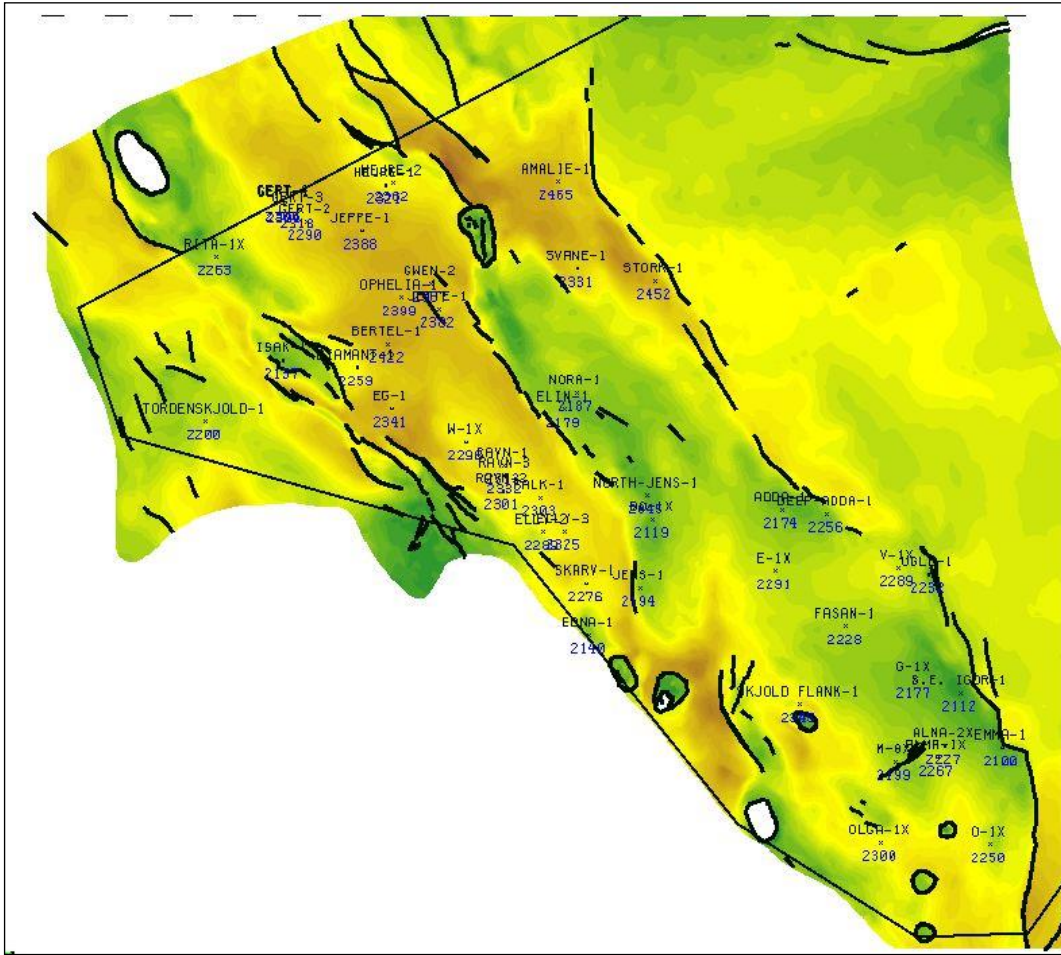


Fig. 1.8: Average velocity for interval PSS\_BCU-PSS\_31 plotted at Chalk Group Isochores

Average velocities to all well-picks of the interpreted horizons versus two-way-travel time are shown in Fig.1.9. In spite of the large variation an overall general depth-related trend is observed. However, separate trend lines can be isolated depending on the geographical position of the well. High depth related trend lines are found in wells located both to the south in the Salt Dome Province and in the east along the Coffee Soil Fault Zone with the Cleo-1 and Amalie-1 wells forming pronounced outliers. In contrast a low trend can be distinguished in wells located to the far west where most of the wells only penetrated a rather thin chalk section.  $V_{avg}$  derived (and extrapolated) from these trend lines have been used to calculate depths to event-splits below PSS\_15\_TopRavn in pseudo-wells for 1D maturity modelling. This rude approach gives rise to considerable uncertainty in the deep undrilled parts of the basin taking the sampling bias in consideration.

The well-derived average velocities have been compared with the available RMS velocity cubes from the DUC2005 and the MC3D-Angelina2007 surveys. At the level of PSS\_15\_TopRavn the RMS velocities are typically about 10% higher than in the wells. Even higher discrepancies up to 15% are recorded at deeper stratigraphic levels.

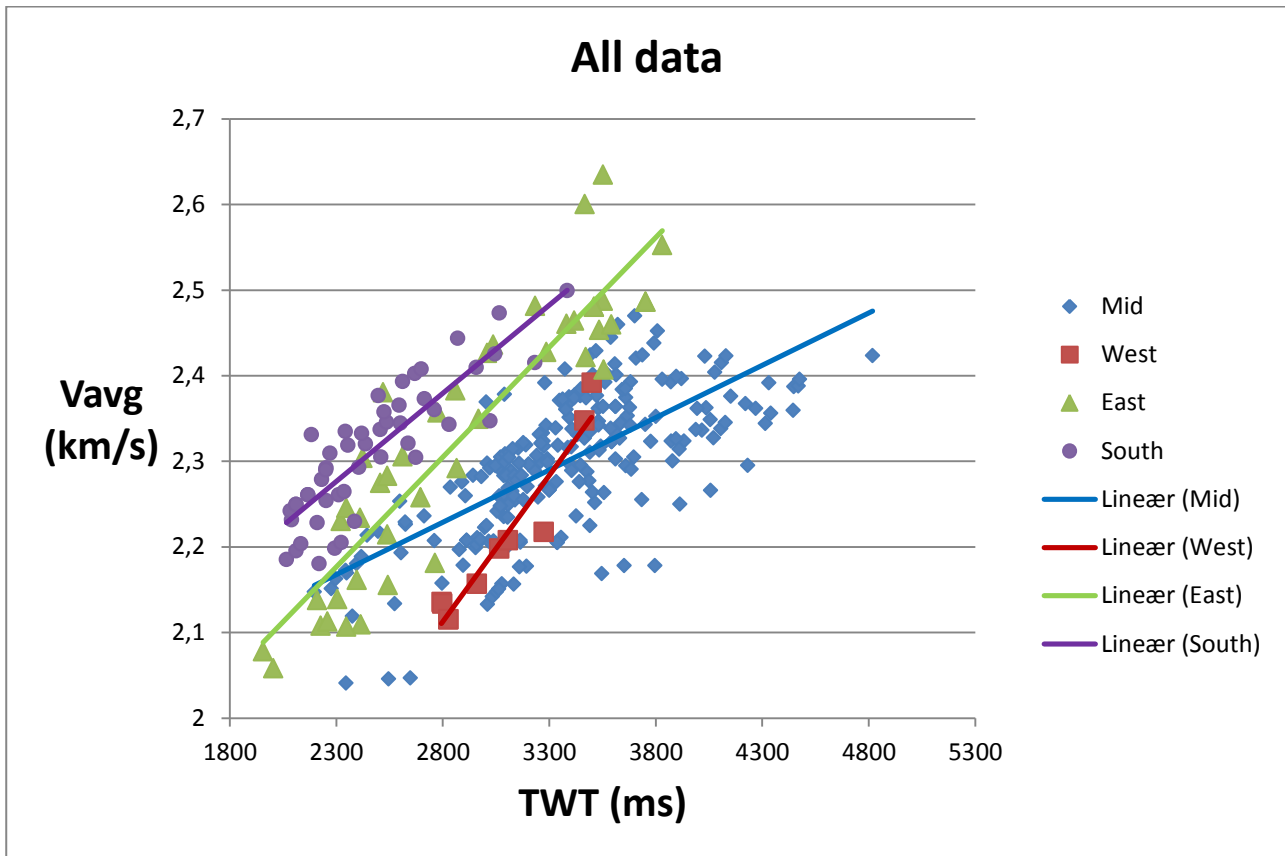


Fig. 1.9: Average velocity to all well picks vs two-way-traveltime

## 1.9 Depth structure maps

Depth structure maps to PSS\_BCU, PSS\_31 and PSS\_15\_TopRavn have been generated using the Z\_MAP Plus software in order to facilitate input for maturity modelling exercises of the potential source rocks intervals in the Farsund Formation. The gridded maps are available in the map menu on the Website. A brief description of the workflow is given below.

The depth-conversion of the time-grids is performed using the layer-cake method whereby interval thickness grids sequentially are added to the overlying surface.

The Base Cretaceous Unconformity surface is calculated by using an average velocity grid to BCU applied to the PETSYS PSS-BCU time-grid. The velocity grid was calculated from already existing time and depth grids from Britze et al., 1995b and shown in the Website map menu. The existing time grid was based primarily on 2D data and the depth grid was generated by the layer-cake method by adding 5 thickness grids of post-Jurassic intervals.

The thicknesses of the PSS\_BCU – PSS\_31 and PSS\_31 – PSS\_15\_TopRavn intervals were calculated using constant  $V_{int}$  of 2.693 km/s and 2.765 km/s, respectively. These figures are arithmetic averages of  $V_{int}$  of drilled intervals (Fig1.6). It is stressed that the well-based velocity database is biased as no data are available where the intervals are very thick.

At each step a back-interpolation of the depth grid was carried out in order to match the depth-values at well locations. The generated error-grid was then added to the depth grid.

The PSS\_15\_Top Ravn is a key surface as it represents both the base of an interval rich in TOC below PSS\_29 in the north and the top of the Heno Formation sandstones and the mass-flow sandstone encountered in the Svane-1 well. The surface show very large variation in depth spanning from about 2400 m on the crests of salt pillows in the south to maximum 6600 m in the Tail End Graben.

## 1.10 Schematic spatio-temporal structural activity maps

A series of schematic maps have been produced to highlight active faults and location of depocentres in each of the intervals bounded by the regionally mapped reflectors in order to summarise the temporal structural style and development and provide an input to guide generation of palaeo-geographic maps. The maps found in the 'structural element' folder on Website have been constructed from the time-isochores maps. The syn-kinematic faults have been located when abrupt jumps in time-thickness occur and further supported by check on flattened sections. On all maps present-day salt piercements are shown.

Remarks to the maps with references to relevant structural profiles are given below.

*Interval PSS\_1 – PSS\_9* comprises the Lower and Middle Jurassic strata combined although a major hiatus between the Fjerritslev and Bryne Formation is recorded in wells. The interval occurs with varying thickness in the eastern DCG and onlaps seismically Triassic on the Heno Plateau. Remnants possibly occur in the Eg Sub-basin and in the northernmost Danish part of the Feda Graben. The active faults have a dominant N-S direction and are linked to faults cutting the Pre-Zechstein level (e.g. structural profile 6, 7, 10, 11 and 14). An exception is faults in the Salt Dome Province in the south-east where faults are detached in Triassic and Zechstein and associated depocentres and abrupt changes in interval thickness along the Coffee Soil Fault Zone. This is attributed to halokinesis and salt withdrawal of mobile Zechstein salt (Duffy et al., 2013).

A rather abrupt thickness change is mapped at the rather small areal overlap between the DUC2005 and Pam-99 South surveys extending WNW from the present kink in the Coffee Soil Fault Zone. It is not clear if this feature represents an ancient transfer zone or is an artefact caused by picking of a too shallow PSS\_1 reflector in the deep northern part of the DUC2005 survey.

*Interval PSS\_9 – PSS\_13* comprises the time span Oxfordian –Lower Kimmeridgian and corresponds roughly lithostratigraphically to the Lola Formation. The interval oversteps the underlying interval to the west with the extension controlled by truncation. The thickness variation is large with a number of narrow deep elongate, partly overstepping depocentres located in the Tail End Graben extending southwards into the Rosa Basin. Small isolated, high amplitude hangingwall depocentres are found adjacent to the southern segment of the Coffee Soil Fault Zone witnessing continued salt withdrawal.

The mobile salt is responsible for the majority of the syn-kinematic cover faults, which are mechanically decoupled from the deep Pre-Zechstein faults in this area (e.g. structural profile 1 & 2).

A mosaic of tilted faulted blocks characterise the interval on the southern Heno Plateau.

*Interval PSS\_13 – PSS\_15A, 15B and PSS\_TopRavn* comprises an Intra Upper Kimmeridgian interval corresponding to the Ravn Member of the Heno Formation and the drilled section from top of mass-flow sandstones to TD in the Svane-1 well. The base is further south correlated to the top of the Lola Formation. In the east the depocentres mostly have the character of forced low amplitude folds, which along the southern segment of the Coffee Soil Fault Zone become more distinct. Duffy et al. (2013) have proposed a positive feedback mechanism to have developed here, whereby sediment accumulation in the accommodation generated by both border fault displacement and evaporate withdrawal, resulted in loading and further withdrawal of evaporates, which, in turn generated accommodation. A cluster of N-S trending growth faults affect this area (e.g. structural profile 2 and 6).

In the north-west the Gert Ridge starts to develop and is associated with development of minor depositional thicks to the west.

*Intervals PSS\_TopRavn - PSS\_29 and PSS\_15 – PSS-25* is combined into one map. It represents intervals in the Upper Kimmeridgian and Intra Lower Volgian belonging to the lower part of the Farsund Formation. The thickness distribution is rather similar to the underlying interval with maximum thicknesses confined to a number of elongate depocentres in the Tail End Graben. Of special interest is small depocentres mapped along the Ringkøbing-Fyn High master fault (structural profile 11 and 14). Detailed mapping of this area by Bruhn and Vagle (2005) has suggested that these depocentres were associated short-lived relay ramps delineated by overstepping normal faults supplying material from the high, which later became breached.

In the north-west a continuous fault zone developed from the Gert Ridge south-eastwards to the Gwen structure. Tilted fault blocks are developed in the Gertrud Graben area (e.g. structural profiles 17 and 22).

*Intervals PSS\_29 – PSS\_31 and PSS\_25 – PSS\_31* includes a lower Volgian interval of the Farsund Formation. Maximum thickness is found in a broad depocentre located centrally in the Tail End Graben. To the south the interval is thin (less than 100 ms) and to the north in the Søgne Basin area and neighbouring Mandal High it is eroded by the BCU reflector (structural profile 22), the latter high believed to have been an area of non-deposition during most of the late Jurassic (Rosslund et al., 2013). The interval is thin in the Heno Plateau area and is locally truncated by the intra-Volgian Unconformity, PSS\_31 (e.g. structural profile 13).

The structural grain in this interval is dominated by syn-kinematic faults with a NW-SW orientation.

*Intervals PSS\_31 – PSS\_35 and PSS\_35 – PSS\_BCU* is only displayed in the eastern area delimited by the areal interpretation of seismic marker PSS\_35. Maximum deposition in the lower interval took place in the Adda area south of the WNW-ESE trending segment of the Coffee Soil Fault Zone (structural profile 5), whereas the deposition in the upper interval occurred in smaller isolated basins. Both intervals in the south are thin to absent and the upper interval is even truncated at BCU in the John structure area and at part of the Kraka structure.

The structural grain during the Middle Volgian – Ryazanian interval is dominated by NW-SE syn-kinematic faults. This includes development of growth faults in the North Jens (structural profile 8) and Tyra area. The structural complex Arne-Elin Graben also developed during this time span with large deposition rates (structural profile 11).

*Combined Interval PSS\_31 – PSS\_BCU* is displayed to illustrate the structural grain over the entire part of DCG. The fault pattern is everywhere dominated by NW-SE directions. This is independent of the nature of the faults ranging from growth faults in the south to basement attached faults like the Gert-Gwen ridges in the north-west. The latter separates the young opposite dipping Feda of Gertrud Grabens, respectively (structural profile 20).

## 1.11 Jurassic subcrop and supercrop maps

Simplified subcrop and supercrop maps of the Jurassic in DCG are found in the structural element folder on the map menu.

On the subcrop map a distinction is made between a Triassic, Zechstein or Pre-Zechstein sub-stratum. Triassic deposits are present everywhere in the eastern part. Zechstein evaporates underlie Middle Jurassic of the Bryne Formation on the Lulu-Lulita salt ridge in the Søgne Basin. The northern and southern limits of mobile salt, which to a large extent control the structural style of the Jurassic rift basin are shown. In the western part Rotliegende sediments and volcanics underlie the Jurassic. The boundaries between Triassic and older rocks are often controlled by old N-S trending fault segments. On the footwall of the Coffee Soil Fault Zone crystalline basement rocks have been drilled in e.g. Per-1.

The supercrop map shows the extension of Lower Cretaceous sediments of the Cromer Knoll Group and where Upper Cretaceous chinks directly overlie the Jurassic following the outlines from Japsen et al. (2003). Severe ringing and interbed multiples masking the image of the uppermost Jurassic section is a problem in the latter areas.

The fault traces mapped on the PSS\_BCU surface are shown with two colours. The black fault traces marks reactivated faults, which were active already during deposition of the PSS\_31 – PSS-BCU interval. Faults marked in red are all post-Jurassic faults affecting the surface. This includes reverse faults caused by widespread Cretaceous inversion in the form of compression along former extensional faults resulting in flexuring and folding of basin infill (Vejbæk & Andersen, 2002).

## 1.12 Rock physics templates

Both Vp- and Vs logs have been run in the Jurassic section in 9 study wells. We have crossplotted Vp/Vs ratios versus acoustic impedance (AI) using the rock physics template facilities in the *Hampson – Russel* software. For each well two colour-coded crossplots are produced to differentiate populations either by lithostratigraphic unit, depth or GR-values. It was necessary to edit the logs in zones, where especially the Vs logs are of poor quality. The crossplots can be accessed on the PETSYS Website under Wells.

The intension with this exercise on a restricted data-set is to analyse if robust separations of different lithologies can be demonstrated. Below a few observations are commented upon.

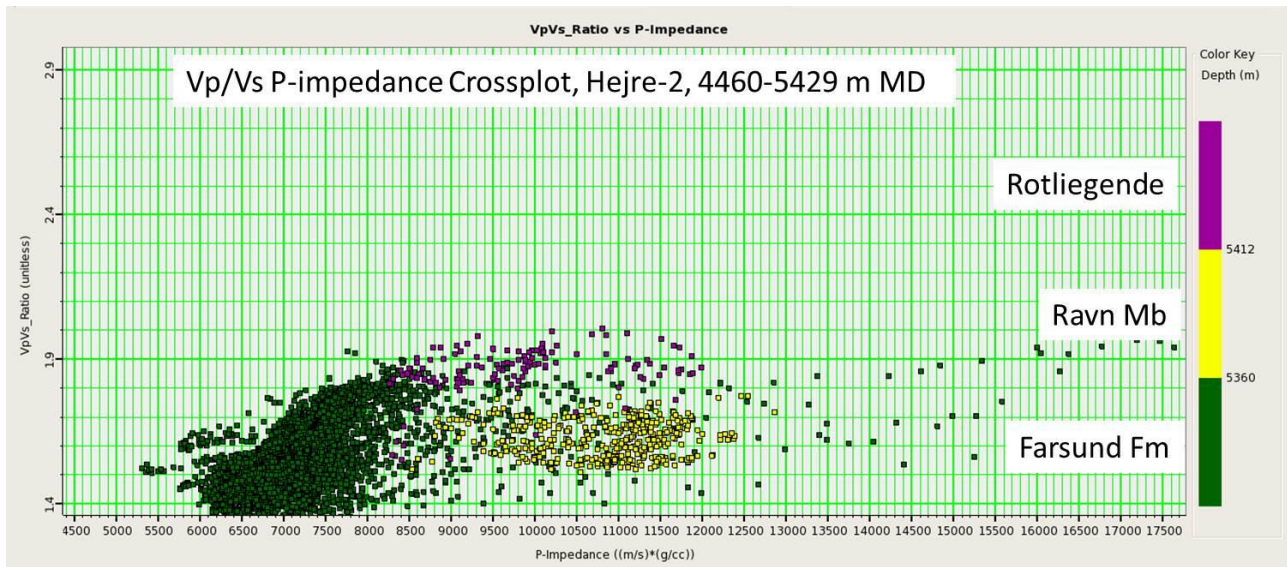


Fig. 1.10: Vp/Vs P-impedance crossplot, Hejre-2, 4460-5429 m (MD). Lithostratigraphic units used for colour coding

In most of the analysed wells the (e.g. Hejre-2, Fig1.10) the crossplots show clear separation between the often TOC-rich mudstones of the Farsund Formation and the sandstones of the Ravn Mb. The mudstones are characterised by both low Vp/Vs ratio and AI in contrast to the higher AI-values in the sandstones. The underlying Rotliegende section forms a separate population with higher Vp/Vs ratios. The crossplot of the deep TOC-rich Farsund Fm interval at depth of about 5000 m MD in this well is shown separately in Fig. 1.11. The low AI-values are noted. This observation is in line with experience from the Norwegian shelf (Løseth et al., 2011).

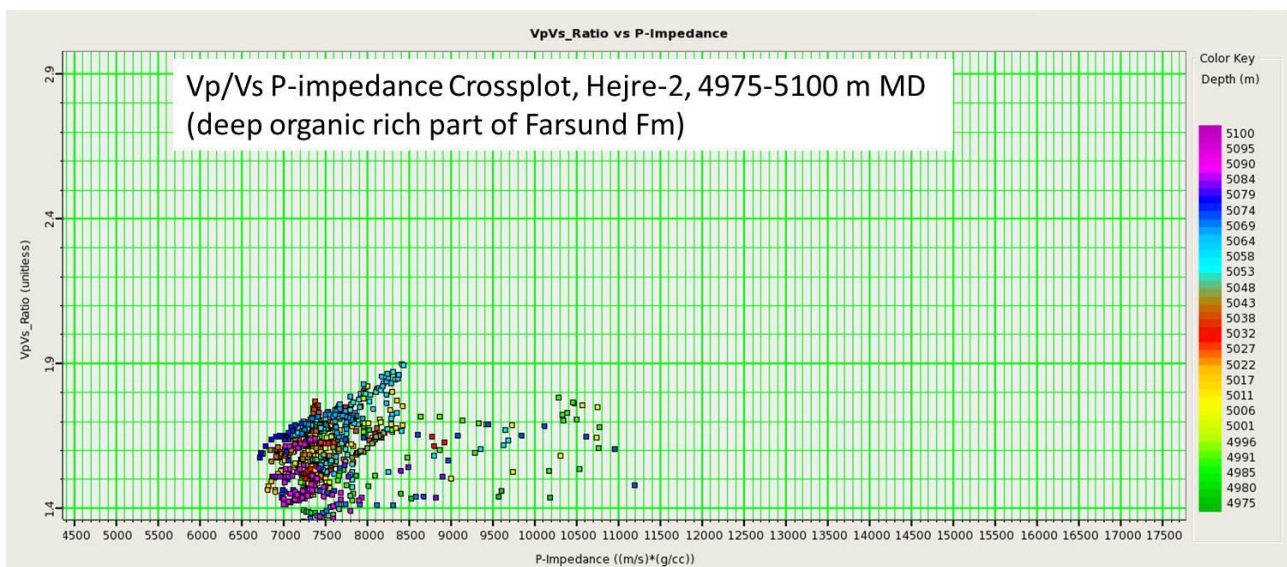


Fig. 1.11: Vp/Vs P-impedance crossplot, Hejre-2, 4975-5100 m MD (deep organic rich part of Farsund Fm). Depth scale used for colour coding

The Fasan-1 well (Fig. 1.12) has only penetrated the Farsund Formation. The crossplot with GR-values used for colour coding shows a cluster with both very low Vp/Vs and AI values separated by low GR-rocks representing tight carbonate or carbonate-cemented lithologies with much higher values. The very low Vp/Vs ratio (1.4 -1.6) in the high GR-intervals as also seen in the Hejre-2 example are noteworthy. Ultrasonic measurements on samples from the Bakken shales in the Williston Basin (Vernik & Nur, 1992) have shown that such low values are typical for anisotropic organic-rich shales. Vp/Vs variation to lower ratios is influenced by gas in the pore fluid and further enhanced by overpressure conditions (Rojas et al., 2005)..

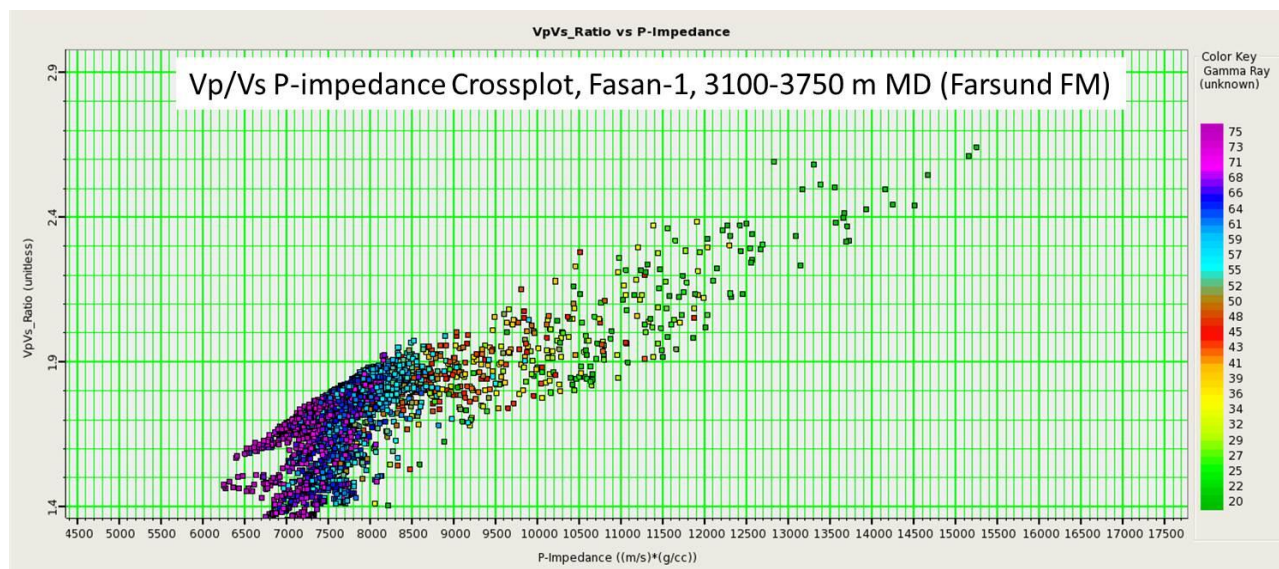


Fig. 1.12: Vp/Vs P-impedance crossplot, Fasan-1, 3100-3750 m MD (Farsund Fm). GR values used for colour coding

### 1.13 References

- Britze P., Japsen P. & Andersen C. 1995a: Geological map of Denmark, 1:200 000: The Danish Central Graben.'Base Chalk and the Chalk Group' (two-way-traveltime and depth, interval velocity and isochore). Danmarks Geologiske Undersøgelse Kortserie 48, 7 pp., 4 maps.
- Britze P., Japsen P. & Andersen C. 1995b: Geological map of Denmark, 1:200 000: Danish Central Graben 'Base Cretaceous and the Cromer Knoll Group' (two-way-traveltime and depth, interval velocity and isochore). Danmarks Geologiske Undersøgelse Kortserie 49, 7 pp., 4 maps.
- Bruhn R. & Vagle K. 2005: Relay ramp evolution and mass flow deposition (Upper Kimmeridgian – Lower Volgian) in the Tail End Graben, Danish North Sea. Basin Research 17, 551-567.
- Duffy, O.B., Gawthorpe, R.L., Docherty, M. & Brocklehurst, S.H. 2013: Mobile evaporite controls on the structural style and evolution of rift basins: Danish Central Graben, North Sea. Basin Research 25, 310-330.
- Japsen P., Britze, P. & Andersen C. 2003: Upper Jurassic – Lower Cretaceous of the Danish Central Graben: structural framework and nomenclature. Geol. Surv. Den.Green. Bull. 1, 233-246.

Løseth, H., Wensaas, L., Giding, M., Duffaut, K. & Springer, M. 2011: Can hydrocarbon source rocks be identified on seismic data? *Geology* 2011; 39; 1167-1170

Rojas, E., Davis, T.L., Batzle, M., Prasad, R.L. & Michelena, J. 2005: Vp-Vs ratio sensitivity to pressure, fluid and lithology changes in tight sandstones. Extended abstract. SEG/Houston 2005. Annual Meeting.

Rosland, A., Escalona, A. & Rolfsen, R: 2013: Permian – Holocene tectonostratigraphic evolution of the Mandal High, Horth Sea. *AAPG Bull.* V.97, No. 6. pp. 923-957.

Vejbæk, O.V. & Andersen, C. 2022: Post mid-Cretaceous inversion tectonics in the Danish Central Graben – regionally synchronous tectonic events? *Bulletin of the Geological Society of Denmark* 49, 129-144.

Vernik, L. & Nur, A. 1992: Ultrasonic velocity and anisotropy of hydrocarbon source rocks. *Geophysics*, Vol. 57, 727-735.



## 2 Results of log interpretation, including the methodology used for the screening procedure, preparing CPI plots, calculation of reservoir parameters and the GR/DT log facies analysis of the Jurassic succession

The petrophysical evaluation is based on wireline log data and core analysis data from selected Danish wells using a standard approach for interpreting the log data. The results of the petrophysical evaluations are listed as LAS files including depth columns, effective porosity (PHIE), shale volume (Vshale) and saturation (Sw). The current log analysis focuses on sand-rich layers within the Jurassic succession, i.e. potential reservoir units. Furthermore, CPI plots of 68 wells have been generated and compiled in a “CPI Catalogue”. Moreover, reservoir parameters, such as sandstone thickness (net & gross), average porosity, shale volume and net-to-gross ratio are calculated and subsequently tabulated in two Excel files. These parameters are calculated on the basis of no porosity cut-off and 12% porosity cut-off, respectively. Maps showing average porosity, net sand thickness, gross thickness, shale volume and net-to-gross ratio are to be plotted interactively from the PETSYS Website. The methodology used for the preparation of GR/DT logs (log facies) is described in more details below.

### 2.1 Petrophysical evaluation (screening procedure):

- **Generally, the shale volume (Vshale)** is calculated from the gamma-ray log using a linear model.
- **The porosity (PHIE)** is determined from density log, calculated shale volume and various fluid densities.
  - It is taken into account that the sandstone matrix density may be higher than 2.65 g/cc (i.e. quartz density) due to the presence of dolomite, siderite, calcite cement etc.
  - Grain density measurements, combined with cross-plots of neutron-density log responses, have been used for lithology determination, i.e. lithology identification plots.
  - Various fluid densities were applied: Water-Based Mud systems: 1.05 -1.10g/cc for oil and water, 0.90g/cc for gas. Oil-Based Mud systems: 0.95g/cc for oil and water, 0.80g/cc for gas.
  - The porosity interpretation was calibrated to core porosity data, when available. The core data have been depth-shifted.
- **The hydrocarbon saturation (Sh) were calculated from resistivity logs and various petrophysical parameters:**
  - Petrophysical parameters  $a$ ,  $m$ ,  $n$  and  $R_w$  were extracted from Well Completion Reports.

- Otherwise  $a = 1$ ,  $m = 2$ ,  $n = 2$  and  $R_w$  from Pickett Plots; i.e. standard approach.
- The calculation of the hydrocarbon saturation is based on the Indonesian Equation.
- $S_w = 1 - S_h$ .

## 2.2 CPI Plots

The generated CPI plots, or petrophysical result displays, deal primarily with the reservoir layers and the sand-rich formations of the Jurassic succession. CPI plots of 68 wells are compiled in a catalogue that has been uploaded onto the PETSYS Website (see “WELLS” – “CPI files”). An example is shown in **Figure 2.1**. Each CPI plot includes the following information, if available:

- Lithostratigraphic subdivision of the Jurassic succession
- DeltaLogR curve.
  - *To connect to Total Organic Carbon (TOC)*
- Lithology interpretation; classic interpretation & GR/DT log facies, i.e.
  - Sandstones: High porosity (yellow), Medium porosity (light green), Low porosity (dark green)
  - Clays: High clay content (grey), Moderate clay content (dark brown), Low clay content (light brown).
- Porosity; log-derived porosities and core porosity data. The core data have also been used for calibrating the log-derived porosities.
- Hydrocarbon Saturation.
- Acoustic Impedance, i.e. log-derived using sonic and density logs.
  - *To connect to the seismic interpretation.*
- Sequence stratigraphic subdivision of the Jurassic succession
- Cored intervals, caliper logs, casing shoes
- Comments on depositional environment, diagenesis and permeability
  - *To link to geological aspects and permeability.*

The calculation of the DeltaLogR curve is described in Passey et al. (1990), and they suggest the following algorithm for determining DeltaLogR ( $\Delta\log\_R$ ) on the basis of a resistivity log and a sonic log:

$$\Delta\log\_R = \log_{10}(\text{Resistivity}/\text{Resistivity}_{\text{baseline}}) + 0.02 * (\text{Sonic}\Delta t - \text{Sonic}\Delta t_{\text{baseline}})$$

# HEJRE-2

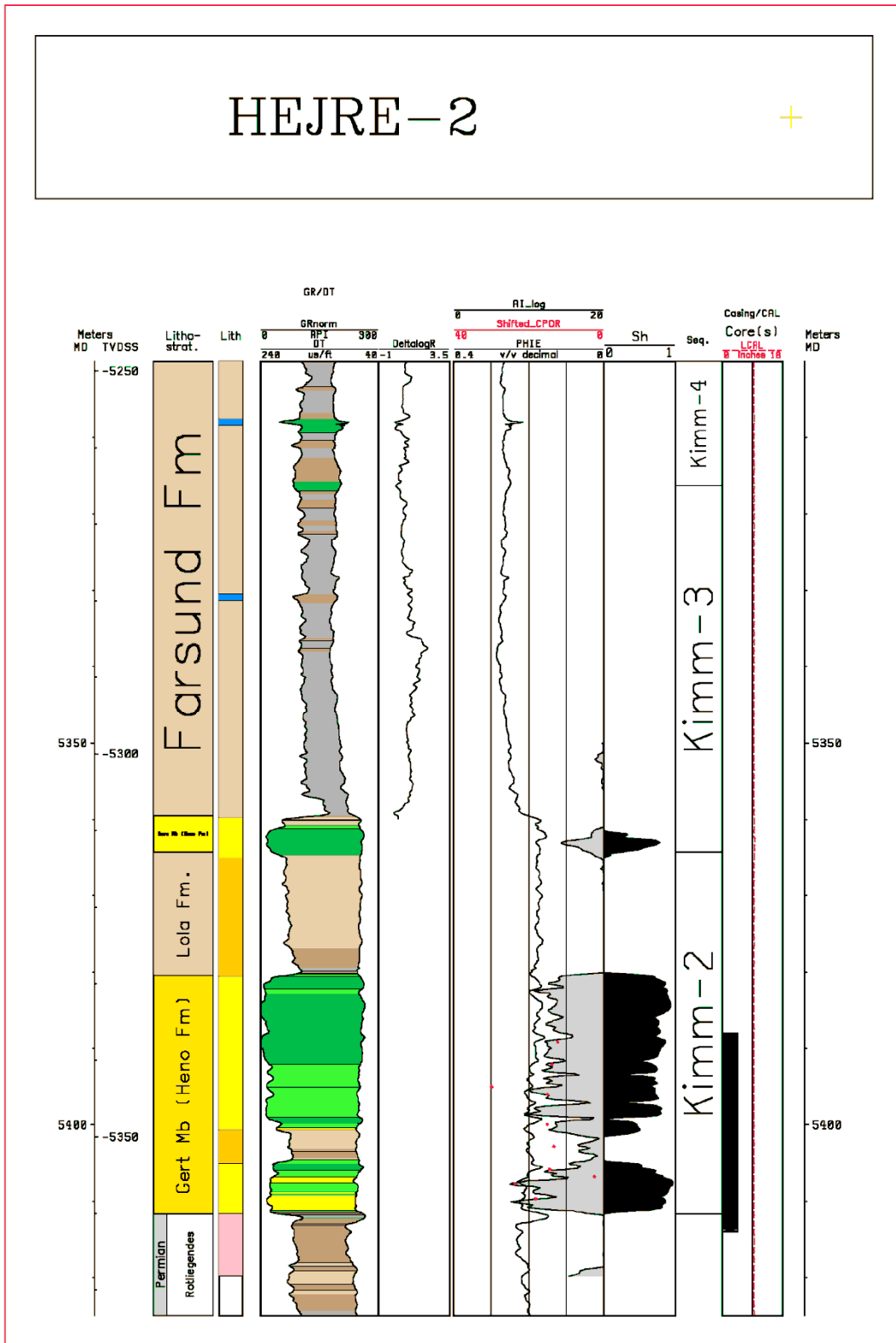


Figure 2.1: Example of an extended CPI plot prepared for this study. Stratigraphy, lithology, raw log curves, interpreted curves. Comments associated with plotted curves and cored intervals are given below. The GR/DT log facies are plotted in between the gamma-ray and sonic logs.

Comments associated with the CPI plot presented in Figure 2.1:

**Depositional sand environments:**

Farsund Fm: Offshore gravity-flow

Ravn Mb: Shoreface

Gert Mb: Shoreface

**Petrography and diagenesis of cored section:**

Calcite cement (associated with shell debris), when present, results in very low porosity and permeability (< 5 %, < 0.1 mD)

Quartz cementation (stylolitization associated with micaceous rock fragments), in upper part of cored interval, results in medium porosity and low permeability (10 – 15 %, 0.1 -1 mD)

Early zeolite cement (associated with volcanic rock fragments), in lower part of cored interval, are inferred to result in high porosity and medium-high permeability (20 -25 %, 10 - 300 mD).

**Qemscan analyses of cored sections:**

Illitic clay content (up to 6%)

Calcite (up to 59%)

In general, the comments associated with the plotted log curves etc. in the CPI catalogue deal with:

- Deposition sand environments, e.g. offshore gravity-flow, shoreface, back-barrier etc.
- Petrography and diagenesis of cored sections, including information about cementation, cements, quartz overgrowths, dissolution leading to secondary porosity, illite coatings etc. The diagenetic development is linked to porosity and permeability, if possible.
- Results of the qemscan analyses of cores sections (e.g. clay content, calcite percentage)
- Results extracted from Neutron-Density cross-plots or lithology identification plots, providing information about the presence of calcite and dolomitic cements and lithologies other than sandstones.

## 2.3 LAS files

Apart from CPI plots, the result of the log interpretation is presented as LAS files, which list log-derived shale volume, porosity and saturation for each ½ ft. The LAS files have been uploaded onto the PETSYS Website (see “WELLS” – “LAS files”). The LAS files can fairly easily be downloaded from the Website and then uploaded into a company database.

## 2.4 Reservoir parameters

The interpreted log data form the basis for calculating reservoir parameters for each lithostratigraphic unit, i.e. tops, unit thickness, gross sand thickness, net sand thickness, average porosity, shale volume and net-to-gross ratio. These parameters are listed in two excel spread sheets, applying a 30% Vshale cut-off along with 0% (no) porosity cut-off and 12% porosity cut-off, respectively. In case of no porosity cut-off, the net sand thickness equals the gross sand thickness.

The net-to-gross ratio is herein defined as net sand thickness divided by unit thickness. The basic unit for calculating these parameters in each well is the lithostratigraphic unit sub-division, which was updated and revised during the study period as a consequence of the establishment of a new seismo-stratigraphic framework. These point data can be plotted interactively on maps using the “Map” button on the PETSYS Website, and then pressing “Map Data” – followed by “Log-derived Sand Thickness”. The two Excel files, which list the basic data, are also stored in this folder; press the “description” button for accessing data sheets and legend.

The tables and maps are related to the following lithostratigraphic units set up for the Jurassic succession:

- Poul Mb,
- Outer Rough Sand,
- Ravn Mb,
- Gert Mb,
- Middle Graben Fm,
- Lulu Fm and
- Bryne Fm

In summary, the reservoir parameters can be **plotted as point data** on maps, or the parameters can be **exported as Excel files** directly from the PETSYS Website (refer to the description section). The database includes: unit thickness, net sand thickness based on 12% porosity cut-off, gross sand thickness corresponding to net sand thickness at 0% porosity cut-off, along with matching porosities, shale volumes and net-to-gross ratios.

## 2.5 GR/DT log facies

The GR/DT log facies illustrates the distribution of sandstone relative to porosity along with the clay content in a particular formation relative to GR response. The sandstone facies are subdivided into 3 classes (tight, porous, and very porous sandstone) and similarly, the claystones are also subdivided into 3 classes (**Figure 2.2**). The classification of the sandstones is more or less based on porosities derived from the sonic log, and it should be noted that the sonic porosities may deviate from porosities derived from a petrophysical evaluation based on neutron-density logs.

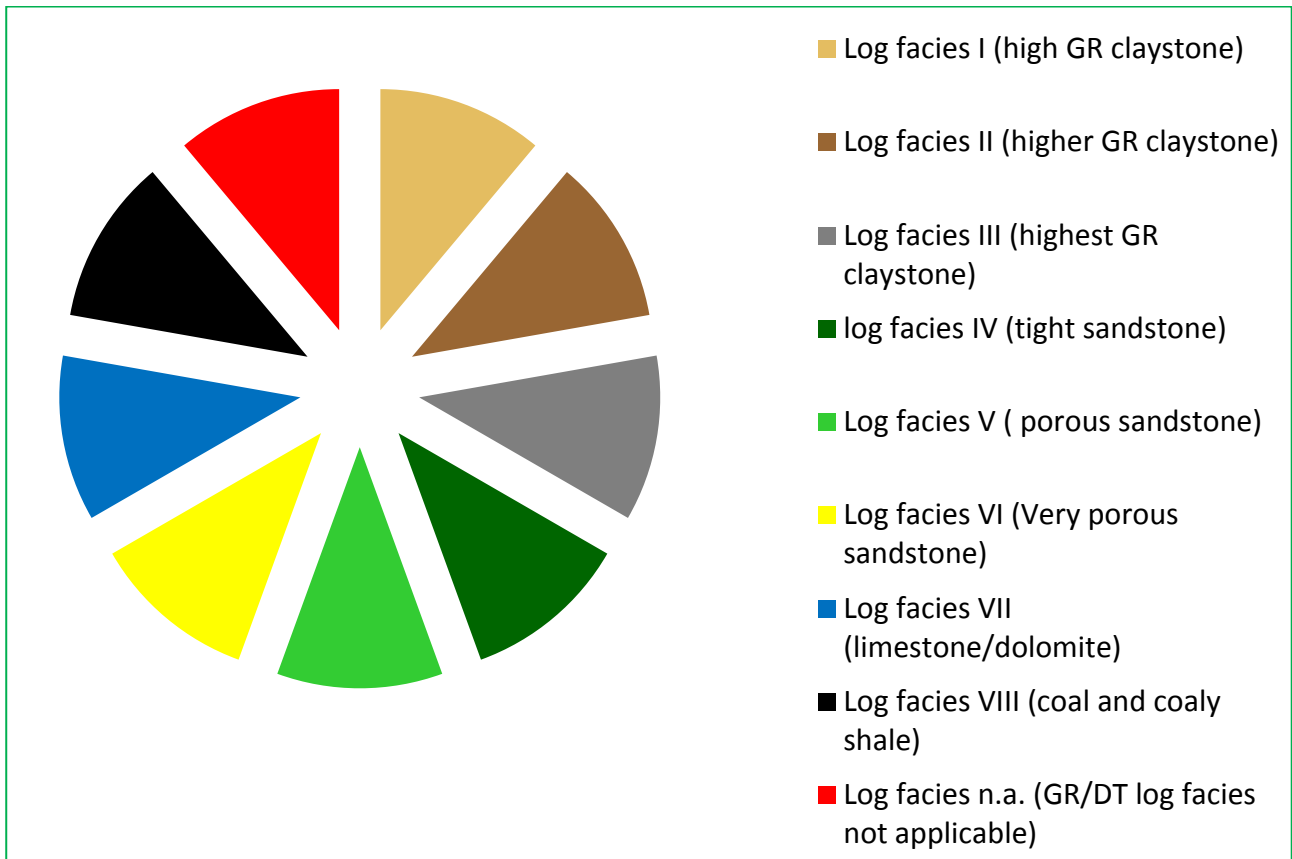


Figure 2.2: The various log facies, classes, and colour coding. GR/DT log facies analysis.

For a particular well, the GR/DT logs (log facies) were prepared on the basis of sonic and gamma-ray logs. Firstly, a normalized GR log is generated and two GRnorm baselines are introduced as described in the text box below (part 1). Secondly, the sandstone log facies are defined on the basis of low GR response combined with two sonic (DT) baselines (also described below; part 2).

- **Preparation of GR/DT log facies, part 1:**
- The lithological interpretation tool in Landmark-Stratworks is used to analyse the GR and DT log responses
- A normalized GR curve in each well is prepared, i.e. GRnorm
- For each well three GRnorm-Base Line values are calculated from the GRnorm-minimum and maximum values.
- The minimum value is most important, because ideally, it should separate sandstone from more clay-rich lithologies. It is picked in sandy intervals (cf. completion report/mudlog). We term this line GRnorm 1
- Pick the highest value in intervals with the highest gamma response. We term this line GRnorm 3
- Pick the middle value in an intermediate GRnorm position. We term this line GRnorm 2
- Log responses to the right of GRnorm 1, 2 and 3, respectively, delineate claystones with high-GR, higher-GR and highest-GR responses. They are termed log facies I, II and III
- 
- **Preparation of GR/DT log facies, part 2:**
- Two DT-Base Line values are used to divide the sandstone intervals into three porosity classes, i.e. tight, porous and very porous
- Fix a baseline for DT at a value of 70. We term this baseline DT 1
- Fix a baseline for DT at a value of 81. We term this baseline DT 2
- Find an area where the sonic response is located to the right of DT 1. This is termed log facies IV, i.e. tight sandstone
- Find an area where the sonic response is located to the right of DT 2. This is termed log facies V, i.e. porous sandstone
- Find an area where the sonic response is located to the left of DT 2. This is termed log facies VI, i.e. very porous sandstone
- Sections where the GRnorm response is lower than GRnorm 1 and where the sonic response is higher than DT 2 or even DT 1 is marked as limestone/dolomite and termed log facies VII
- Sections where the density response is very low and DeltalogR is high is marked as coaly shale/coal and termed log facies VIII
- Sections where GR/DT logs cannot be prepared due to missing logs or poor log quality are termed log facies n.a. (not applicable)
- The log facies and their corresponding colour codes are shown in Figure 2.2.

## 2.6 Quantification of GR/DT log facies

For a particular well, the thickness of the tight, porous, and very porous sandstone facies, along with thicknesses of the remaining GR/DT log facies, can be extracted from the PETSYS Website using the “Map button” from the main menu, followed by:

- Go To “Map data” (folder)
- Select ‘Log facies vs stratigraphic units’
- Select ‘Sequence stratigraphic unit’
- Press ‘Update map’, and for **each well**, a pie diagram with the %-distribution of the various log facies is plotted. In addition, 3 numbers (x, y, z) appear below each pie-diagram; these (x, y, z) data refer to the amount of tight, porous and very porous sandstone, respectively, that is present in a particular sequence. The unit is **metres**. Note that the sand-bearing units correspond to log facies IV–VI.

- Use the cursor to select a particular well located on the map, and one well-specific pie-diagram appears along with a text box listing the thickness (in metres) of all individual log facies present in the well.
- For the well in question, press “See all well data for well”, forwarding to ‘the GR/DT log facies vs. sequence stratigraphy’ folder in the PETSYS database. For **each sequence**, a pie diagram with the %-distribution of the various log facies is plotted along with a text box listing the thickness of each facies in %.
- Go to bottommost part of the window for displaying thickness data **in metres**
- For each sequence in a particular well, the thicknesses of the various log facies (I–VIII) are tabulated. These thickness data can be exported to Excel files.

**Similarly for mapping “sand vs. Clay” data; again, press the “MAP” button followed by:**

- Go To “Map data” (folder)
- Select ‘Sand vs. Clay’
- Select ‘Sequence stratigraphic unit’
- Press “Update map”. For **each well**, a pie diagram with the %-distribution of “sand/ clay/ other” is plotted the specified sequenc stratigraphic unit along with the sandstone thickness in metres (listed in brackets below pies).
- Use the cursor to select a particular well located on the map,
- For the well in question, press “See all well data for well”, forwarding to ‘the GR/DT log facies vs. sequence stratigraphy’ folder in the PETSYS database. For **each sequence**, a pie diagram with the thickness distributions of “sand/clay/other” is plotted along with a text box listing thicknesses in metres.
- Go to bottommost part of the window for displaying thickness data **in metres**
- For each sequence in a particular well, the thicknesses of the various log facies (I–VIII) are tabulated. These thickness data can be exported to Excel files.

## 2.7 Porosity considerations

The log facies dealing with sandstones are log facies IV-VI as defined in Figure 2.2. Estimates on corresponding porosities are listed below:

Log facies IV, Tight Sandstone, dark green, characterized by a sonic porosity < c. 10%

Log facies V, Porous Sandstone, light green, characterized by a sonic porosity in the range c. 10–15%

Log facies VI, Very Porous Sandstone, yellow, characterized by a sonic porosity > c. 15%.

## 2.8 Porosity-permeability plots

A number of porosity-permeability plots have been constructed on the basis of core analysis data from relevant wells. Press the “Porosity-Permeability Relations” button for getting access (under ‘Wells’ in the main menu). The plots are connected to the current lithostratigraphic subdivision



that result from the PETSYS Study work, and deals with the following formations and units: Bryne Fm., Lulu Fm, Heno Fm (Ravn and Gert Members), and Outer Rough Sand. For each unit, an attempt to correlate porosity and permeability has been made, and a trend line - or a reference line - is suggested.

## **2.9 Database with core analysis data**

Furthermore, histograms of conventional core analysis data are available from the PETSYS Website. These plots encompass porosity, permeability and grain density measurements plotted for each drill core in a particular well. In addition, more core analysis data that are related to a specific lithostratigraphic unit, are plotted together (combined plots). Press the “Core analysis” button (under ‘Wells’ of ‘Lab. Datasets’) to get access to the plots dealing with core analysis data originating from selected wells penetrating the Jurassic succession.

## **2.10 Reference**

Passey, Q.R., Creaney, S., Kulla, J.B., Moretti, F.J. & Stroud, J.D. 1990: A practical model for organic richness from porosity and resistivity logs. AAPG Bulletin, V. 74, No. 12, pp 1777-1794.



### 3 Stratigraphy and depositional environments

The stratigraphic frame established within the PETSYS project for the Jurassic succession in the Danish Central Graben area consists of combined and integrated lithostratigraphic, biostratigraphic, sequence stratigraphic, chemostratigraphic and seismic studies. The databases, concepts and methods used for the first four studies are presented below, while the seismic study are presented elsewhere (“Technical notes” – “Regional seismic interpretation and mapping”). Picks with depths (measured depth) to all stratigraphic surfaces and to bioevents for each well can be downloaded from the PETSYS Website (“Picks”). The integration between the stratigraphic disciplines is presented in a “Chronostratigraphic Chart” (Figure 3.1). The chart can be downloaded from the PETSYS Website (“Stratigraphy”).

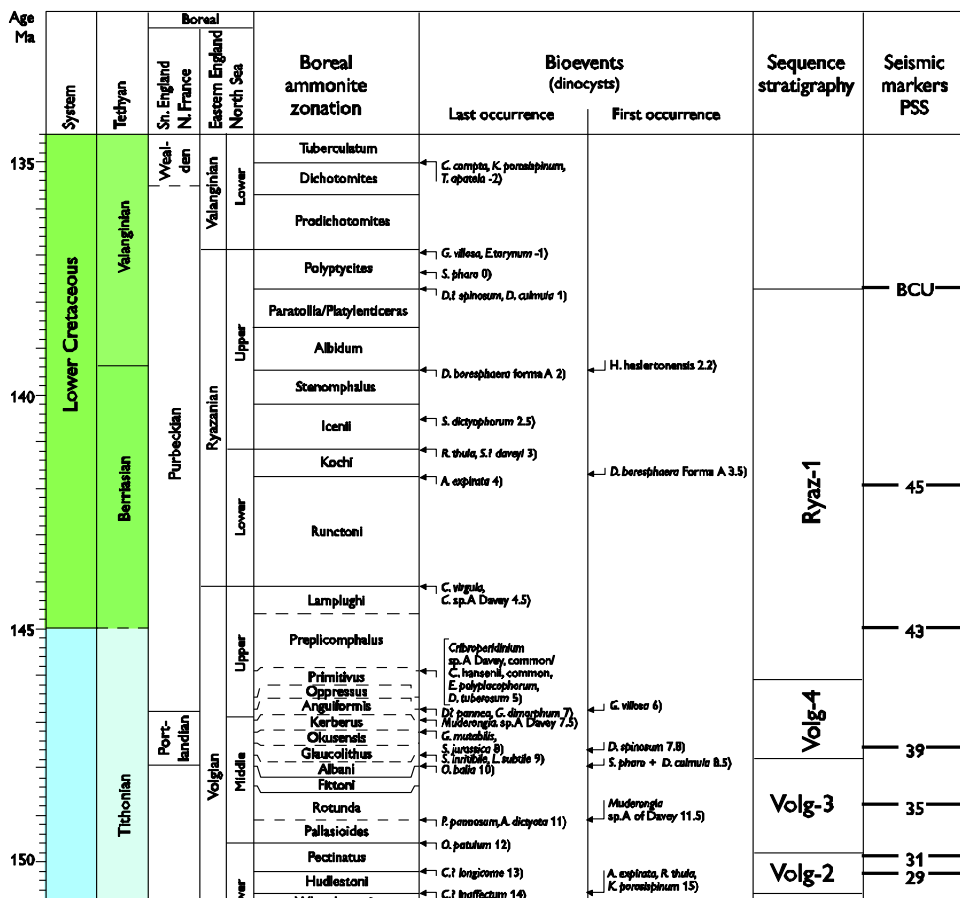


Fig.3.1. Part of the Chronostratigraphic Chart which integrates the chronostratigraphy, biostratigraphy, sequence stratigraphy and the seismic markers. The correlations between bioevents and chronostratigraphy are based on; Costa & Davey (1992), Davey (1982), Dybkjær (1998), Heilmann-Clausen (1987), Herngreen et al. (2000); Ineson et al. (2003); Poulsen (1996); Poulsen & Riding (2003), Riding & Thomas (1992) and Abbink et al. (2012).

#### 3.1 Lithostratigraphy

##### Database

The interpretation of the lithology in the 87 wells included in the PETSYS project is based on Gamma- and Sonic logpatterns and on information from Completion Reports. The locations of the wells are shown in Figure 3.2. Cored intervals gave invaluable information about lithology,

depositional environments and chemical composition. In addition, lithology interpretations based on a GR/DT log facies study was included (see "Technical Note" - "Log interpretation").

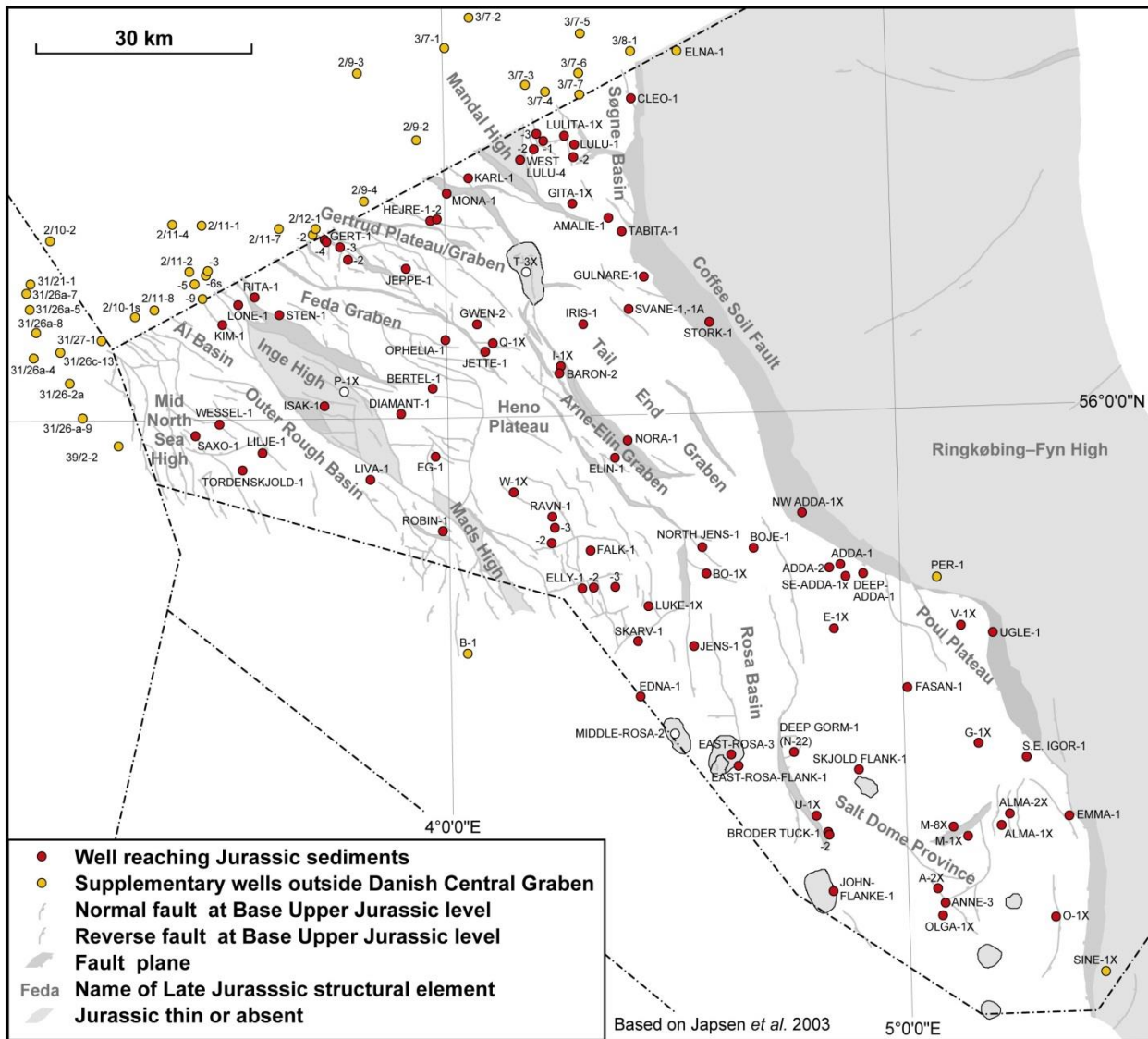


Fig. 3.2. Map of the Danish Central Graben showing the structural elements and the position of wells (red dots) penetrating Jurassic deposits. Faults at Base Upper Jurassic level. Structural elements are based on Japsen *et al.* (2003).

### Approach

All lithostratigraphic formations and members used in the project are illustrated in a simplified scheme for the whole Danish Central Graben (Figure 3.3). The lithostratigraphic subdivision follows generally the lithostratigraphy of Michelsen *et al.* (2003) for the Danish Central Graben. No new lithostratigraphic units have been defined formally in the PETSYS project, but the informal unit, "Outer Rough Sand", is used for the shallow marine, Lower Volgian, sand present in the Outer Rough Basin. The lithostratigraphic scheme can also be downloaded from the PETSYS Website ("Stratigraphy").

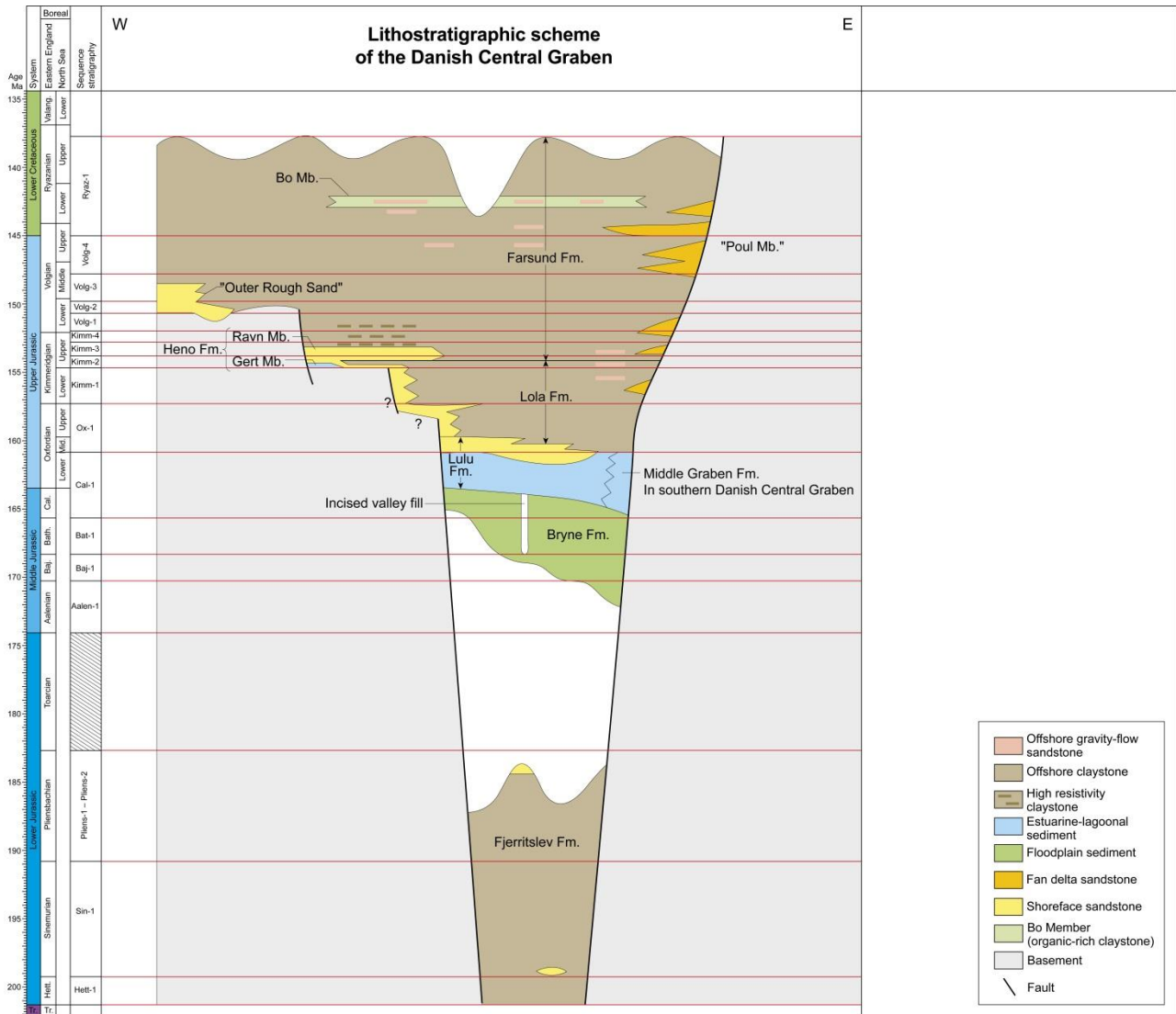


Fig. 3.3. Lithostratigraphic units used in the PETSYS project, correlated with sequence stratigraphy and chronostratigraphy.

In some wells it was possible to interpret the Rhaetian Winterton Formation below the Lower Jurassic Fjerritslev Formation. Otherwise, the lithological units underlying the Jurassic succession have not been referred to lithostratigraphic units.

The Fjerritslev Formation is only present in a few wells located in the Salt Dome Province. However, the distribution of this shallow marine claystone is thought to have been much larger. Reworked clayclasts containing Lower Jurassic palynomorphs were found in Upper Kimmeridgian cores from the Gwen-2 well (see Johannessen et al. 1996).

The Middle Jurassic fluvio-deltaic lithostratigraphic units, the Bryne, Middle Graben and Lulu formations, are separated on the basis of the depositional environment and their geographical occurrence within the study area, see further Andsberg (2003) and Michelsen et al. (2003).

The boundary between the clayey Lola and Farsund formations is defined in the U-1 well. In wells located in the deep parts of the basin, this boundary correlates with the MFS Kimm-2. In wells

located in more shallow marine/plateau areas, with Ravn Member (Heno Formation) sandstone present, the base of the Farsund Formation is located at the top of the Ravn Member, while MFS Kimm-2 is interpreted to occur within the Ravn Member (see examples on the PetSys Website: "Sections" - "Log correlation profiles", profiles 6 and -8). The seismic marker PSS\_13 (= "near top Lola") correlates in wells from the deeper parts of the basin generally to MFS Kimm-2. In wells located more shallow, on the Heno and Gertrud Plateaus, this seismic marker is registered as the transition downwards in the wells from the sandy Ravn Member to the shaly Lola Formation. In this way PSS\_13 is not synchronous from the shallow to the deeper parts of the basin, but is found "too deep" in the shallow areas.

The lowermost member of the sandy Heno Formation, the transgressive Gert Member, occurs only in the southern Feda Graben/northern Heno Plateau/Gertrud Plateau area and consists of back-barrier deposits overlain by back-stepping shoreface sandstones. In this area the shoreface sandstone referred to the Ravn Member is represented by one progradational-retrogradational unit. In the southern parts of the Heno Plateau area, Gert Member is not present, while two progradational-retrogradational units occur which both are referred to the Ravn Member as they both consist of shoreface sandstone. Thin transgressive sandstone intervals within the Lola Formation, e.g. in Falk-1, have not been referred to separate lithostratigraphic units.

The results from the chemostratigraphic study turned out to be very useful in distinguishing between the Lola and Farsund formations, and between the Gert and Ravn members of the Heno Formation, see also Weibel et al. (2010).

The Lower Volgian sandstones deposited in the Outer Rough Basin are referred to the informal unit "Outer Rough Sand".

The gravity-flow sandstones of different ages occurring in deeper marine settings, e.g. in Svane-1, Amalie-1, Iris-1 and Jeppe-1 are not referred to separate lithostratigraphic units. The Upper Kimmeridgian gravity flow sandstones present e.g. in the deepest part of the Svane-1 well and in Amalie-1 is interpreted to be timeequivalent with the Ravn Member.

The Poul Formation (Michelsen et al. 2003) is here renamed as "Poul Member" as the geographical distribution of these sandstones seems to be limited and the sandstones occur as isolated lobes along the Coffee Soil Fault. The sandstones referred to the Vyl Formation by Jensen et al. (1986), occurring in the V-1 well, are here included in the "Poul Member" as they overlap stratigraphically and probably represent the same depositional environment (gravity-flow sandstones). "Poul Member", as used here, is dated as Middle Volgian to Ryazanian.

Bo Member (= the informal "Hot Unit", Jensen et al. 1986) represents a very organic rich interval in the uppermost Jurassic to lowermost Cretaceous part of the succession (Ineson et al., 2003). Bo Member correlates with the upper part of the Mandal Formation (Vollset and Doré, 1984) defined in the Norwegian Sector (Dybkjær 1998).

The boundary between the Farsund Formation and the Cromer Knoll Group is in some wells not easily defined based on log-patterns. The occurrence of sand and marl in the Cromer Knoll Group was used as additional criteria for locating this boundary.

## Data quality

The quality of the gamma- and sonic logs used for the lithostratigraphic subdivision is variable from well to well and in some occasions also from one part of the studied succession to another (from one log-run to another). In intervals where the logpattern is obscured due to a casing, the lithology interpretation is based solely on informations from the Completion Report.

### *3.2 Bio- and chronostratigraphy*

#### Database

Biostratigraphic data from 87 wells are included in the project. These are all the non-confidential wells which penetrate parts of the Jurassic succession. The biostratigraphic data used for dating and correlation of the Jurassic succession are restricted to palynological data. Palynomorphs are the microfossil-group, which is used by far the most service companies for the Jurassic within the North Sea Basin. In a few wells no palynological data is available for the Jurassic succession. The biostratigraphic database comprises all published data, all existing consultant reports and in addition all relevant inhouse GEUS data from the 87 wells.

#### Selection of bioevents and chronostratigraphy

A series of stratigraphically usefull bioevents (first occurrence, last occurrence and abundance variations of palynomorph species or genera) were selected for correlation between the wells. The selected bioevents are those used by most service companies and which can be correlated with the standard ammonite zonation and thus with chronostratigraphy, see the "Chronostratigraphic Chart" (Figure 3.1). The correlations between bioevents and chronostratigraphy are based on published studies from onshore England; the references are listed in the figure text and included in the reference list. The timescale used is that of Gradstein et al. (2012). Stipled arrows indicate that the bioevent in question is not tied directly to the standard ammonite biozones. In order to facilitate communication within the project group and to include the bioevents in the Stratwork log-correlation tool, every bioevent is provided with a specific number. The lowest numbers correspond to the stratigraphically youngest bioevents and increase with increasing ages. In this chart the integration between the biostratigraphy, the sequences and the seismic markers defined in the PETSYS project is shown and correlated with the chronostratigraphy.

The bioevents for each well are included in the "Stratigraphic Summary Charts" (Figure 3.5). In these summary charts, which can be downloaded from the PETSYS Website ("Stratigraphy" - "Stratigraphic Summary Charts") also additional information, such as occurrences of taxa which may have a stratigraphic potential, but is not recognized in other wells, are included. In the "Stratigraphic Summary Charts" the depth of the sample in which either the "Top" or "Base" occurrence of a specific biostratigraphic taxa are shown, while in the "Picks-database" in the Website "Top" is indicated as "First" (corresponding to "First downhole occurrence") and "Base" is indicated as "Last" (corresponding to "Last downhole occurrence").

Bioevents recorded from core-samples may have one depth in the "picks-database" and occur with another depth in the "Stratigraphic Summary Chart". This difference in depth for the same bioevent

occurs in cores for which the core depth has been shifted relative to the logs. For example is the depth for the bioevent "Base of *Dichadogonyaulax? pannea*" = 12593.58' in the Stratigraphic Summary Chart for Diamant-1, while the depth for the same bioevent is indicated as 12579' in the "picks database" for Diamant-1. The core has been shifted appr. 14' (4 m) downwards.

To support the correlations between the palynological data and the chronostratigraphy, ammonites found in corepieces from the NW Adda-1XA well and from the Elly-3 well, have been studied (Alsen, 2014a, b).



Fig. 3.4. Photo of ammonites from a corepiece from the NW Adda-1XA well.

## Approach

The biostratigraphic data was used in guiding the seismic interpretation. Both the seismic markers and the bioevents (as numbers) were uploaded in the StratWorks log-correlation tool and were used for guiding the sequence stratigraphic correlation between the wells.

## Data quality

Due to caving the last occurrences of specific bioevents are sometimes found "too low", in relation to where we would expect to find them (e.g. indicated by crossing well-defined seismic markers between wells). Reworking has also been recorded, especially in deposits immediately above a major unconformity, in the "transgressive lag deposits" and in wells located close to major faults, e.g. the Coffee Soil Fault. In addition, increasing degradation of the palynomorphs with depth is an obvious problem within the dataset.



## Abbreviations

The following abbreviations have been used in the Stratigraphic Summary Charts:

Rew: Presumed reworked

T.p.: Triassic palynomorphs recorded

P.p.: Permian palynomorphs recorded

C.p.: Carboniferous palynomorphs recorded

C: Presumed caved

Occ.: Occurrence of the taxa in question

Ufo: Uncertain first occurrence

Questionable identification to species is indicated by a questionmark before the genus name, e.g. *?Scriniodinium crystallinum*. In some cases the genus-name is followed by a questionmark, e.g. *Corculodinium? inaffecta* or *C.? inaffecta*. In this case the questionmark relates to the taxonomy - whether the species should be referred to this genus or to another genus.

### 3.3 Sequence stratigraphy

#### Background and sequence stratigraphic concept

The sequence stratigraphic interpretations takes offset from the well-based study of Andsbjerg & Dybkjær (2003). The number of sequences within the Jurassic succession is generally the same, except for a few changes (Hett-2 and Ox-2 have been excluded in the PETSYS Project, due to different interpretation and correlation) and the dating of the individual sequences is almost the same – in both cases based on the palynological data. However, in contrast to the study by Andsbjerg & Dybkjær (2003), the PETSYS sequence stratigraphic study is strongly guided by a robust, regional seismic study, providing an overall stratigraphic frame and, in addition, information about e.g. unconformities, condensed/expanded parts of the succession and fault-planes obscuring the log-patterns in various wells. Furthermore, the PETSYS project includes many new wells and also some older wells, which were not included in the study by Andsbjerg & Dybkjær (2003). The latter study included about 50 wells while the PETSYS project includes 87 wells.

The sequence stratigraphic concept applied in the present study is that of the Exxon group (Posamentier et al. 1988; Posamentier & Vail 1988; Van Wagoner et al. 1988; 1990). Each sequence is confined by a lower and an upper sequence boundary (SB) and is subdivided into a transgressive systems tract (TST) and a highstand systemtract (HST). The two systemtracts are separated by a maximum flooding surface (MFS).

## Methods

The sequence stratigraphic interpretations were carried out using the StratWorks (Landmark) log-correlation tool. The subdivision into sequences and systems tracts is based on variations in lithology, interpreted mainly from the gamma-ray logs, but supported by the sonic logs. Information about lithologies was also taken from the Completion Reports. In addition, lithology interpretations based on a combined GR/DT-study was included - the method for this study is described a Technical Note found at the PETSYS Website ("Technical Notes" - "Log interpretation". Caliper logs, neutron-density logs and resistivity logs were also included in the template in order to give information about hole-quality (caliper), and to support the correlations between wells, based on log-patterns. In some areas, on the Heno and Gertrud Plateaus, the resistivity log turned out to be very usefull for detailed correlation.

Key surfaces such as sequence boundaries and maximum flooding surfaces have been correlated between wells from platform areas characterized by upward coarsening shoreface sandstones out in the deep parts of the basin dominated by offshore claystones. In such cases the sequence boundary is placed at maximum regression of the shoreface sandstones (the most coarse-grained sand or gravel) and correlated out into the offshore claystone in the basin and picked at the most "coarse-grained" part of an upward coarsening claystone succession. These correlations are guided by biostratigraphy and seismic surfaces. In areas with several stacked upward coarsening shoreface successions, a maximum flooding surface is placed at the most fine-grained interval, between the prograding shoreface sandstones.

In some areas in the deep part of the basins, an abrupt increase in grain-size from claystones to a succession characterized by inter-bedded sandstones and claystones is seen. This is the case in the northern part of the Tail End Graben (Svane-1 and Amalie-1 area). The sandstone beds are interpreted as deposited by sediment gravity-flow processes in an offshore environment. In such cases the sequence boundary is placed at the sharp based sandstone-claystone succession, inferring that these sediments were deposited during a fall in relative sea-level and probably followed by a relative rise in sea-level and therefore interpreted as a lowstand systems tract.

In non-marine sediments it is more difficult to carry out sequence stratigraphic interpretations and correlations, because it is more difficult to interpret changes in relative sea-level. An incised valley filled with estuarine sediments has been recognized in the Søgne Basin due to the high quality data: large amounts of cored intervals and the close position of wells (Andsbjerg 2003). Here a sequence boundary is placed at the base of the incised valley succession, because the incision of older sediments was caused by a fall in relative sea-level (Andsbjerg 2003; Andsbjerg and Dybkjær 2003).

The key surfaces, used for correlation between wells are the SB's and the MFS's. The SB's are located at the culmination of coarsening upwards trends, while MFS's are located where the gamma-ray values indicate the most finegrained lithologies. Thin carbonate beds are represented by low-value gamma-ray/high value sonic spikes. The location of the sequence stratigraphic surfaces and the correlations between wells, were guided by the biostratigraphic events and the seismic markers, both of which were included in the template used for the sequence stratigraphic study within the StratWorks log-correlation tool.

The Jurassic succession in the Danish Central Graben area has been subdivided into 18 sequences, named according to their ages, e.g. Kimm-1 for the oldest sequence referred to the Kimmeridgian. All sequences probably correspond to 3rd order sequences as defined by Vail et al. (1977) and Van Wagoner et al. (1990). However, due to variations in subsidence rate, the duration of the sequences recognised in the Lower and Middle Jurassic is somewhat longer than for the Upper Jurassic sequences. The overall correlation between the sequence stratigraphy, biostratigraphy, the seismic markers and the chronostratigraphy is presented in the Chronostratigraphic Chart (Figure 3.1). The two pliensbachian sequences, Pliens-1 and Pliens-2, are not separated in the chart, but shown as Pliens-1 - Pliens-2. This is because it is not possible based on the available biostratigraphy to correlate the sequence boundary SB Pliens-2 with the chronostratigraphy in detail.

For the individual wells, the correlation between the sequences, the lithostratigraphic units, the seismic markers, the bioevents and the chronostratigraphy is presented in the "Stratigraphic Summary Charts" (Figure 3.5). Summary Charts for 87 wells have been uploaded onto the PETSYS Website ("Stratigraphy" - "Stratigraphic Summary Charts").

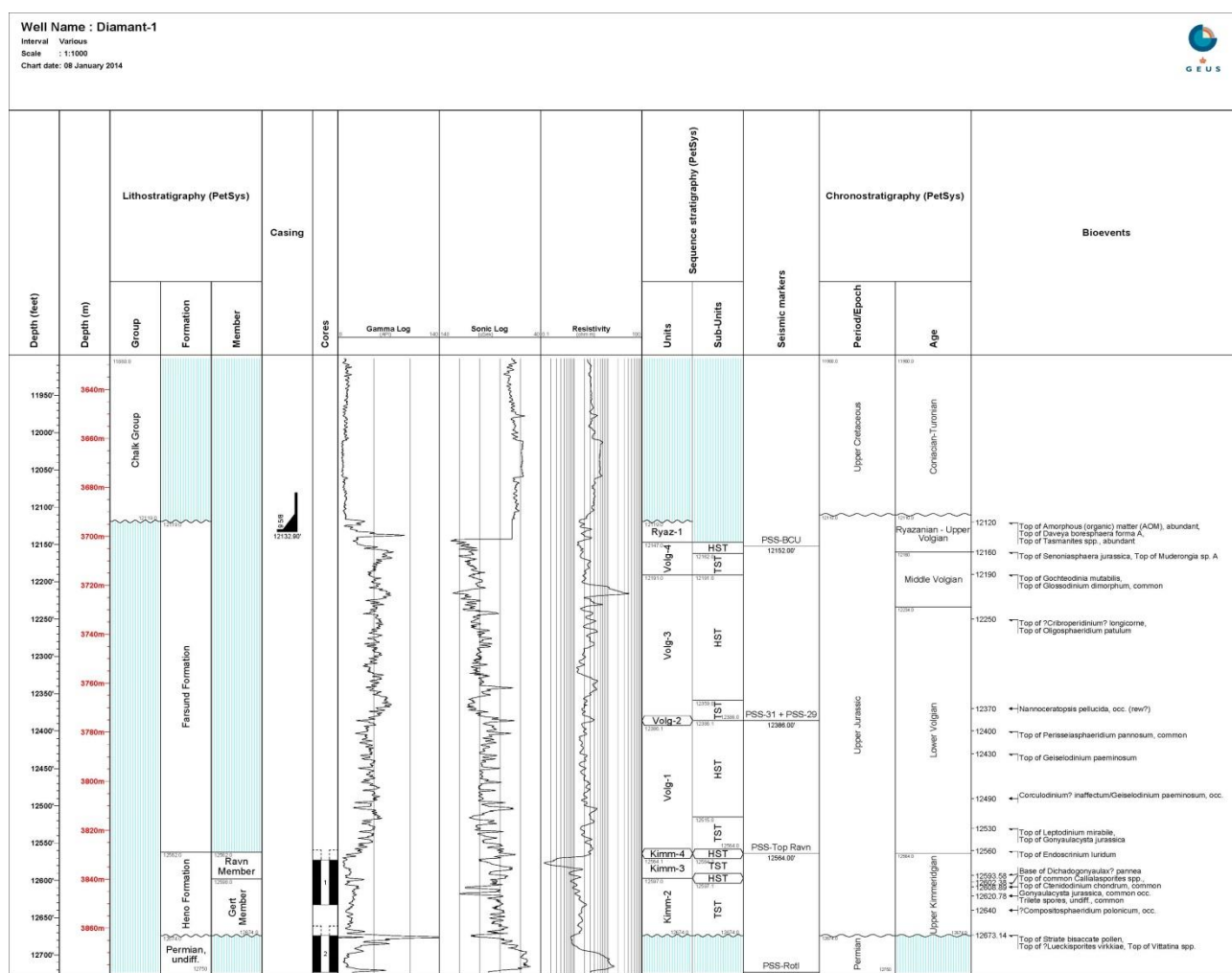


Fig.3.5. Example of a "Stratigraphic Summary Chart", here for the Diamant-1 well, showing the stratigraphy for the well (litho-, sequence and chronostratigraphy), the seismic markers and the bioevents. Furthermore, a gamma-log, sonic-log and restivity-log are shown together with the location of casings and cored intervals.

Eight log-correlation profiles have been produced, to show the distribution of the sequences in different parts of the study area and the correlation between them (Figure 3.6). The panels have been uploaded onto the PETSYS Website ("Sections" – "Log Correlation Profiles").

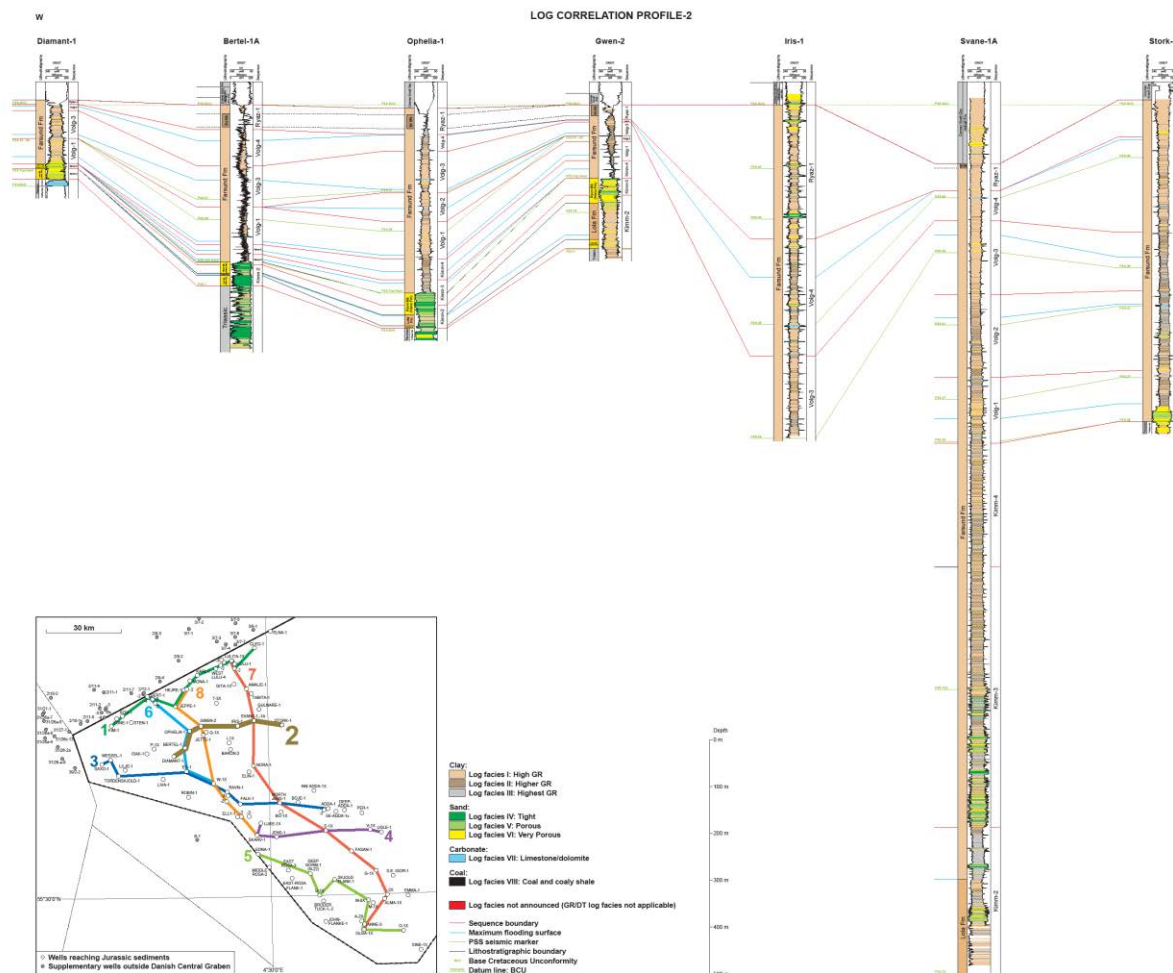


Fig.3.6. Example of a Log Correlation Profile. Profile 2 is shown here.

The depositional history for the studied succession is further illustrated by a series of 6 time stratigraphic panels (Figure 3.7). The panels illustrate the distribution of depositional environments through time (18 sequences) in different parts of the Danish Central Graben. Hiatuses are also presented on these panels. Each well in the panels shows the depositional environments in dark colors. Depositional environments between the wells are illustrated in light colors. The panels can be downloaded from the Website ("Sections" – "Time Stratigraphic Panels").

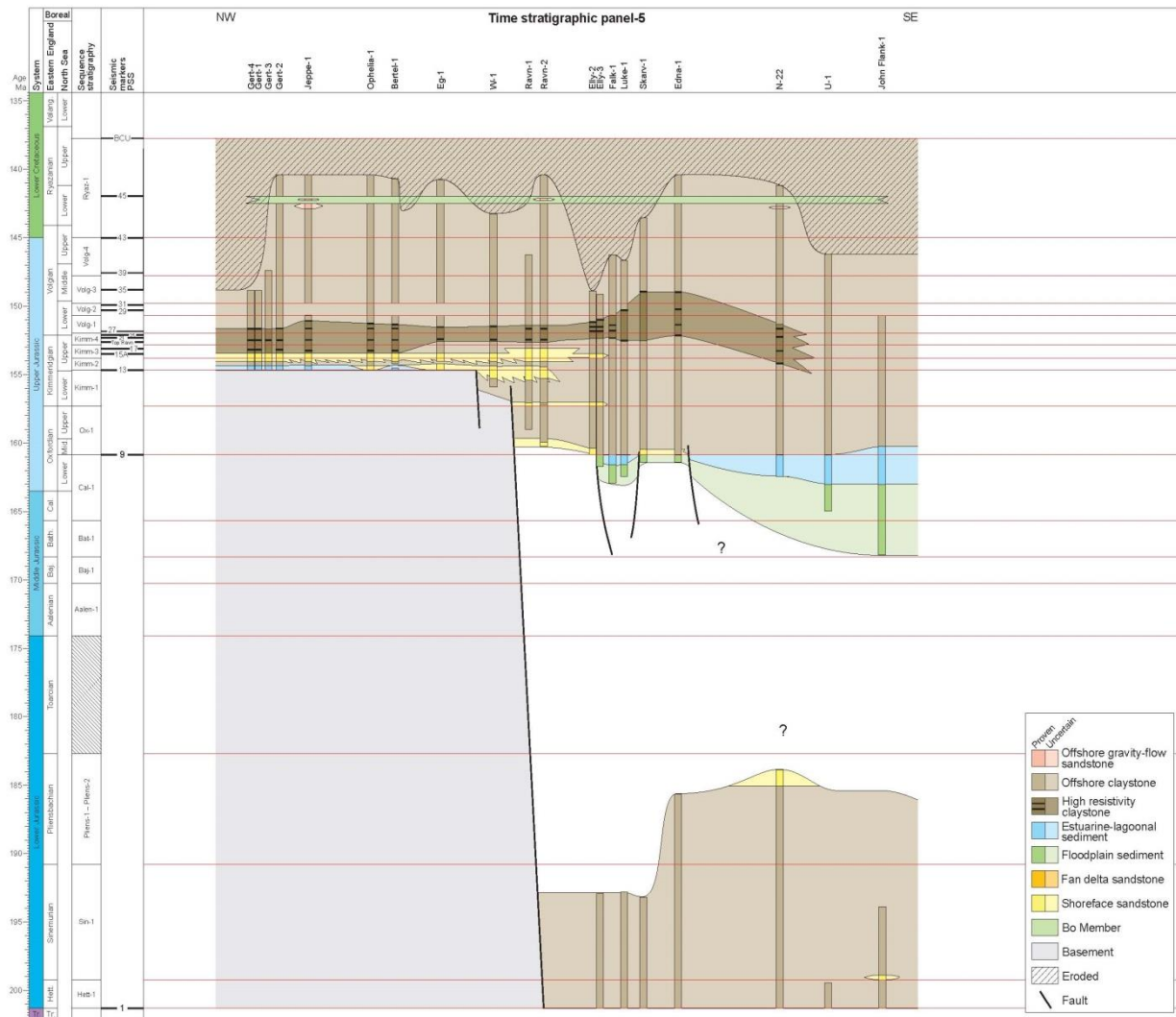


Fig. 3.7. Example of a Timestratigraphic Panel.

### Data quality

The quality of the logs used for the sequence stratigraphic interpretation varies between wells. Intervals with "bad hole" were identified using the caliper log. The location of casings was also included in the StratWorks template in order to guide the interpretation and to avoid to locate SB's in intervals contaminated by cement at casing points. Intervals representing fault planes, identified from the seismic data, were marked as a warning against overinterpretation in these intervals. In some wells the logging did not reach TD. In such cases, the sequence stratigraphic interpretation has been prolonged to TD in spite of the missing information from log-patterns.

### 3.4 Chemostratigraphy

#### Database

Chemostratigraphic investigations include cored intervals of the Heno Formation in 14 wells and cored intervals of gravity flow deposits from the Farsund Formation and the Cromer Knoll Group in 7 wells. Application of chemostratigraphy on cuttings samples has been attempted for 4 wells. On the PETSYS Website it is possible to make graphical comparison of oxides (major elements), elements (trace elements) or ratios versus measured depth (Figures 3.8 and 3.9) or versus other oxides or elements (Figure 3.10); and finally ternary plots of elements, oxides or ratios (Figure 3.11).

The chemostratigraphical dataset can be accessed by selecting “Wells” – “Chemostrat” or “Lab. Datasets” – “Chemostrat “ at the PETSYS Website. An additional feature, average fractions as pie diagrams for each well (Figure 3.12), is available at “Maps” - “Map data” - “Chemostratigraphy”.

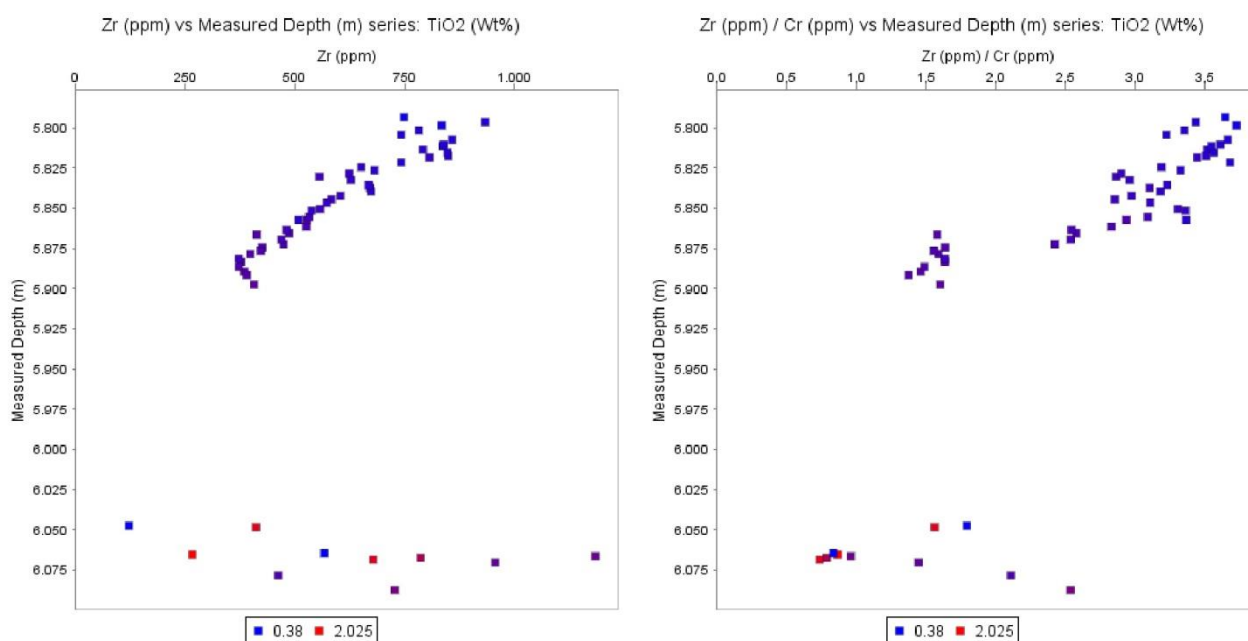


Fig.3.8. Example from PETSYS Website of element versus depth graphs, here illustrating Zr content and Zr/Cr ratio versus measured depth for the Gert-4 well; note each square is coloured according to  $\text{TiO}_2$  content.

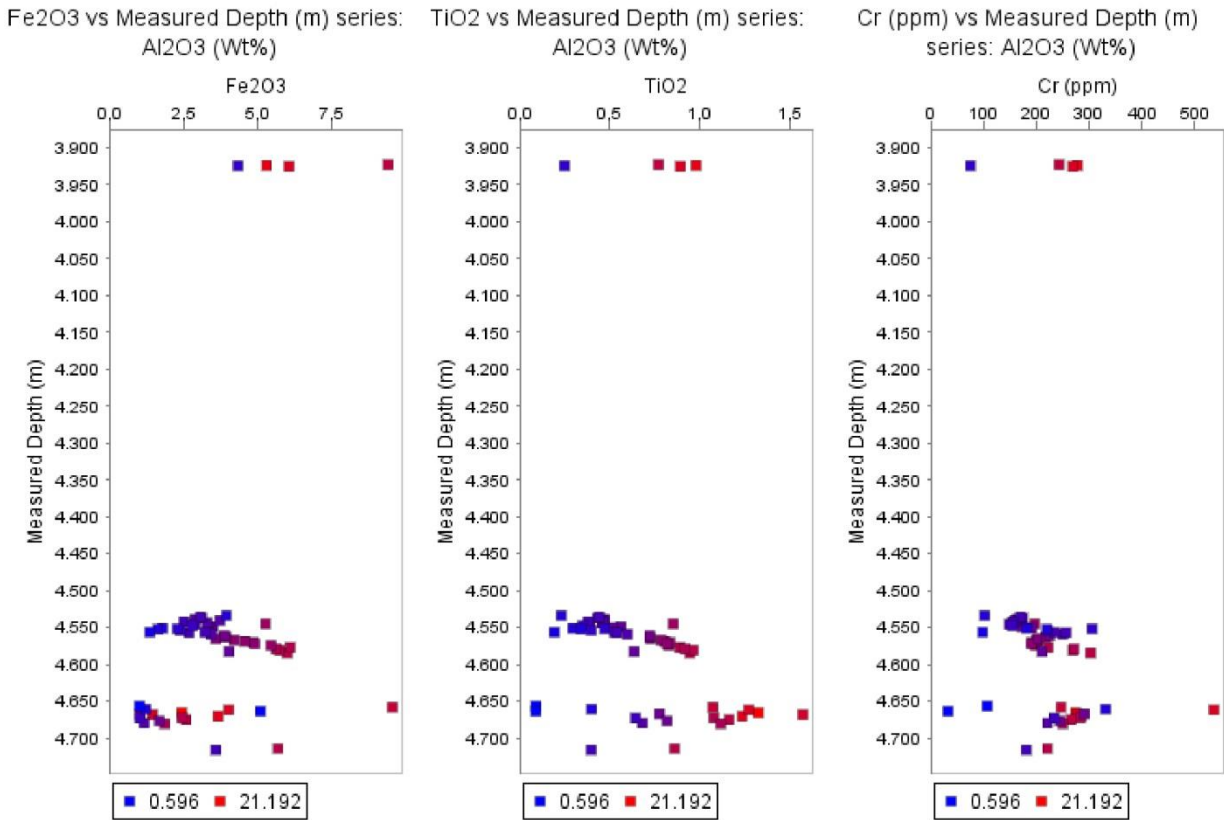


Fig. 3.9. Example from PETSYS Website of element versus depth list, here illustrating  $Fe_2O_3$ ,  $TiO_2$  and Cr versus measured depth for the Rita-1 well; note the colour of each square represent the  $Al_2O_3$  content.

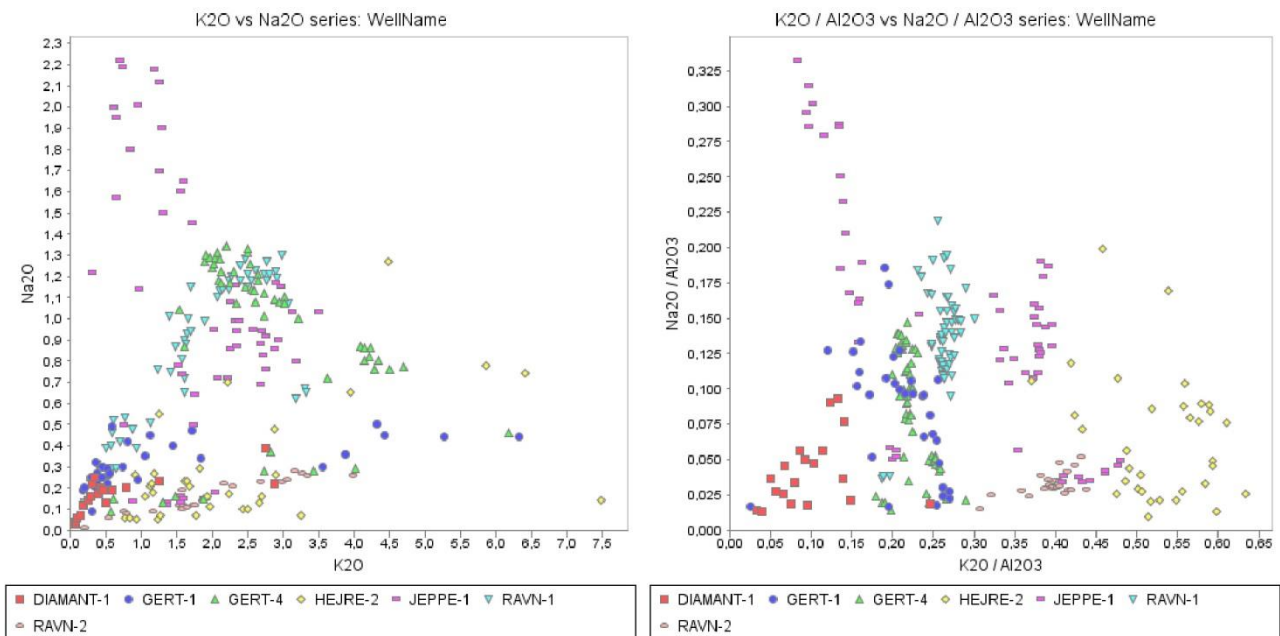


Fig. 3.10. Example from PETSYS Website of element versus element cross plots, here illustrating  $Na_2O$  versus  $K_2O$  and the  $Na_2O/Al_2O_3$  versus  $K_2O/Al_2O_3$  ratio; note each symbol represent one well.

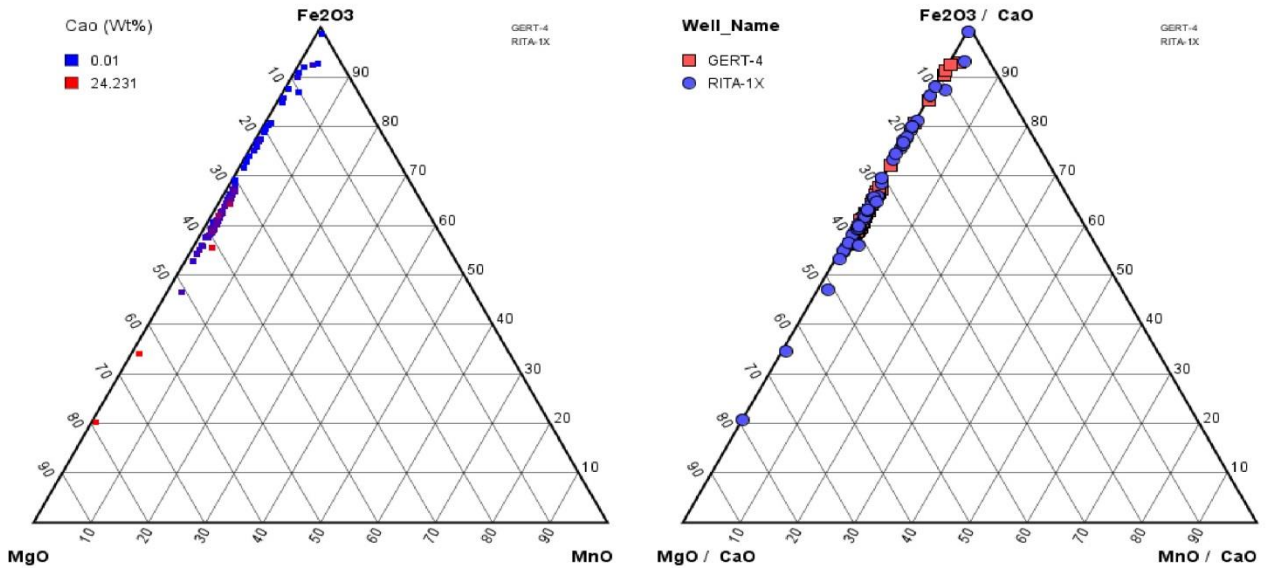


Fig. 3.11. Example from PETSYS Website of ternary plots, here illustrating Fe<sub>2</sub>O<sub>3</sub>, MgO and MnO relative proportions or the ratios of Fe<sub>2</sub>O<sub>3</sub>/CaO, MgO/CaO and MnO/CaO for the Gert-4 and Rita-1 wells. Note the symbol colour shows the relative CaO content in the left ternary plot, but the wells in the right ternary plot.

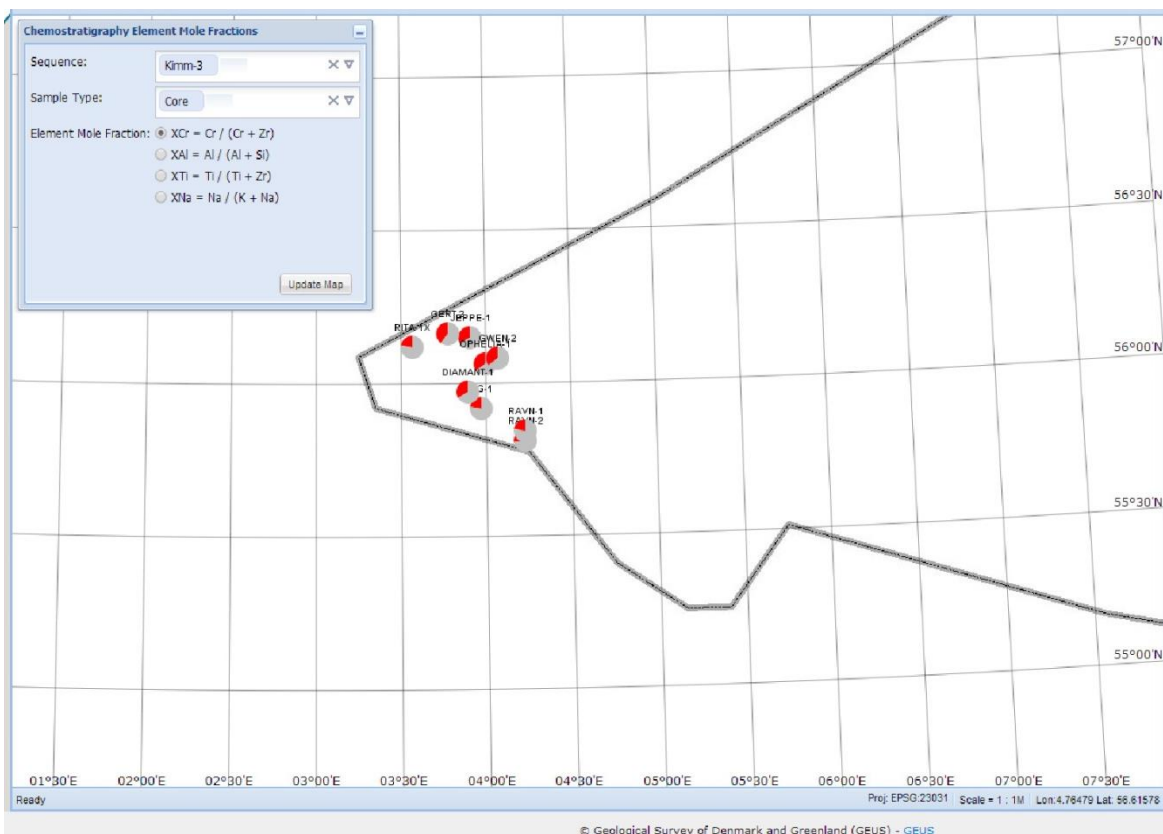


Fig. 3.12. Example from the PETSYS Website of a map showing the element mole fraction here Cr / (Cr + Zr) for the Kimm-3 sequence based on cored samples.



## Approach

The chemostratigraphical results are integrated with the lithostratigraphy and sequence stratigraphy. Cored sandstone samples can relatively easily be related to Ravn or Gert members, and cored mudstones can be related to the Farsund or Lola formations based on the approach given in a previous study (Weibel et al. 2010). Subdivision of the Heno Formation into Ravn Member and Gert Member has in particular been based on immobile elements assumed to be related to heavy minerals (e.g. Ti, P, Zr, Cr, Nb, Ce, La, Th, V, U) and less stable elements like Na, K and Al, which may reflect the variation in feldspar and clay mineral composition.

Cutting samples have been compared to the cored samples (which chemical composition is assumed to define each particular member/formation), and here it has been necessary to rely on the affinity of the cuttings samples for Ravn or Gert members or the Lola or Farsund formations for which reason the conclusions on the cuttings samples are more subtle.

## Methods

Core plugs were taken parallel to the bedding plane, and with a diameter of 1" (2.54 cm) and a length of approximately 3 - 5 cm. The cuttings samples were washed and dried. Samples were crushed in either wolfram-carbid or steel mortars. Geochemical analyses were performed at GEUS laboratory or at "Acme Labs".

At GEUS major elements were in general analysed by XRF (X-ray Fluorescence) and trace elements by ICP-MS (inductively coupled plasma - mass spectrometry). Contents of organic matter and volatiles were analysed by ignition (1 hour at 1000°C) of the powdered samples. Glass discs were prepared by fusing the ignited powder with sodium tetraborate and shaping it in Pt/Au moulds (Kystol and Larsen, 1999). The glass discs were analysed with a Phillips PW 1606 wavelength dispersive multi-channel XRF spectrometer equipped with a Rh-anode X-ray tube operated at 50 kV and 50 mA. Na<sub>2</sub>O and Cu were determined by atomic absorption spectrometry (AAS). Dried samples were treated with hydrofluoric acid; the residue, after evaporation, was dissolved in a hydrochloric acid – potassium chloride solution and measured on a Perkin Elmer PE2280 AAS instrument. Kystol and Larsen (1999) recommend detection limits for main elements (Si, Ti, Al, Fe, Mn, Mg, Ca, Na, K, P) varying from 0.01 wt% for P<sub>2</sub>O<sub>5</sub> to 0.3 wt% for SiO<sub>2</sub>. Trace elements (V, Cr, Ni, Zn, Rb, Sr, Nb with the exception of Ba, Y) are determined by XRF on reconnaissance basis at the > 50 ppm level (Kystol and Larsen 1999).

A piece of the glass disc was dissolved in a mixture of HCl and HNO<sub>3</sub>. The diluted solutions were sprayed, using a Meinhard nebulizer, into the argon carrier gas and analysed by the Perkin Elmer 6100 DRC quadrupole ICP-MS. The following elements were analysed: Ba, Ce, Co, Cr, Cs, Cu, Dy, Er, Eu, Ga, Gd, Hf, Ho, La, Lu, Mn, Nb, Nd, Ni, Pb, Pr, Rb, Sc, Sm, Sr, Ta, Tb, Th, Ti, Tm, U, V, Y, Yb, Zn, Zr. Detection limits vary with sample type and elements analysed, from < 100 ppb to < 1 ppt (Frei and Kystol 2004). Routine analyses of international standards and in-house standards have demonstrated that the analytical precision and the accuracy are better than 5 % for the majority of elements analysed.

At “Acme Labs”, the major oxides and several minor elements were analysed by ICP-ES (inductively coupled plasma-emission spectrometry); and rare earth and refractory elements were determined by ICP-MS (inductively coupled plasma-mass spectrometry). Both methods applied 0.2 g sample fused by Lithium metaborate/ tetraborate and digested in dilute nitric acid. In addition a separate 0.5 g aliquot digested in Aqua Regia (mixture of nitric acid and hydrochloric acid) was analysed by ICP-MS to report the precious and base metals (Au, Ag, As, Bi, Cd, Cu, Hg, Mo, Ni, Pb, Sb, Se, Tl, Zn). Generally, ICP-MS can determine concentrations that are 1 to 2 orders of magnitude lower compared to ICP-ES. Detection limits were 0.01 % for all major elements; with exception of 0.04% for Fe (ACME labs 2009). Detection limits were less than 1 ppm for trace elements including most REE (rare earth elements). The exception were Ba (5 ppm), Co (20 ppm), Nb (5 ppm), Ni (20 ppm), Sr (3 ppm), V (8 ppm), Y (2 ppm), Zn (5 ppm), Zr (5 ppm) and Ce (30 ppm). Total S and C were analysed by LECO with detection limits of 0.01 % and 0.02 %, respectively. Loss on ignition (LOI) was given as weight difference after ignition at 1000°C.

For cuttings samples comparison has been done on the data set after correction for Ba, assuming zero in the sediments and 100% Ba from barite in the drilling mud (the data set available on the PETSYS homepage is raw data, which has not been changed by any corrections). Cr and other metals have not been used in case it originates from impurities in the cuttings samples, as the contents of specific metals vary between wells.

#### Data quality

Different laboratories have been applied hence with different detection limits as result.

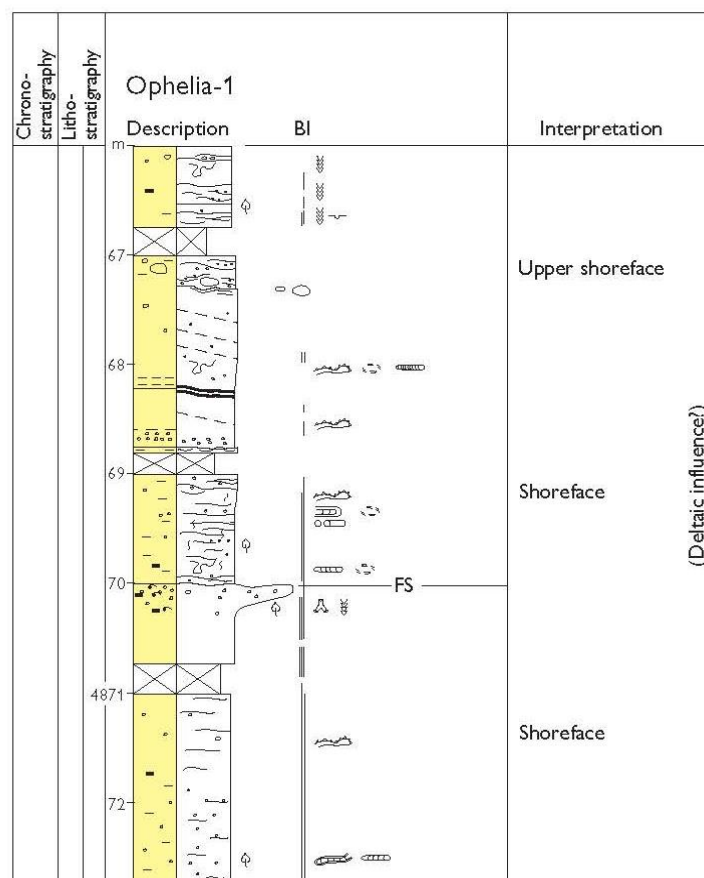
Cuttings samples were washed and dried but otherwise not modified. Cuttings samples commonly contain impurities which vary between wells, which hamper comparison by multivariate analysis.

### *3.5 Depositional environments*

The interpretations of depositional environments presented in the following are based on data from previous and new core-descriptions, from descriptions of cuttings and sidewallcores found in the completion reports and from lithology interpretations based on logs. Previous interpretations of the depositional environments for the studied succession includes Johannessen et al. (1996), Andsbjerg et al. (2001), Andsbjerg (2003) Andsbjerg and Dybkjær (2003), Johannessen (2003), Ineson et al. (2003), Michelsen et al. (2003) and Johannessen et al. (2010).

### 3.6 Core descriptions

Core descriptions from selected wells, presented as sedimentological logs (Figure 3.13), can be found at the PETSYS Website within "Wells" – "Core Descriptions". The cores have been described (lithology, grain size, sedimentary structures, fossils, trace fossils, and degree of bioturbation) in order to interpret depositional environments. The interpretations of depositional environments have been expanded above and below the cored sections using petrophysical logs. Upward coarsening sandstone successions inferred from petrophysical logs are interpreted as prograding shoreface. Upward-fining sandstone successions are interpreted as a back-stepping shoreface. Upward-fining sandstone successions in a non-marine setting are interpreted as fluvial



channel fill.

Fig. 3.13. Example of a sedimentological log. Ophelia-1. Shoreface sandstones of the Ravn Mb.

### 3.7 Palaeogeographic maps

A series of 17 palaeogeographic maps (Figure 3.14) illustrates the depositional history and the changes in the distribution of depositional environments up through the Jurassic. Each map represents a timeinterval, as indicated on the figure. The influence of structural elements active within the timeinterval in question, on the distribution of sediments and environments, has been taken into account (faults, axis of depocentre and structural highs). The palaeogeographic maps can

be downloaded from the PETSYS Website ( "Maps" – "Palaeogeography"), the legend appears when pressing the "i"-icon.

The Coffee Soil Fault zone separates the easternmost Danish Central Graben and the Ringkøbing-Fyn High. It is not clear if there was deposition of Jurassic-Lower Cretaceous sediments on the Ringkøbing-Fyn High. The two gravity-flow sand units in the northern part of the Tail End Graben (Svane-1 and Amalie-1) were deposited at the same time as the maximum shoreface regression on the Heno Plateau, suggesting that the sand was derived from the Heno Plateau. As the Mandal High probably wasn't a structural high at this time, the sand from the Heno Plateau may also have been transported from the Heno Plateau to the Søgne Basin.

As all wells are sub-divided in sequences, it is possible to illustrate the palaeogeography for each sequence. Pie-diagrams (GR/DT sand-clay type) are also constructed for each sequence ("Map" - "Map data" – "Log facies versus sequence stratigraphy", see further the technical note entitled "Results of log interpretation..."). An overlay of a pie-diagram on the palaeogeographic map for the same sequence, shows the overall reservoir quality of the sand in all wells in, for example, a prograding shoreface sand unit. It is also possible to show the thickness of sandstone units for each sequence on the palaeogeographic maps using the pie-diagram overlay. Another example of the use of combining the palaeogeographic maps and the pie-diagrams is for the sequences Kimm-3, Kimm-4 and Volg-1. This combination illustrates how the lowermost part of the Farsund Formation in wells on the Heno Plateau shows a high proportion of log facies III (highest GR claystones). This is confirmed by very high resistivity log values and TOC-HI values. It thus seems that the clay deposited in the Heno Plateau area in the uppermost Kimmeridgian – Lower Volgian had a different composition than the same succession elsewhere in the basin.

The series of palaeogeographic maps shows an overall transgression from east towards west from the Baj-1 sequence to the Ryaz-1 sequence. Two regressive shoreface sandstone events happened during deposition of sequences Kimm-1 to Kimm-2 and Kimm-2 to Kimm-3, respectively.

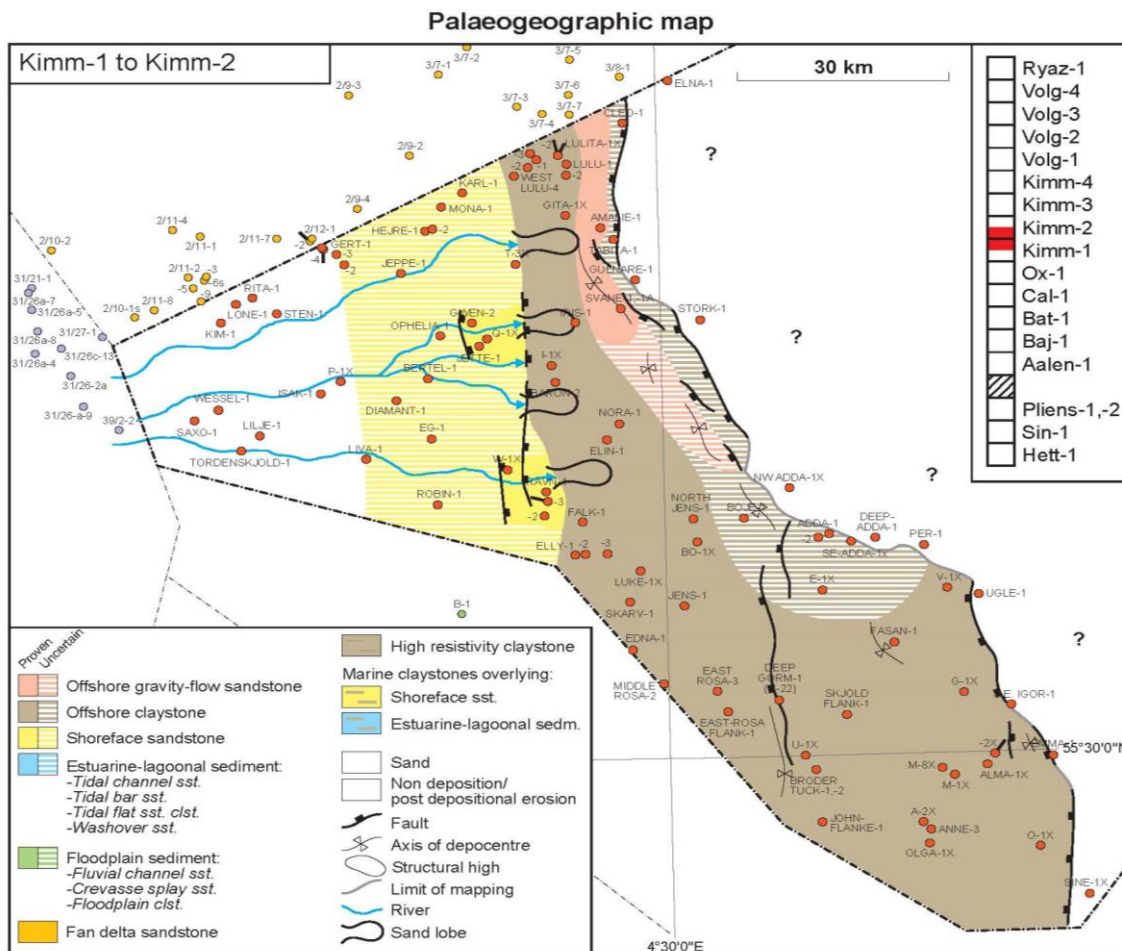


Fig. 3.14. An example of a palaeogeographic map. This map represents the timeinterval during which the upper part of Sequence Kimm-1 and the lower part of Sequence Kimm-2 were deposited.

### 3.8 References

ACME Labs, 2009: Schedules of services and fees, 33p.

Abbink, O.A., Callomon J.H., Riding, J.B., Williams, P.D.B., Wolfard, A., 2012. Biostratigraphy of Jurassic–Cretaceous strata in the Terschelling Basin, The Netherlands. *Proceedings of the Yorkshire Geological Society*, 53 (4), 275–302.

Alsen, P., 2014a. Ammonite stratigraphy in the NW Adda-1Xa well. A contribution to The Jurassic Petroleum System in the Danish Central Graben – The PETSYS Project. *Danmarks og Grønlands geologiske Undersøgelse Rapport 2014/27*, 10pp.

Alsen, P., 2014b. Ammonite stratigraphy in the Elly-3 well. A contribution to The Jurassic Petroleum System in the Danish Central Graben – The PETSYS Project. *Danmarks og Grønlands geologiske Undersøgelse Rapport 2014/26*, 12pp.

Andsbjerg, J., Nielsen, L.H., Johannessen, P.N., Dybkjær, K., 2001. Divergent development of two neighbouring basins following the Jurassic North Sea doming event: the Danish Central Graben and

the Norwegian-Danish Basin. *Sedimentary Environments Offshore Norway – Palaeozoic to Recent*. Eds: O.J. Martinsen and T. Dreyer. NPF Special Publication, Elsevier, Norwegian Petroleum Society, 10, 175–197.

Andsbjerg, J., 2003. Sedimentology and sequence stratigraphy of the Bryne and Lulu formations, Middle Jurassic, northern Danish Central Graben. In: Ineson, I. and Surlyk, F. (eds.): *The Jurassic of Denmark and Greenland*. Geological Survey of Denmark and Greenland Bulletin 1, 301–347.

Andsbjerg, J., Dybkjær, K., 2003. Sequence stratigraphy of the Jurassic of the Danish Central Graben. In: Ineson, I. and Surlyk, F. (editors): *The Jurassic of Denmark and Greenland*. Geological Survey of Denmark and Greenland Bulletin 1, 265–300.

Costa, L.I., Davey R.J., 1992. Dinoflagellate cysts of the Cretaceous System. In: Powell, J. (Ed.): *A stratigraphic index of dinoflagellate cysts*. British Micropalaeontological Society Publication Series, Chapman & Hall, 99–153.

Davey, R.J., 1982. Dinocyst stratigraphy of the latest Jurassic to Early Cretaceous of the Haldager No. 1 borehole, Denmark. Geological Survey of Denmark Ser. B 6, 57pp.

Dybkjær, K., 1998. Palynological dating of the Mandal Formation (Uppermost Jurassic – lowermost Cretaceous, Norwegian Central Graben) and correlation to organic-rich shales in the Danish sector. *Marine and Petroleum Geology* 15, 495–503.

Frei, D. & Kystøl, J. 2004: Inductively coupled plasma mass spectrometry (ICP-MS) Laboratory. <http://www.geus.dk/departments/geol-mapping/projects/spectrometry-dk.htm>.

Gradstein, F.M., Ogg, J.G., Schmitz, M.D., Ogg, G.M., 2012. *The geological timescale 2012*. Elsevier, Oxford, U.K.

Heilmann-Clausen, C., 1987. Lower Cretaceous dinoflagellate biostratigraphy in the Danish Central Trough. Geological Survey of Denmark Ser. A 17, 89pp.

Herngreen, G.F.W., Kerstholt, S.J., Munsterman, D.K., 2000. Callovian-Ryazanian ("Upper Jurassic") palynostratigraphy of the Central North Sea Graven and Vlieland Basin, the Netherlands. *Mededelingen Nederlands Instituut voor Toegepaste Geowetenschappen TNO*, nr. 63, 99pp.

Ineson, J.R., Bojesen-Koefoed, J.A., Dybkjær, K., Nielsen, L.H., 2003. Volgian-Ryazanian "hot shales" of the Bo Member (Farsund Formation) in the Danish Central Graben, North Sea: stratigraphy, facies and geochemistry. In: Ineson, J.R. & Surlyk, F. (eds): *The Jurassic of Denmark and Greenland*. Geological Survey of Denmark and Greenland Bulletin 1, 403–436.

Japsen, P., Britze, P., Andersen, C., 2003. Upper Jurassic-Lower Cretaceous of the Danish Central Graben: structural framework and nomenclature. In: Ineson, J.R. & Surlyk, F. (eds): *The Jurassic of Denmark and Greenland*. Geological Survey of Denmark and Greenland Bulletin 1, 233–246.

Jensen, T.F., Holm, L., Frandsen, N., Michelsen, O., 1986. Jurassic – Lower Cretaceous lithostratigraphic nomenclature for the Danish Central Trough. Geological Survey of Denmark, Series A, 12, 65pp.

Johannessen, P.N., Dybkjær, K., Rasmussen, E.S., 1996. Sequence stratigraphy of Upper Jurassic reservoir sandstones in the northern part of the Danish Central Trough, North Sea. *Marine and Petroleum Geology* 13 (5), 755–770.

Johannessen, P.N., 2003. Sedimentology and sequence stratigraphy of paralic and shallow marine Upper Jurassic sandstones in the northern Danish Central Graben. In: Ineson, I. and Surlyk, F. (eds.): *The Jurassic of Denmark and Greenland*. Geological Survey of Denmark and Greenland Bulletin 1, 367–402.

Johannessen, P.N., Dybkjær, K., Andersen, C., Kristensen, L., Howikoski, J., Vosgerau, H., 2010. Upper Jurassic reservoir sandstones in the Danish Central Graben: new insights on distribution and depositional environments. In: Vining, B.A. & Pickering, S.C. (eds): *Petroleum Geology: From Mature Basins to New Frontiers*. Proceedings of the 7th Petroleum Geology Conference. Petroleum Geology Conference series 2010, v. 7, 127–143. Geological Society, London.

Kystol, J. & Larsen, L. M., 1999: Analytical procedures in the rock geochemical laboratory of the Geological Survey of Denmark and Greenland. *Geology of Greenland Survey Bulletin*, 184, 59-62.

Michelsen, O., Nielsen, L.H., Johannessen, P.N., Andsbjerg, J., Surlyk, F., 2003. Jurassic lithostratigraphy and stratigraphic development onshore and offshore Denmark. In: Ineson, I. and Surlyk, F. (eds.): *The Jurassic of Denmark and Greenland*. Geological Survey of Denmark and Greenland Bulletin 1, 147–216.

Posamentier, H.W., Jervey, M.T., Vail, P.R., 1988. Eustatic controls on clastic deposition I – conceptual framework. In: Wilgus, C.K. *et al.* (eds.): *Sea-level changes – an integrated approach*. Society of Economic Paleontologists and Mineralogists Special Publication 42, 109–124.

Posamentier, H.W., Vail, P.R., 1988. Eustatic controls on clastic deposition II – sequence and systems tract models. In: Wilgus, C.K. *et al.* (eds.): *Sea-level changes – an integrated approach*. Society of Economic Paleontologists and Mineralogists Special Publication 42, 125–154.

Poulsen, N., 1996. Dinoflagellate cysts from marine Jurassic deposits of Denmark and Poland. *AASP Contribution Series* 31, 227pp.

Poulsen, N.E., Riding, J.B., 2003. The Jurassic dinoflagellate cyst zonation of Subboreal Northwest Europe. In: Ineson, J.R. & Surlyk, F. (eds): *The Jurassic of Denmark and Greenland*. Geological Survey of Denmark and Greenland Bulletin 1, 115–144.

Riding, J.B., Thomas, J.E., 1992. Dinoflagellate cysts of the Jurassic System. In: Powell, J. (Ed.): *A stratigraphic index of dinoflagellate cysts*. British Micropalaeontological Society Publication Series. London: Chapman & Hall, 7–97.

Vail, P.R., Mitchum, R.M., Thompson, S., 1977. Seismic stratigraphy and global changes of sea level; Part 3: relative changes of sea level from coastal onlap. In: Payton, C.E. (ed.): *Seismic stratigraphy – applications to hydrocarbon exploration*. American Association of Petroleum Geologists Memoir 26, 63–81.

Van Wagoner, J.C., Posamentier, H.W., Mitchum, R.M., Vail, P.R., Sarg, J.F., Loutit, T.S., Hardenbol, J., 1988. An overview of the fundamentals of sequence stratigraphy and key definitions.

In: Wilgus, C.K. *et al.* (eds.): Sea-level changes – an integrated approach. Society of Economic Paleontologists and Mineralogists Special Publication 42, 39–45.

Van Wagoner, J.C., Mitchum, R.M., Campion, K.M., Rahmanian, V.D., 1990. Siliciclastic sequence stratigraphy in well logs, cores and outcrops: concepts for high-resolution correlation of time and facies. American Association of Petroleum Geologists Methods in Exploration Series 7, 55pp.

Vollset, J., Doré, A.G., 1984. A revised Triassic and Jurassic lithostratigraphic nomenclature for the Norwegian North Sea. Bulletin of the Norwegian Petroleum Directorate, 3, 53pp.

Weibel, R., Johannessen, P., Dybkjær, K., Rosenberg, P., Knudsen, C., 2010. Chemostratigraphy of upper Jurassic reservoir sandstones, Danish Central Graben, North Sea. Marine and Petroleum Geology 27, 1572–1594.



## 4 Petrography and diagenesis

### 4.1 Database

Petrography and diagenesis studies are based on cored intervals of the Heno Formation in 14 wells and of the Outer Rough Sand (Farsund Formation) in two wells. Diagenesis and its relation to the porosity and permeability are presented in datasheets for each thin section and in summaries for each well. Datasheets and summaries are available on the PETSYS Website by selecting 'Wells' followed by 'Diagenesis' or 'Lab. Datasets' followed by 'Diagenesis'.

Additional petrographical studies have been performed on gravity flow sediments of the Farsund Formation and Cromer Knoll Group from 6 wells. No porosity and permeability measurements were performed on these sediments, but datasheets with the characteristic composition and petrography are available on the PETSYS Website.

### 4.2 Approach

The focus of the diagenetic examinations has been on the Heno Formation, which has the widest extent (compared to other Upper Jurassic sandstones) in the Danish Central Graben and therefore represents variations in depositional environment, paleogeographic position in the basin, provenance, burial depth, burial history etc. The objective was to find the major diagenetic influence on the porosity and permeability of each sample and for each well core. The Outer Rough Sand was included in the diagenetic investigations in order to understand the observed differences in porosity and permeability between the two wells.

### 4.3 Microscopy

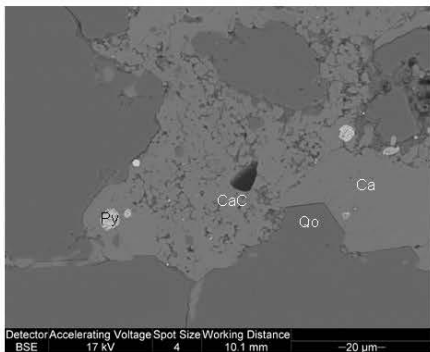
Polished thin sections were prepared from sedimentary rocks impregnated with blue epoxy, for easy identification of porosity. The polished thin sections were studied by transmitted and reflected light microscope. Descriptive terms for clay minerals are used according to Wilson and Pittman (1977) and for carbonate cement morphologies modified from Harwood (1988). Supplementary studies of crystal morphologies and paragenetic relationships were performed on gold-coated rock chips mounted on stubs and on carbon-coated thin sections using a Phillips XL 40 scanning electron microscope (SEM). The electron beam was generated by a tungsten filament operating at 17 kV and 50-60  $\mu$ A. Mineralogy, petrographic relations, texture, grain size and sorting were described for each thin section (Fig. 4.1). Relative timing of the diagenetic phases for each well is presented in a diagenetic sequence (Fig. 4.2).

Thin section grain size analysis underestimates the dimensions relative to sieving analysis (Johnson 1994). Rather than attempting to correct for this bias, we have chosen to give the grain size as an estimated average and range of grain sizes (minimum to maximum). The grain size nomenclature is applied according to the Wentworth Class (Wentworth 1922). Sorting is estimated petrographically from sorting comparators by Longiaru (1987), which is based on the sorting classes of Folk (1966). The sorting classes are defined for eight relative phi classes that range from very well to poorly sorted. The phi values range from 0 for very well sorted sand to 2.0 for poorly–very poorly sorted sand.

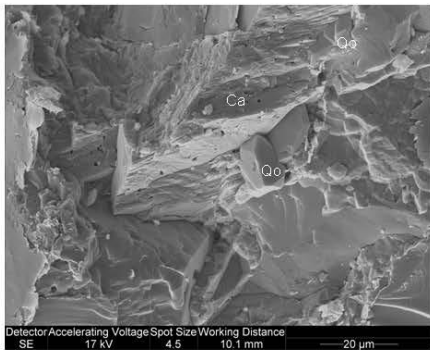
Thin section/sample: JE1-He4938.01



Overview.



Dominating authigenic phases, quartz overgrowths (Qo) and calcite cement (Ca). Calcite cement (Ca) post-date pyrite framboids (Py) and quartz overgrowths, which encloses detrital calcite clasts (CaC) (Backscatter electron micrograph).



Calcite cement (Ca) post-dating authigenic quartz (Qo) (Scanning electron micrograph).

GEUS

**Well / locality:** Jeppe-1  
**Depth:** 4938.01 m b. Kb.  
**Fm / Mb:** Heno Fm / Ravn Mb  
**Depositional envr.:** Middle shoreface  
**Sample preparation:** Blue epoxy  
**Grain size (range):** 175 µm (50 – 350 µm)  
**Sorting:** Moderately well – moderately  
**Plug porosity and permeability at thin section:** 8 % and 0.2 mD

**Framework grains:**

Quartz dominates. K-feldspar is common, whereas plagioclase is rare. Mica is rare. Apatite fossil fragments are rare. Organic matter is rare. Glauconite is rare. Heavy minerals (rutile) are rare.

Detrital smectitic clays are minor in the upper part of the sample, though abundant in the lower part.

**Diagenetic changes in paragenetic order:**

Apatite (rare) occurs in local areas as tiny crystals.

Pyrite, framboidal, (rare).

K-feldspar overgrowths (rare) are commonly partly dissolved or illitized.

Illitization of smectitic detrital clays (minor-abundant).

Quartz overgrowths (minor-common) on detrital quartz grains are often partly replaced by calcite cement. Authigenic quartz is well-developed when growing into fossil fragments.

Calcite cement (abundant in the upper part of the sample, common in the lower part), is sparry.

Secondary porosity after feldspar dissolution.

**Conclusion:**

Fine-grained sandstone of low porosity and low permeability due to abundant calcite cement and/or illitized clays.

Fig. 4.1. Example of datasheet for the thin section JE1-He4938.01.



## 4.4 Qemscan

Mineral quantification by the Qemscan method is based on carbon coated polished blocks analysed by a scanning electron microscope (SEM) coupled with 2 - 4 energy dispersive X-ray spectrometers to rapidly image and chemically/mineralogically map samples.

Qemscan uses the level of backscatter electron brightness to distinguish the sample from the impregnated epoxy, i.e. 'background', in the sample block. Therefore, at each stepping interval, a backscatter electron (BSE) brightness reading is taken and, if above a 'background' threshold, an X-ray spectrum is acquired. Conversely, if the BSE value is below the threshold, no X-ray spectrum is acquired. Each analysis point (or pixel in the mineralogical image) is made with a distance of 10  $\mu\text{m}$  and a measurement takes between approximately 1 and 4 ms. The resultant X-ray spectrum is compared with a table of known mineral compositions and chemical compositions. If a previously unclassified mineral phase is encountered during analysis, it is marked as 'other'.

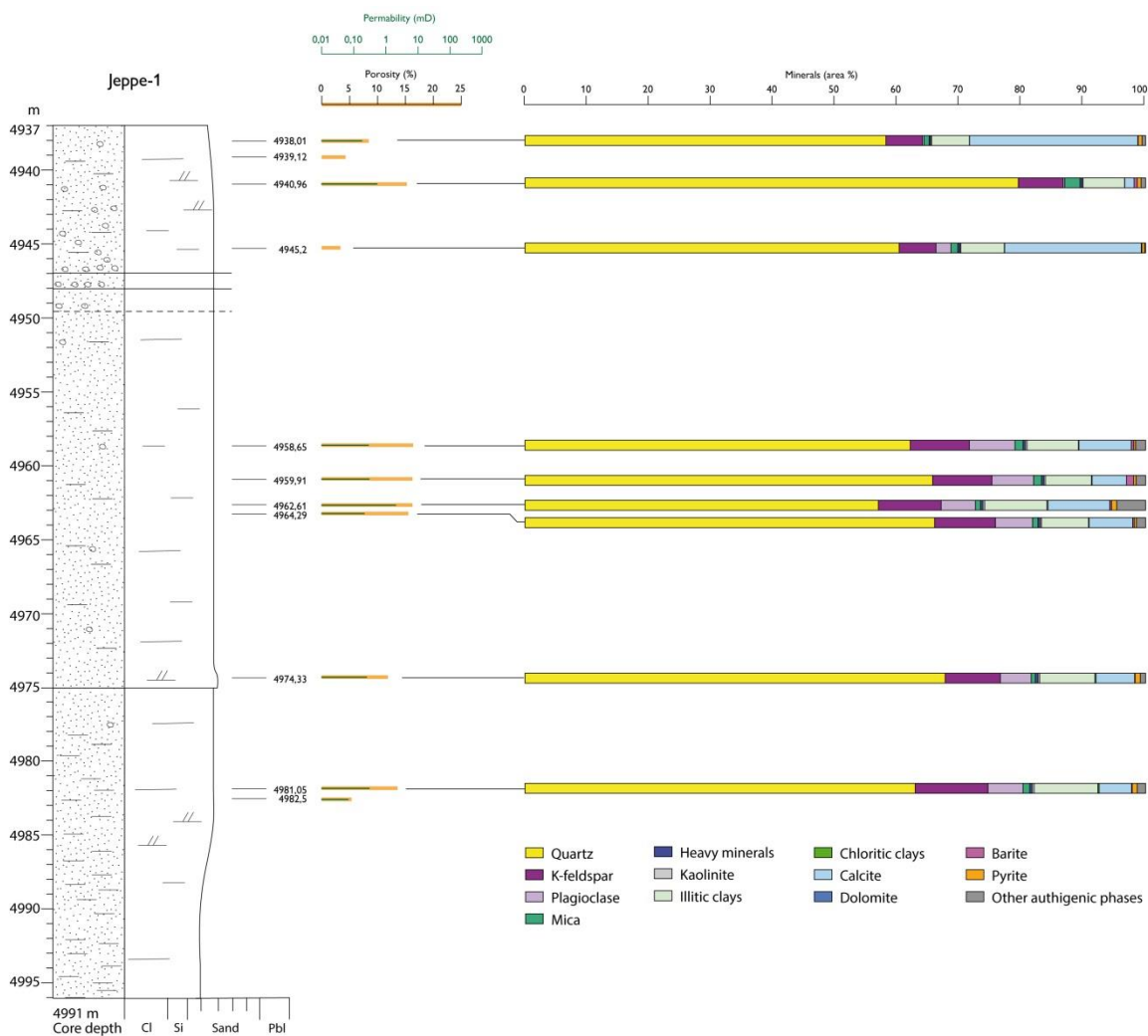


Fig. 4.3. Example of sedimentary log with combined information about mineralogy from Qemscan analyses and porosity and permeability measurements for the Jeppe-1 well.

## 4.5 X-ray diffraction (XRD)

Bulk samples for X-ray diffraction analysis (XRD) were crushed in a steel or wolfram-carbide mortar and mounted with random orientation. Samples were scanned on an automated Philips© PW 3710 X-ray or a PANalytical X'Pert Pro MPD diffractometer with automatic divergence slit, using graphite monochromated CuK $\alpha$  radiation. Quantification of major mineral phases based on bulk samples was done by Rietveld analysis of X-ray diffractograms.

For clay mineral analysis the samples were crushed manually and dispersed ultrasonically in distilled water. The fraction >30  $\mu\text{m}$  was removed by sedimentation and the 2-30  $\mu\text{m}$  by centrifugation in a centrifugal particle size analyser using the method described by Slater & Cohen (1962). The suspensions were flocculated in 1 M NaCl and following this excess salt was removed by centrifugation and washing with water and ethanol. Oriented specimens were prepared by pipette of the < 2  $\mu\text{m}$  clay fraction, which were either Mg-saturated, K-saturated, Mg-saturated and ethylene glycolated or K-saturated and heated for an hour at 300°C. The clay specimens were analysed by a Phillips 1050 X-ray diffractometer with pulse-height selection and  $\beta$ -filtered Co-K $\alpha$  radiation. The discrete minerals were identified from peak positions on the X-ray diffractograms. The clay mineralogy of the investigated sandstones is incorporated in the mineralogical description in the datasheets.

## 4.6 Porosity and permeability

Plug porosity and permeability is measured according to the API RP-40 standard (API 1998). Gas permeability was measured at a confining pressure  $\sim$  2.8 MPa (400 psi), and at a mean N<sub>2</sub> gas pressure of  $\sim$  1.5 bar (bar absolute) = 0.15 MPa (permeabilities below 0.05 mD were not measured or measured using a bubble flowmeter). He-porosity was measured at unconfined conditions. The measured effective porosity corresponds to the total porosity, as most reservoir rocks contain only few isolated pores (API 1998). Thin sections were made from the plug trims and cut offs; for which reason the porosity and permeability can be directly correlated to petrographic observations.

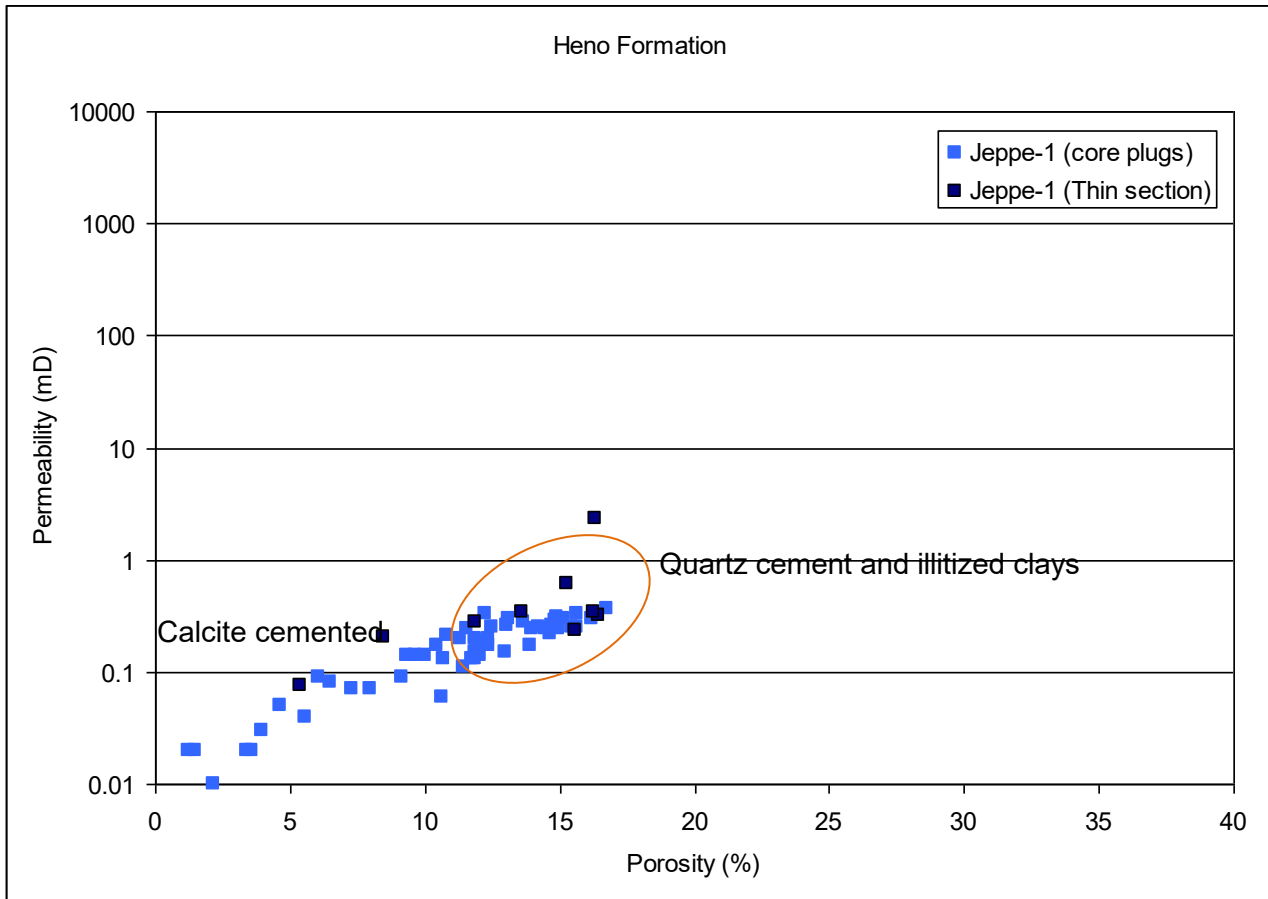


Fig. 4.4: Example of plug porosity and permeability related to major diagenetic changes in the Jeppe-1 well.

#### 4.7 Data quality

Heterogeneities in plugs can result in differences between plug porosity and permeability measurements and thin section petrography, although thin sections are made from plug cut offs. When difference has been recognised, this has been noted in the datasheet.

Modal composition obtained by traditional point counting and Qemscan quantification supplement each other. Point counting will typically underestimate the amount of feldspar present, especially when the thin sections are not stained as in this case. Remnants after partly dissolved or carbonate replaced feldspar grains are difficult to recognise. Clay minerals can be overestimated during point counting, as clay minerals are commonly smaller than the thickness of the thin section and consequently surrounded by porosity, which is not counted.

The Qemscan method cannot distinguish between authigenic and detrital phases. Rock fragments are not identified by the Qemscan method, but spilt into separate minerals. Some minerals are grouped due to similar chemical composition.

## 4.8 References

- API. 1998. API RP 40, Recommended practice for core analysis, second edition, American Petroleum Institute, Washington DC.
- Dunham, R.J. (1962). "Classification of carbonate rocks according to depositional texture". In: Ham, W.E. (Ed.) Classification of carbonate rocks. American Association of Petroleum Geologists Memoir 1, 108-121.
- Folk, R. L. 1966. A review of grain-size parameters. *Sedimentology* 6, 73-93.
- Harwood, P. P. 1988. Microscopical techniques: II. Principles of sedimentary petrography. In: Tucker, M. E. (ed.), *Techniques in sedimentology*. Blackwell Scientific Publications, Oxford, 108-173.
- Johnson, M.R., 1994. Thin section grain size analysis revisited. *Sedimentology* 41, 985-999.
- Longiaru, S. 1987. Visual comparators for estimating the degree of sorting from plane and thin sections. *Journal of Sedimentary Research* 57, 791-794.
- McBride, E. F. 1963. A classification of common sandstones. *Journal of Sedimentary Research* 33, 664-669.
- Slater, C., Cohen, L. 1962. A centrifugal particle analyser. *Journal of Scientific Instruments* 39, 614–617.
- Wentworth, C. K. 1922. A scale of grade and class terms for clastic sediments. *Journal of Geology* 5, 377-392.
- Wilson, M. D., Pittman, E. D. 1977. Authigenic clays in sandstones: recognition and influence on reservoir properties and paleoenvironmental analysis. *Journal of Sedimentary Petrology* 47, 3 – 31.



## 5 Hydrocarbon shows/discoveries database

The following note gives a brief description of the hydrocarbon shows/discoveries database that was established as part of the PETSYS project and which is available on the [PETSYS website](#).

All data have been compiled from completion reports (abbreviated CR). Data are presented at depth levels and at stratigraphic levels, using the revised lithostratigraphic subdivision established in the project.

Data can be addressed at map level and at well level.

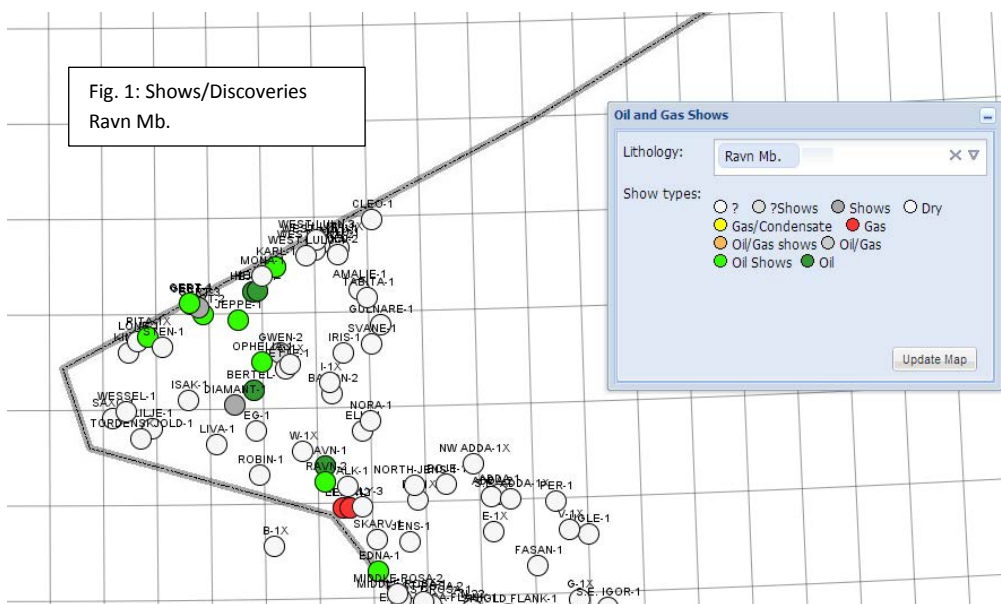
### 5.1 Access at map level

Select "Map" and press "Map data"

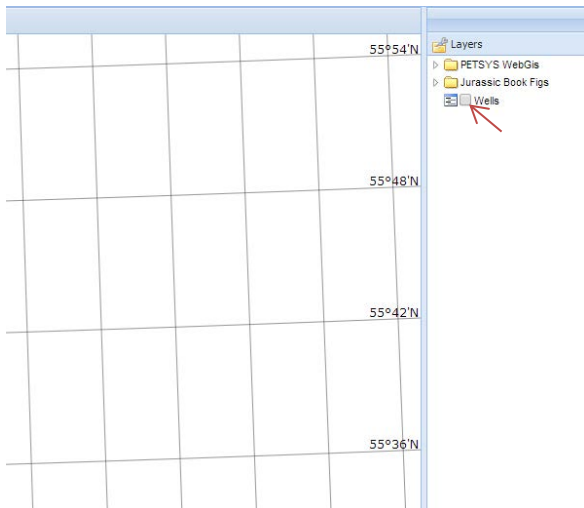
Select "Oil and Gas shows"

Select "lithostratigraphic unit"

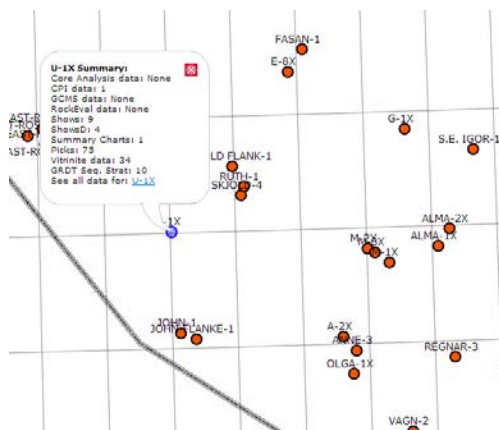
Press "Update map" and for each well the various show categories will be plotted, example Ravn Member in fig.1:



Press the button marked wells:



A map with the position and name of the project wells will be displayed. If you press at a specific well, a list of the information available will be given. See example for the U-1 well:



Press [U-1X](#) and select shows. The following will be given, i.e. a pie diagram and a table with the distribution of shows/discoveries at lithostratigraphic levels. Information is also provided at depth levels. For details see access at well levels.

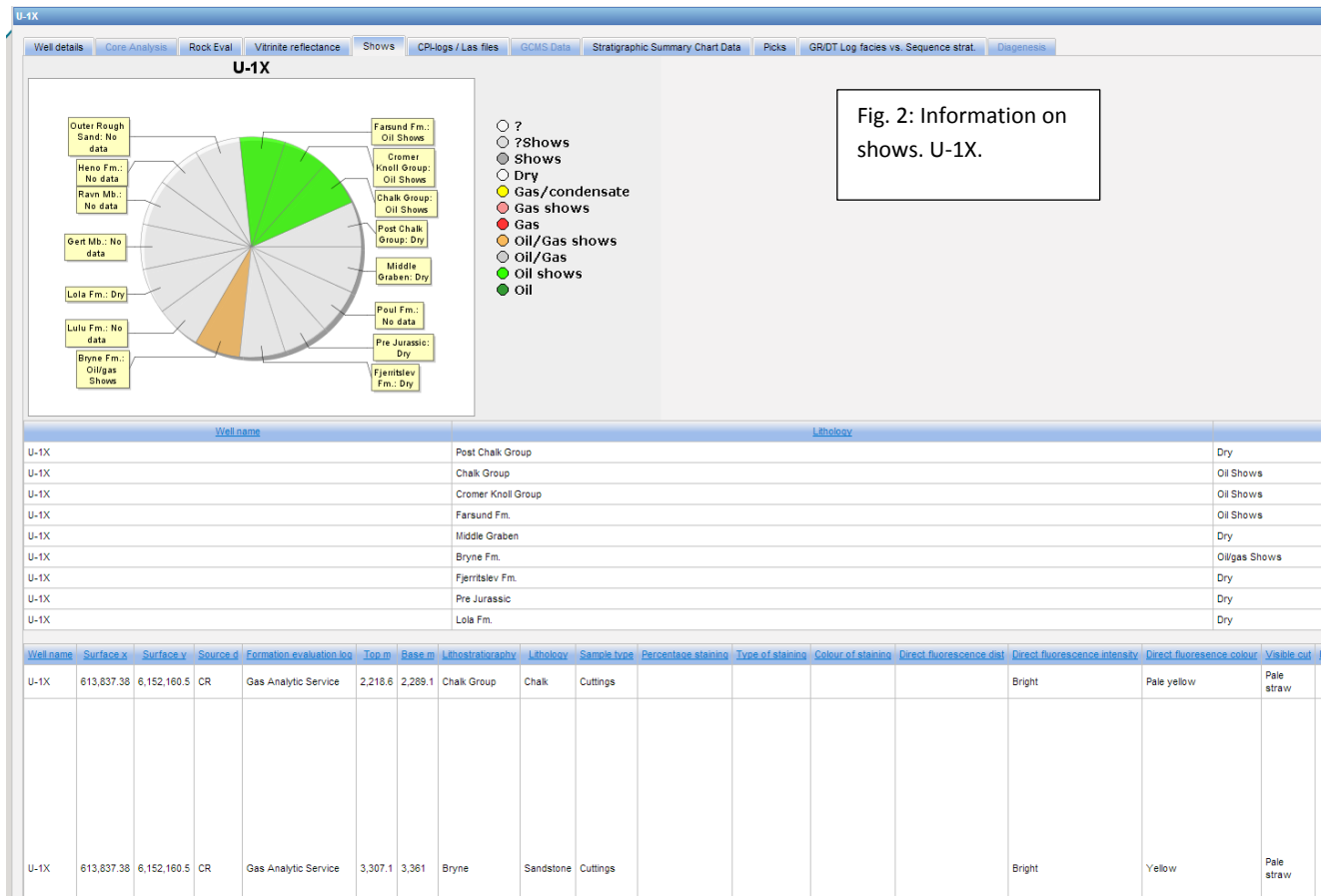


Fig. 2: Information on shows. U-1X.

## 5.2 Access at well level

Select wells in the main menu and press hydrocarbon shows. Information is provided at two levels: lithostratigraphic and depth.

Depending on the methods used by the various companies, information at depth level is provided on the following:

Percentage staining	Type of staining	Colour of staining
Direct fluorescence distribution	Direct fluorescence intensity	Direct fluorescence colour
Visible cut	Fluorescent cut	Crush cut
Fluorescent residue	Visible residue	Odour
Gas	CPI saturation	Comments

An example of information provided under comments is from the Chalk Group in the Anne-3 well:

"Core #1 and 2. Locally bleeding oil and gas. Test #3 in the interval 1903,8 - 1917,2 m produced 970 BOPD and 430 MCFPD of gas. Tests #4 and 4A in the interval 1869,6 - 1894,3 produced 350 BOPD/205 MCFPD and 780 BOPD/460 MCFPD respectively "

## 6 Source rock analyses

### 6.1 Rock-Eval data

Rock-Eval data from the Jurassic section in 76 wells are compiled and quality checked. 12 'new' wells were analysed as part of the project. In total the database consists of 5239 samples. The data can be accessed via the lab dataset and wells buttons and can be shown both in total, by individual well and by lithostratigraphic formation/member or sequence stratigraphic unit. At each selected image frequency plots of hydrogen index (HI), Tmax and TOC appear in addition to crossplots of Tmax vs. HI, TOC vs. S<sub>2</sub> and HI plus TOC vs. depth are displayed.

The Rock-Eval data contained in each image are tabulated below the graphics and can be down-loaded and exported in Excel format. An example of data listed for each well is shown in Fig. 6.1. Total Carbon (TC) and Total Sulphur (TS) values are included for 'new' wells analyses as part of the present project. The type of sample material is generally cuttings, but when oil-based drilling mud has been used cuttings were extracted with organics solvents prior to analysis.

Both TOC- and HI values can be posted for each sequence stratigraphic unit and each interval bounded by mapped reflectors applying the map data folder in the map menu.

**Example of tabulated source rock data**  
Tordenskjold-1 well, Outer Rough Basin

New wells: also TC and TS data

Depth (m)	Type	TOC	Tmax	S1	S2	HI	PI	Formation/Group	Member	Stage
3408	cuttings	2,63	436	0,36	7,79	296	0,04	Farsund		U. Jurassic
3433,85	cuttings	2,53	439	0,71	8,16	323	0,08	Farsund		U. Jurassic
3434,05	cuttings	3,72	436	1,45	17,49	470	0,08	Farsund	Bo (Hot Unit)	U. Jurassic
3434,55	cuttings	3,02	437	1,02	12,35	409	0,08	Farsund		U. Jurassic
3453	cuttings	2,84	439	0,43	6,66	235	0,06	Farsund		U. Jurassic
3462	cuttings	3,5	432	0,89	11,37	325	0,07	Farsund		U. Jurassic
3471	cuttings	3,99	435	1,27	21,59	541	0,06	Farsund		U. Jurassic
3474	cuttings	4,19	435	1,42	17,6	420	0,07	Farsund		U. Jurassic
3480	cuttings	4,33	435	0,89	15,7	363	0,05	Farsund		U. Jurassic
3489	cuttings	5,04	434	1,43	21,56	428	0,06	Farsund		U. Jurassic
3498	cuttings	4,01	434	1,05	13,15	328	0,07	Farsund		U. Jurassic
3507	cuttings	3,25	443	0,53	9,34	287	0,05	Farsund		U. Jurassic
3516	cuttings	2,96	434	0,82	9,04	305	0,08	Farsund		U. Jurassic
3522	cuttings	2,33	437	0,62	6,86	294	0,08	Farsund		U. Jurassic
3534	cuttings	8,82	434	2,39	32,43	368	0,07	Farsund		U. Jurassic
3537	cuttings	3,81	432	2,65	17,55	461	0,13	Farsund		U. Jurassic

Samples with S<sub>2</sub><0.2, TOC<0.5 and Tmax<400 have been removed

Depth (m)	Type	TOC	Tmax	S1	S2	HI	PI	Formation/Group	Member	Stage
Average	cuttings	3,81	436	1,12	14,29	366	0,07	Farsund		U. Jurassic

TOC: Total organic carbon, wt.%  
Tmax: °C  
S1: mg HC/g rock  
S2: mg HC/g rock  
HI: Hydrogen Index, mg HC/g TOC  
PI: Production Index

Fig. 6.1: Example of tabulated source rock data (Tordenskjold-1 well)

An overview of the Rock-Eval data (TOC and HI) well by well is also available as separate traces on the *composite logs* using the well menu. The composite logs compile for the entire drilled Jurassic section both the lithology, GR/DT log-facies, lithostratigraphy, sequence stratigraphic information, seismic picks, reflection coefficients and the Rock-Eval data. In addition a separate *DeltaLogR* is shown. This represents log-derived TOC values calculated from the method described by Passey et al. (1990), using the separation between Resistivity and Sonic logs. This log traces usually mimics the measured TOC values in the wells. An example from the Hejre-2 well is shown in Fig. 6.2.

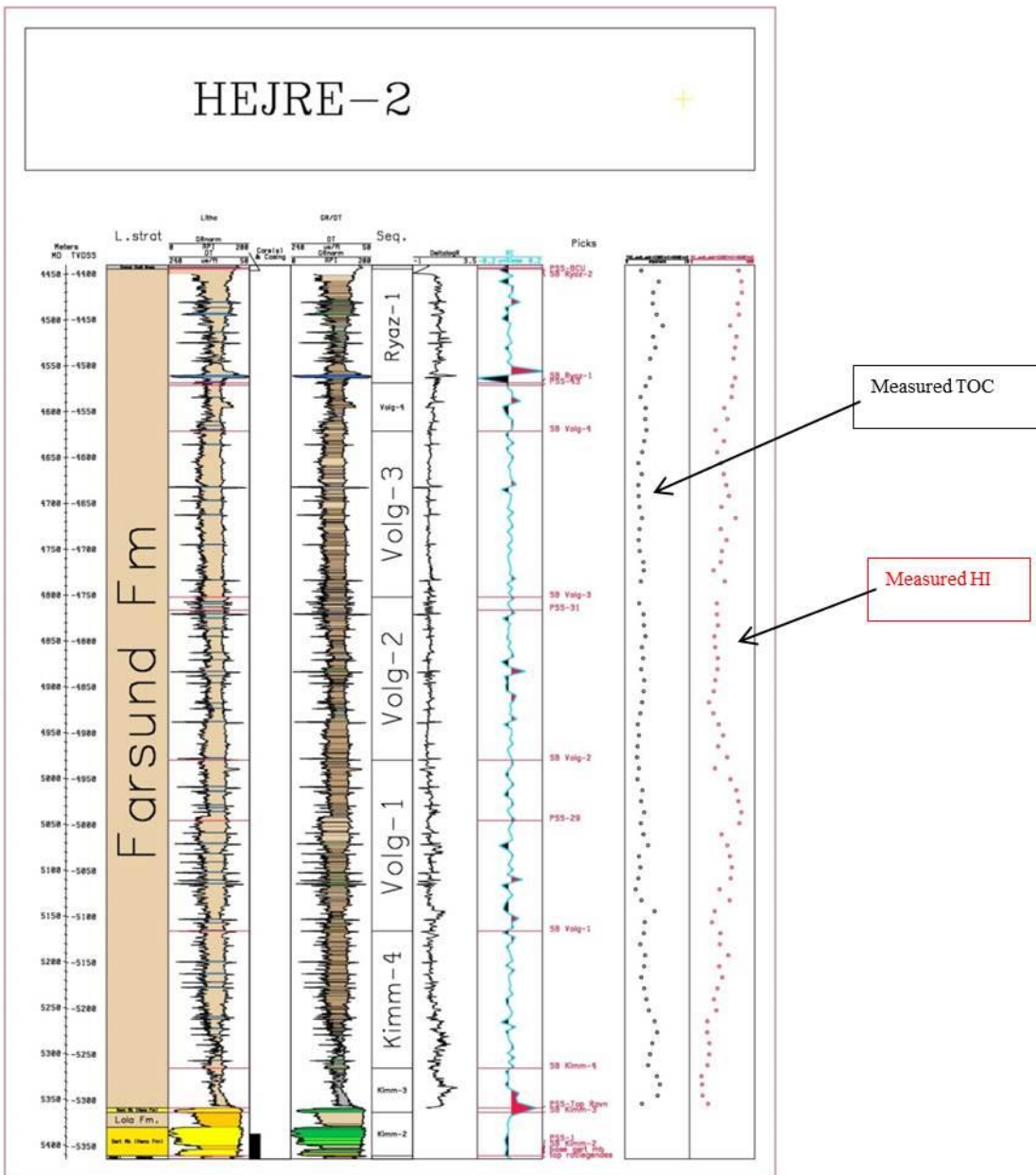


Fig 6.2: Example of composite log (Hejre-2)

The screening data clearly demonstrate that the marine shales of the Farsund Formation are the principal source rocks in the Danish Central Graben (DCG). They correspond to the Kimmeridge Clay Formation (KCF)

and equivalents elsewhere in the North Sea (e.g. Petersen et al., 2013). The uppermost part of the Farsund Formation is commonly characterised as 'hot', because of high gamma-ray (GR) level readings. These hot shales have significantly higher GR responses than the underlying shales and are in DCG referred to as the Bo Member. These shales have generally elevated total organic carbon (TOC) and higher hydrogen index (HI) and contain more oil-prone kerogen than the lower parts of the Farsund Formation. Evaluation of source rock potential in DCG has commonly focussed on the hot, upper part of the formation and largely neglected the remaining part (e.g. Ineson et al., 2003) The present study with a much larger Rock-Eval database shows, however, that also the lower part of the Farsund Formation may contain thick intervals of rich oil-prone shales (Petersen et al. 2012). The Hejre-2 well in the north is shown as an example (Fig. 6.3). Here elevated HI and TOC values are recorded in the Bo Member with gradually decreasing values below. At a depth of about 5000 m a sudden increase in both values occurs. This lower interval corresponds to sequence stratigraphic units Kimm-4 and Volg-1 and the top is marked by seismic reflector PSS\_29. The average TOC values for sequence stratigraphic interval Volg-1 in the wells are posted on the map as Fig. 6.4.

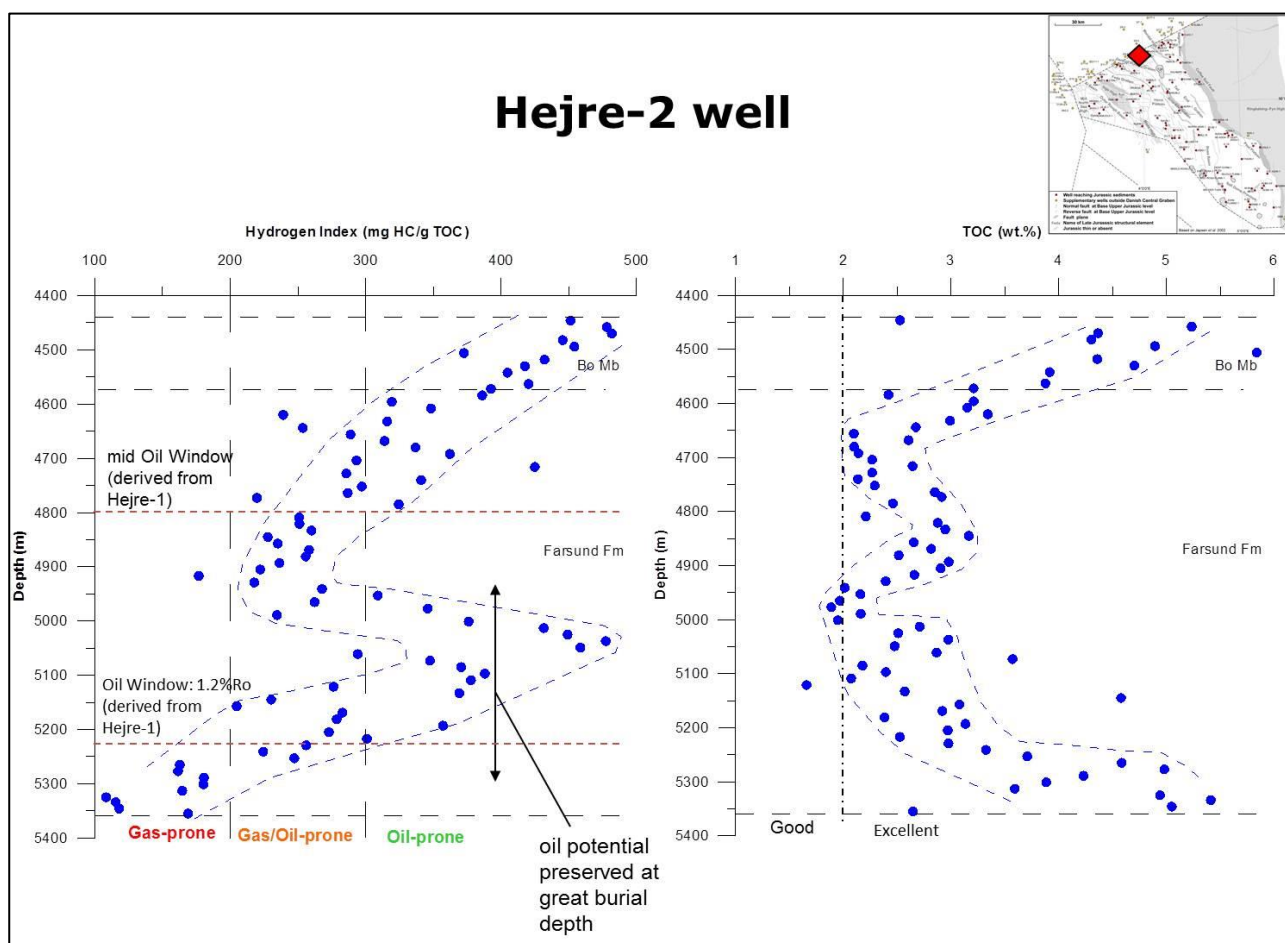


Fig 6.3: HI and TOC data from Hejre-2

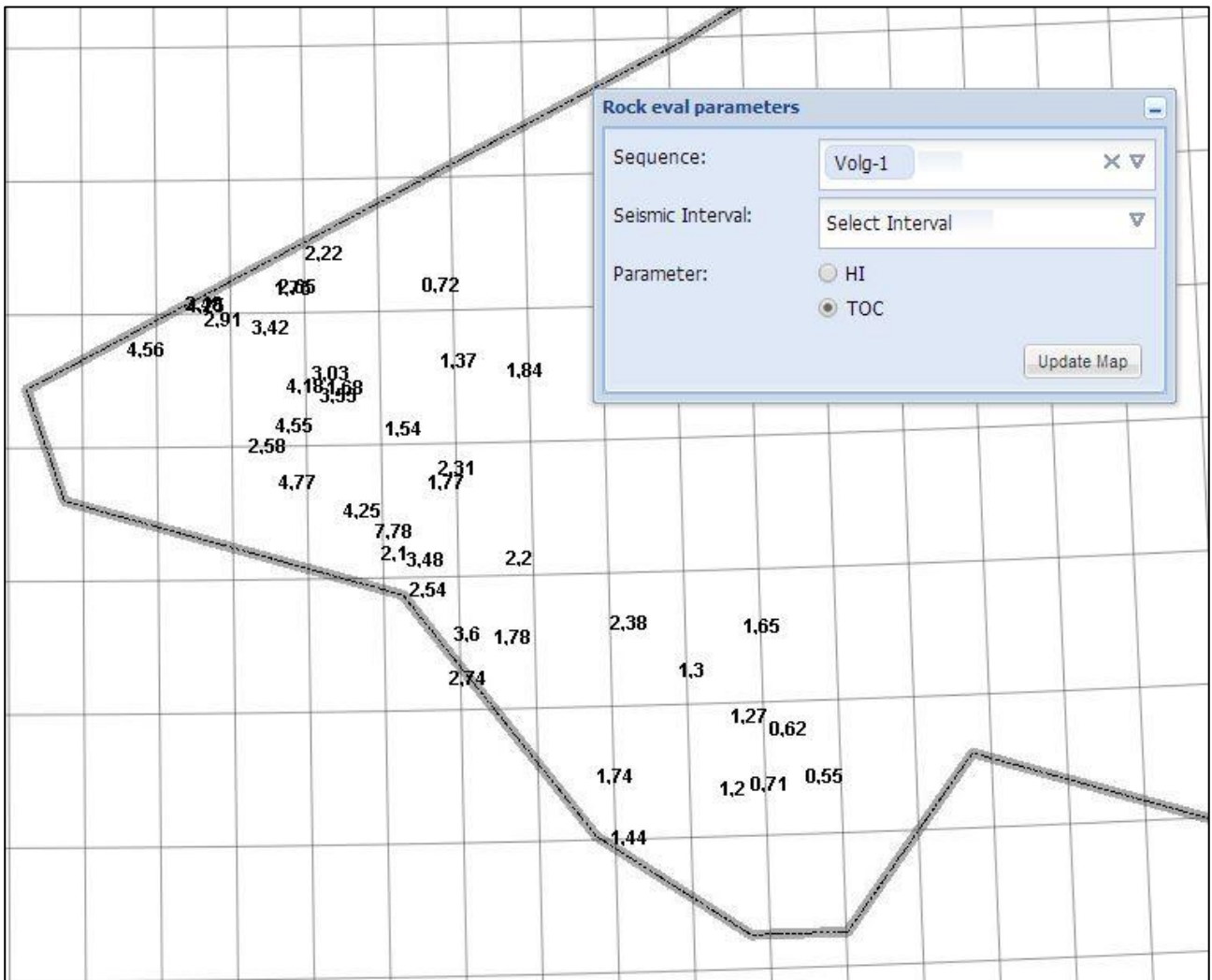


Fig 6.4: TOC values in sequence stratigraphic unit Volg-1

Middle Jurassic coaly intervals are a gas/oil prone source for the HC-accumulations (gas and waxy oil in the Søgne Basin (Petersen et al., 2000, Petersen et al., 2011). Minor amounts of coal are also present in the Bryne Formation in the southern DCG and is a candidate as the gas source to Middle Jurassic reservoirs here.

The shales of the Lower Jurassic Fjerritslev Formation are generally lean in organic matter. However, rather high TOC content is recorded in N-22 on the Gorm Field.

## 6.2 Vitrinite reflectance measurements

Vitrinite reflectance (VR) data from 53 wells are compiled totalling about 1300 data points. This includes 11 'new' wells analysed as part of the project. The data can be accessed via the lab dataset and wells buttons and can be shown both in total, by individual well and by lithostratigraphic formation /member. At each selected image the VR-values are plotted versus depth and are tabulated below. The tables can be exported in Excel format.



The top of the oil window as defined by a VR value at  $R_o\%$  0.6 show large differences in the wells, varying from less than 3000 m to about 4250 m. There is a systematic increasing depth from south to north. In Fig. 6.5 we have plotted the VR values recorded for the uppermost data point in the Farsund Formation in each well. The generally low values imply that the rich potential oil-prone mudstones in this stratigraphic part of the Farsund Formation only are marginally mature at most well locations. We realise that it is problematic to rely on single data points only, if they are not part of a well-established VR gradient. Therefore, the VR ranges shown in the figure should be used as a guide only. However, as depicted in Fig. 6.3. a downward displacement of the mid oil window takes place in the northern wells. In the Hejre-2 example, oil potential may be preserved at great burial depth (> 5000 m). The decrease of HI-values below 5000 m is a result of maturity effects.

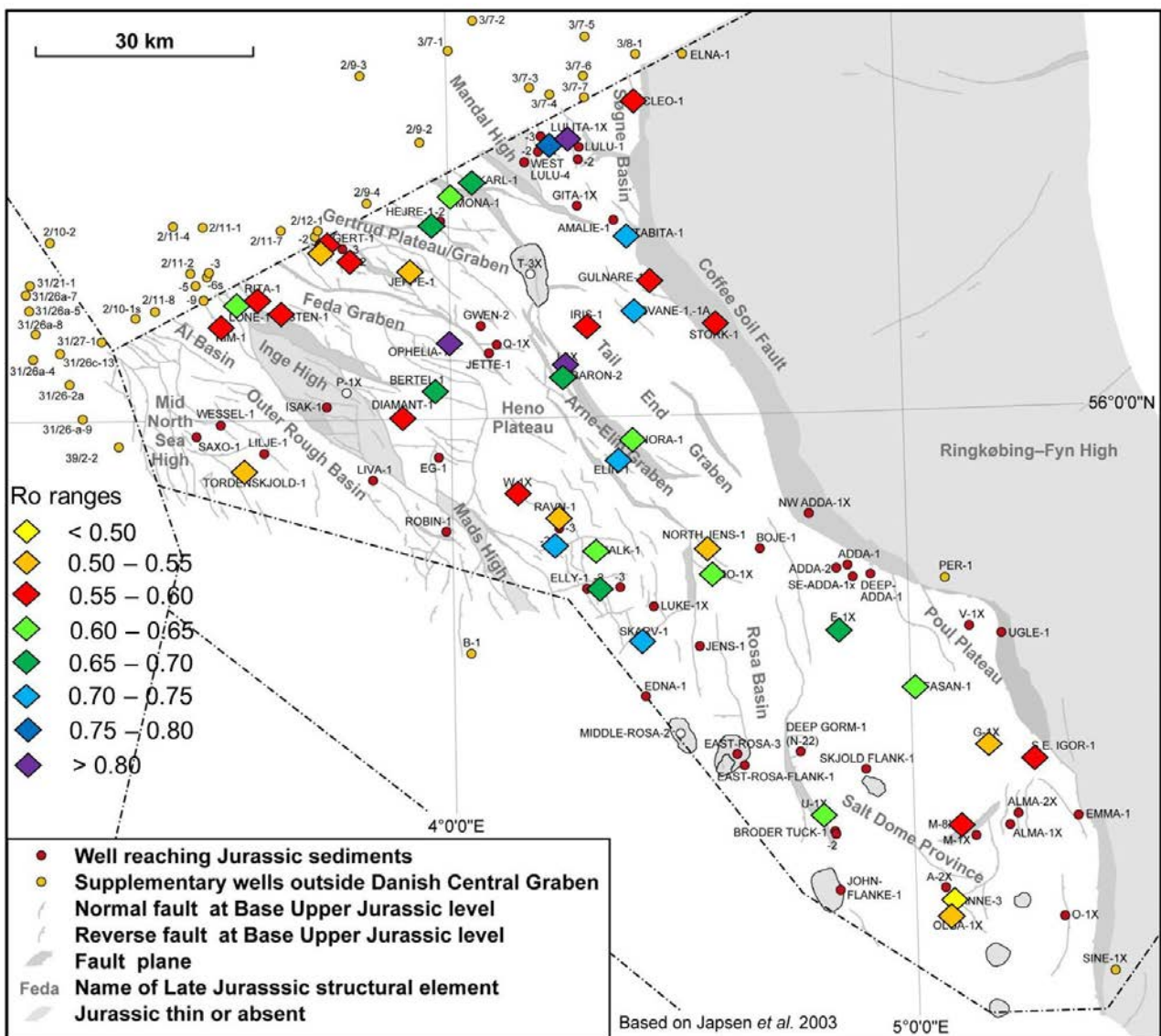


Fig 6.5: VR values recorded for the uppermost data point in the Farsund Formation in analysed wells.

Petersen et al. (2012) have analysed the vitrinite reflectance gradients in a number of deep wells with TD ranging from 4800 m to 5900 m and a thick chalk section located in the northern part of DCG and adjoining part in Norwegian waters. They noticed the overall same VR profiles characterised by three segments: (i) a more or less well-defined increase in VR through the Cenozoic, (ii) an interpolated lower gradient through the chalk section, and (iii) a likewise well-defined increase from the base of the chalk through the Farsund Formation mudstones, but with a higher gradient than determined for the Cenozoic strata. The VR values at the top of the source rock section are much lower than expected indicating that maturation is significantly retarded. It is argued that the lower VR values are controlled by two factors: (i) the high thermal conductivity of chalk accounts for the interpolated lower VR gradients in the thick chalk section, while the higher VR gradients and higher geothermal gradients in the Farsund Formation agree with low thermal conductivity of mudstone, and (ii) the thick section of overpressured mudstones serves as insulator for the overlying chalk and retard source rock maturation as excessive pressure can prevent liquid and gaseous generation products to escape. This prevents condensation and reorganisation of the organic matter, which is necessary to increase maturity. The VR profile and pressure-depth plot for the N2/11-7 well located just north of the Danish-Norwegian borderline is shown as an example (Fig. 6.6).

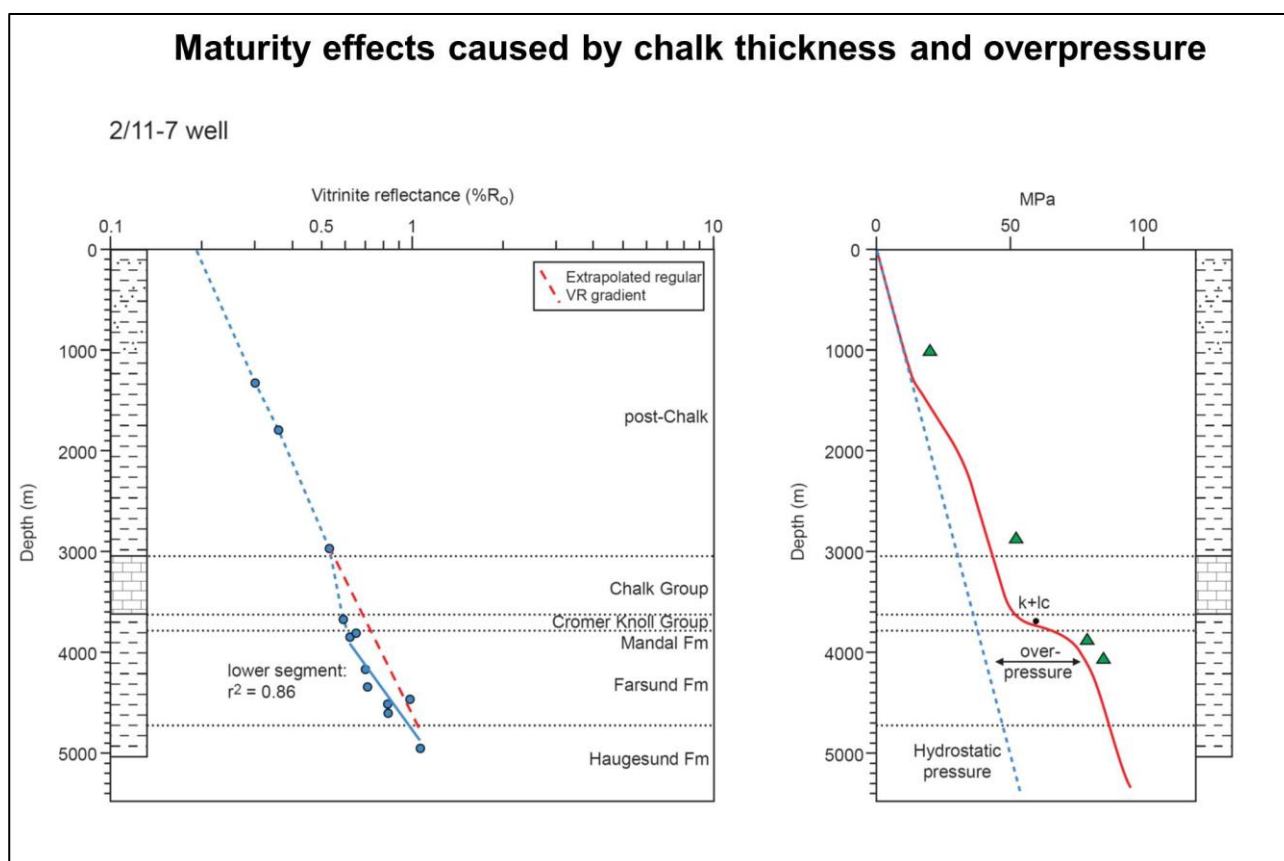


Fig. 6.6: Vitrinite reflectance and pressure gradients for the Norwegian well 2/11-7 (Petersen et al., 2013).

## 6.3 References

- Ineson, J.R., Bojesen-Kofoed, J.A., Dybkjær, K. & Nielsen, L.H. 2003: Volgian – Ryazanian ‘hot shales’ of the Bo Member (Farsund Formation) in the Danish Central Graben, North Sea: stratigraphy, facies and geochemistry. *Geol. Surv. Den.Green. Bull.* 1, 403-436.
- Passey, Q.R., Creaney, S., Kulla, J.B., Moretti, F.J. & Stroud J.D. 1990: A practical model for organic richness from porosity and resistivity logs. *AAPG Bull.*, 74, 1777-1794.
- Petersen, H.I., Andsbjerg, J., Bojesen-Kofoed, J.A., & Nytoft, H.P. 2000: Coal-generated oil: source rock evaluation and petroleum geochemistry of the Lulita oilfield, Danish North Sea. *Journal of Petroleum Geology*, 23, 55-90.
- Petersen, H.I., Holme, A.C., Thomsen, E., Whitaker, M.F., Brekke, T., Bojesen-Kofoed, J.A., Hansen, K.H. & Larsen, B.T. 2011: Hydrocarbon potential of Middle Jurassic coaly and lacustrine and Upper Jurassic – Lowermost Cretaceous marine source rocks in the Søgne Basin, North Sea. *Journal of Petroleum Geology*, Vol. 34(3), pp 277-304.
- Petersen, H.I., Andersen, C., Holme, A.C., Carr, A.D. & Thomsen, E. 2012: Vitrinite gradient of deep wells with thick chalk sections and high pressure: implications for source rock maturation, Danish – Norwegian Central Graben, North Sea. *International Journal of Coal Geology*, 100, 65-81.
- Petersen, H.I., Holme, A.C., Andersen, C., Whitaker, M.F., Nytoft, H.P. & Thomsen, E. 2013: The source rock potential of the Upper Jurassic – lowermost Cretaceous in the Danish and southern Norwegian sectors of the Central Graben, North Sea. *first break volume 32*, April 2013.



## 7 Basin Modelling

Basin modelling is a tool for integrating geological, geophysical, geochemical and petrophysical data. It serves as a framework for testing various hypotheses about the origin and evolution of the basin, its processes and the geological development of its petroleum resources.

In the following procedures are described for 1D modelling using the PetroMod®, v. 2013.2 software.

This software does not allow to model the influence of overpressure.

Event-splitting is described for well based information and information based on seismic interpretation.

### 7.1 Event-splitting using sequence stratigraphy

A fundamental necessity is to define the basin development in terms of chronostratigraphic units (events). The events are characterized by the same duration through the entire model area. However, all other parameters for the events can vary laterally in the model area. The total number of events in the geological model, including deposition, non-deposition and erosion, must be chosen in such a way that all major geological changes can be described.

Event-splitting of the Jurassic-Lowermost Cretaceous is based on the sequence stratigraphy established during the PETSYS project.

The Lower Cretaceous is treated as one event, i.e. the Cromer Knoll Group.

The Chalk Group is divided into 2 events based on GEUS in-house subdivision.

The Post Chalk Group is subdivided into 11 Tertiary Events based on maps published by Rasmussen et al. (2006) and 3 Quaternary events based on GEUS in-house subdivision.

Absolute ages for the Mesozoic are based on the Chronostratigraphic scheme established during the project and Gradstein et al. (2012). Absolute ages for the Tertiary and Quaternary are based on GEUS in-house values.

Assignment of lithologies is based on GR/DT log facies and available information from Completion Reports.

An example is shown for the Hejre-1 well in Figure 7.1.

Hejre-1 - 1D Event-Split									
Layer	Top (m)	Base (m)	Thick. (m)	Eroded (m)	Depo. from (Ma)	Depo. to (Ma)	Eroded from (Ma)	Eroded to (Ma)	Lithology
Quaternary 3	70	196	126		0.50	0.00			Sandstone (clay poor)
Quaternary 2	196	272	76		0.80	0.50			Sandstone (clay rich)
Quaternary 1	272	524	252		1.80	0.80			Sandstone (clay rich)
Sequence I	524	888	364		3.00	1.80			SHALESilt
Sequence H	888	888	0		3.60	3.00			SHALESilt
Sequence G	888	888	0		5.33	3.60			SHALESilt
Sequence F	888	1112	224		11.00	5.33			SHALESilt
Sequence E	1112	1585	473		14.80	11.00			SHALESilt
Sequence D	1585	1791	206		18.70	14.80			SHALESilt
Sequence C	1791	1847	56		21.00	18.70			SHALESilt
Sequence B	1847	1935	88		23.03	21.00			SHALESilt
Sequence A	1935	2391	456		33.90	23.03			SHALEcalc
Horda Fm.	2391	2979	588		56.00	33.90			SHALEcalc
Balder Fm.	2979	3060	81		60.90	56.00			SHALEcalc
Chalk 2	3060	3419	359		80.00	60.90			CHALK
Chalk 1	3419	3666	247		99.00	80.00			CHALK
Cromer Knoll	3666	4268	602		141.00	99.00			SHALEcalc
Ryaz-1	4268	4371	103		146.00	141.00			SHALESilt
Volg-4	4371	4426	55		148.00	146.00			SHALESilt
Volg-3	4426	4561	135		150.00	148.00			SHALESilt
Volg-2	4561	4724	163		151.00	150.00			SHALESilt
Volg-1	4724	4911	187		152.00	151.00			SHALESilt
Kimm-4	4911	4995	84		153.00	152.00			SHALESilt
Kimm-3	4995	5066	71		154.00	153.00			SHALESilt
Kimm-2	5066	5113	47		155.00	154.00			Sandstone (clay rich)
Kimm-1	5113	5113	0		157.00	155.00			SHALE
Ox-1	5113	5113	0		161.00	157.00			SHALE
Cal-1	5113	5113	0		166.00	161.00			SHALE
Bat-1	5113	5113	0		168.50	166.00			SHALE
Baj-1	5113	5113	0		170.00	168.50			SHALE
Aalen-1	5113	5113	0		174.00	170.00			SHALE
Toarc-1	5113	5113	0		183.00	174.00			SHALE
Pliens-2	5113	5113	0		187.00	183.00			SHALE
Plins-1	5113	5113	0		191.00	187.00			SHALE
Sin-1	5113	5113	0		199.50	191.00			SHALE
Hett-1	5113	5113	0		201.00	199.50			SHALE
						201.00			

Fig. 7.1: Hejre-1 well, 1D Event-Split

## 7.2 Boundary conditions

For 1D basin modelling the boundary conditions are palaeowater depth (PWD), sediment water interface temperature (SWIT) and basal heat flow (HF).

The boundary conditions define the basic energetic conditions for the temperature development for all layers, especially the source rock and, consequently, for the maturation of organic matter through time.

### PWD

Palaeowater depth estimates for the Jurassic-Lowermost Cretaceous events are based on the palaeogeographic maps prepared in the PETSYS project. A water depth of 200 m is assumed through most of the Upper Jurassic in areas dominated by offshore mudstones. A water depth of 150 m increasing to 200 and 300 m is chosen during the Cretaceous. For missing sections/hiati the water depth has been lowered to compensate for possible erosion.

Estimates of palaeowater depth for the Tertiary are based on water depth maps published by Rasmussen et al. (2006).

For Quaternary events 1 and 2 water depths are set to zero m, while present day water depth is used for Quaternary event 3.

An example for the Hejre-1 is presented in Figure 7.2.

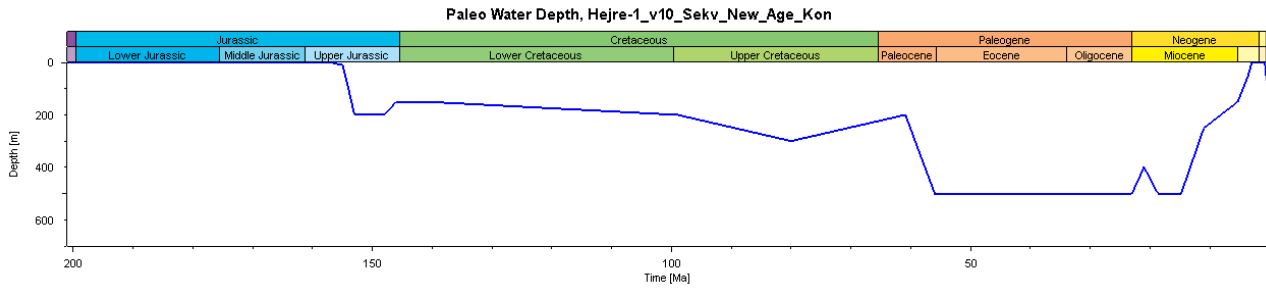


Fig. 7.2: Palaeowater depth variations through time at the Hejre-1 well location.

## SWIT

Sediment water interface temperature for each model event is derived using a build-in method in PetroMod® that based on a world-wide database and the hemisphere and continental location of the study area through time, assigns sediment water interface temperatures. The temperature calculation takes the palaeowater depth into account. An example is presented for the Hejre-1 well:

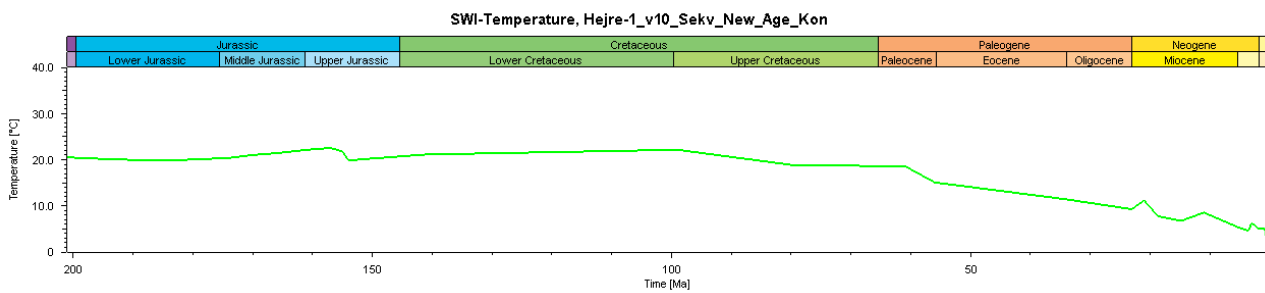


Fig. 7.3: Sediment water interface temperature variations through time at the Hejre-1 well location.

## HF

Two models of the heat flow history have been assessed. A constant heat flow ( $56 \text{ mW/m}^2$ ) model and a heat flow rift-model with a peak in the Upper Jurassic as illustrated in figures 7.4 and 7.5 for the Hejre-1 well:

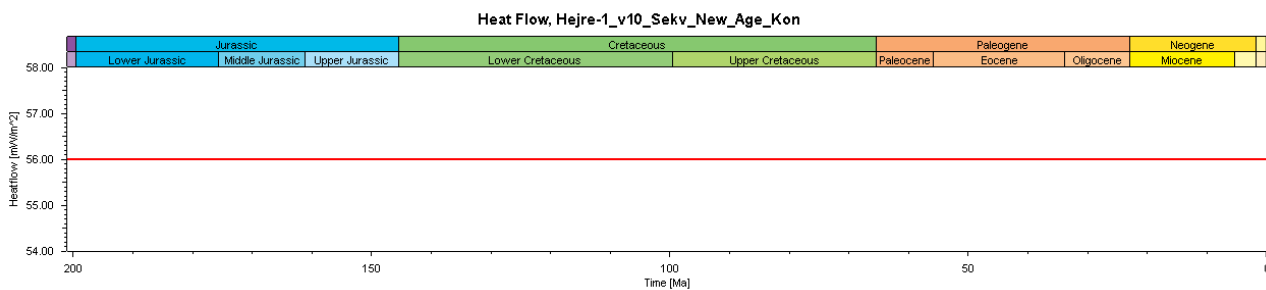


Fig. 7.4: Constant heat flow model, Hejre-1 well

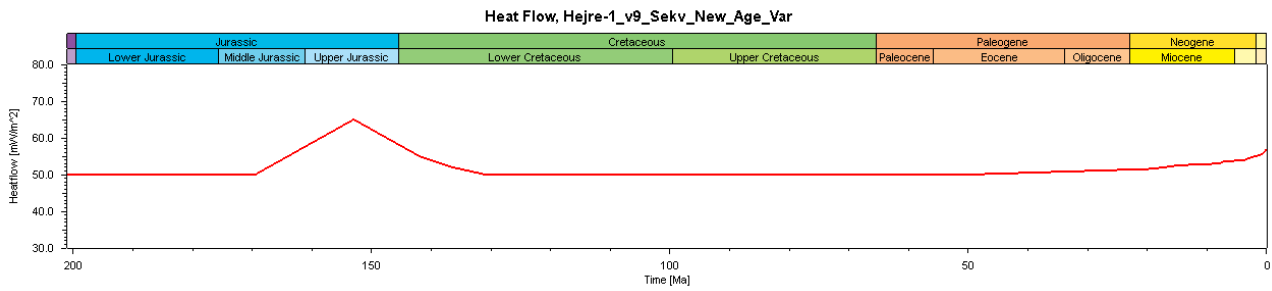


Fig. 7.5: Rift-model for heat flow, Hejre-1 well.

In the rift model a late heat flow increase has been necessary to obtain a proper match between measured and modelled temperature values. Several geological causes have been suggested, i.e. glaciation, rapid subsidence, over-pressuring, fluid flow and changing pore fluids. In addition uncertainties in control data (temperature and maturity) must be considered (Jensen & Dore, 1993).

### 7.3 Calibration

The thermal history during burial of the basin is reconstructed using 1D modelling to calibrate key wells. In PetroMod 1D modelling the EASY  $R_o$  algorithm (Sweeny & Burnham, 1990) has been used to model the maturity in terms of vitrinite reflectance.

For calibration measured vitrinite reflectance and corrected present-day temperatures are compared with the modelled values and the heat flow history is adjusted until a proper match is obtained if possible.

Vitrinite reflectance data are accessible on the [PETSYS Website](#) both under [Wells](#) and [Lab Datasets](#). They can be downloaded as Excel files and imported into the modelling programs applied.

Measured temperature values from all log runs in wells that have TD in or penetrate the Jurassic have been compiled. The temperatures have been corrected according to the correction procedures presented by Waples et al. (2004). Temperatures are accessible on the [PETSYS Website](#) under [Modelling/Calibration Data](#). Data can be downloaded as Excel files. An example is shown for the Hejre-1 well in Figure 7.6.

WELL_NAME	SURFACE_X	SURFACE_Y	KB ELEV(M)	LOG RUN	Bottom depth (m)	BHT Deg.C	Time Since Stop of Circulation (TSC)	Log file nr.	A = 3.07 x B = 0.47 x F = A / B	Ttrue = Tsurf + f x (Tmeas-Tsurf)	T min	T max		
HEJRE-1	559928,1	6233705	36,8	1	3749	101	16	18706	2,392035	1,983961	1,205687	119,9	112,1	127,7
HEJRE-1	559928,1	6233705	36,8	2	5203	156	42	18759	2,193037	2,101078	1,043767	162,4	158,9	166,0
HEJRE-1	559928,1	6233705	36,8	3	5302	160	44	18763	2,183874	2,10802	1,035983	165,4	162,1	168,8

Fig. 7.6: Corrected present-day temperatures in the Hejre-1 well.

For the wells used for modelling, the constant and variable heat flow models, in general, have provided equally good matches as exemplified by modelling results from the Hejre-1 well presented in figures 7.7 and 7.8. Hence a constant heat flow model is applied in the PETSYS project.



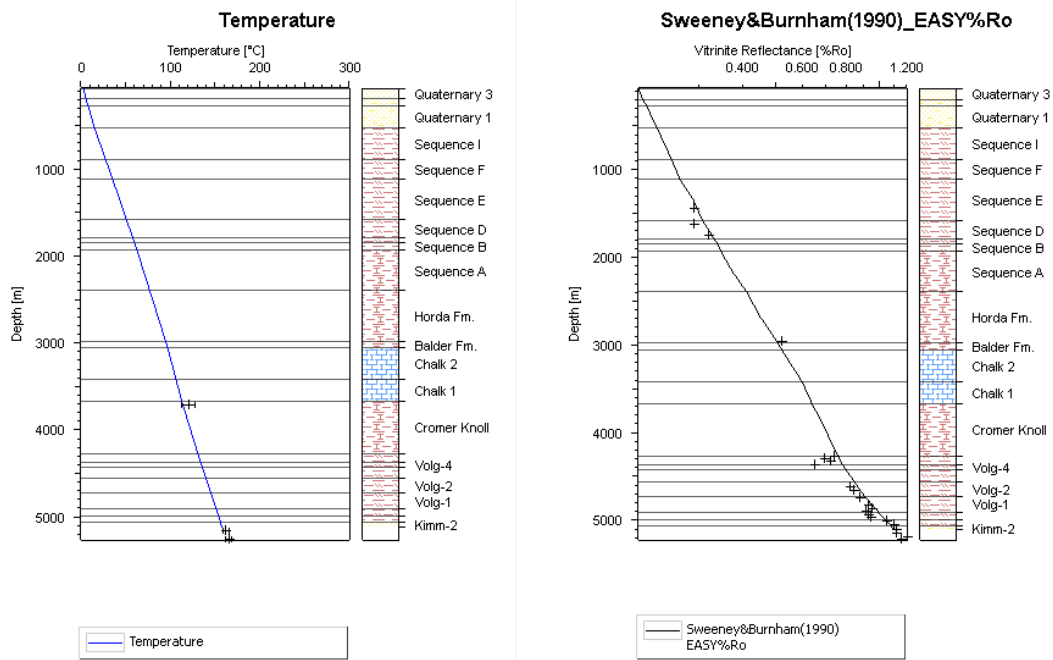


Fig. 7.7: Modelled and measured (+) temperatures and vitrinite reflectance for the Hejre-1 well using a constant heat flow of 56 mW/m<sup>2</sup>

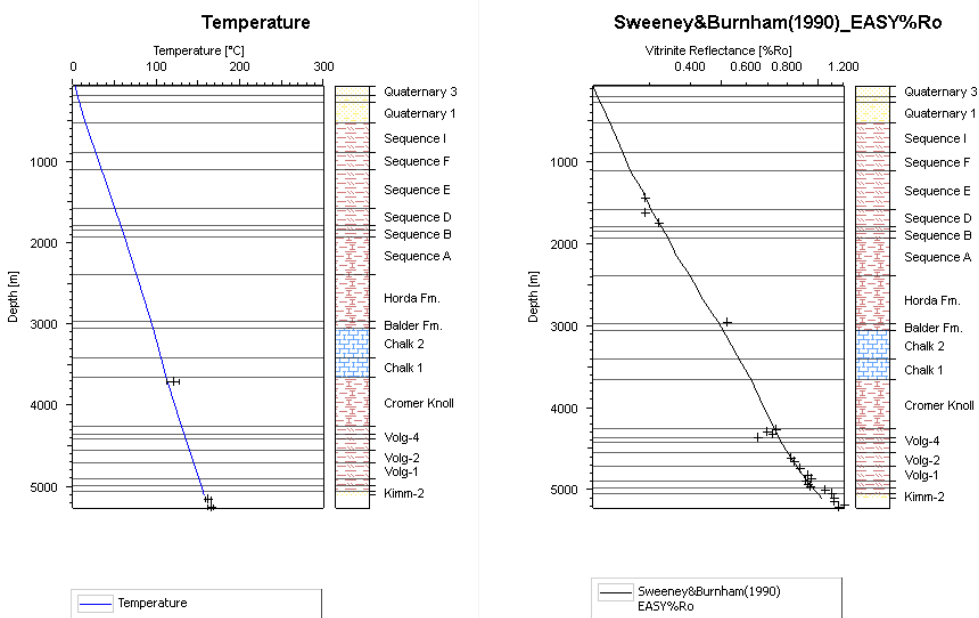


Fig. 7.8: Modelled and measured (+) temperatures and vitrinite reflectance for the Hejre-1 well using a variable heat flow rift-model

## 7.4 Event-split using seismic data

In undrilled areas 1D modelling is carried out on pseudowells (PW's), where the event-splitting is based on the seismic interpretation. An example is presented for a real well, i.e. the Hejre-1 well, where the detailed sequence stratigraphic subdivision of the Jurassic – Lowermost Cretaceous used for event-splitting has been replaced by available seismic data (Fig. 7.9).

Hejre-1 - 1D Event-Split				Simplified							
Layer	Top (m)	Base (m)	Thick. (m)	Eroded (m)	Depo. from (Ma)	Depo. to (Ma)	Eroded from (Ma)	Eroded to (Ma)	Lithology		
Quaternary	70	524	454		1.80	0.00			Sandstone (clay poor)		
Sequence I	524	888	364		3.00	1.80			SHALEsilt		
Sequence H	888	888	0		3.60	3.00			SHALEsilt		
Sequence G	888	888	0		5.33	3.60			SHALEsilt		
Sequence F	888	1112	224		11.00	5.33			SHALEsilt		
Sequence E	1112	1585	473		14.80	11.00			SHALEsilt		
Sequence D	1585	1791	206		18.70	14.80			SHALEsilt		
Sequence C	1791	1847	56		21.00	18.70			SHALEsilt		
Sequence B	1847	1935	88		23.03	21.00			SHALEsilt		
Sequence A	1935	2391	456		33.90	23.03			SHALEcalc		
Horda Fm.	2391	2979	588		56.00	33.90			SHALEcalc		
Balder Fm.	2979	3060	81		60.90	56.00			SHALEcalc		
Chalk 2	3060	3419	359		80.00	60.90			CHALK		
Chalk 1	3419	3666	247		99.00	80.00			CHALK		
Cromer Knoll	3666	4259	593		138.00	99.00			SHALEcalc		
PSSBCU_PSS43/39	4259	4386	127		145.00	138.00			SHALEsilt		
PSS43_PSS29	4386	4799	413		151.00	145.00			SHALEsilt		
PSS29_TopRavn	4799	5064	265		153.00	151.00			SHALEsilt		
TopRavn_PSS1	5064	5113	49		201.00	153.00			Sandstone (clay rich)		

Fig. 7.9: Simplified event-splitting of the Hejre-1 well using seismic data for the Jurassic – Lowermost Crertaceous and a single Quaternary event.

The age of the seismic horizons are taken from the chronostratigraphic chart that is available on the [PETSYS Website](#) under [Stratigraphy/Chronostratigraphy](#).

1D modelling shows a good match between modelled and measured values (Fig. 7.10), hence a seismic based, simplified event-split provides a good frame for the modelling work.

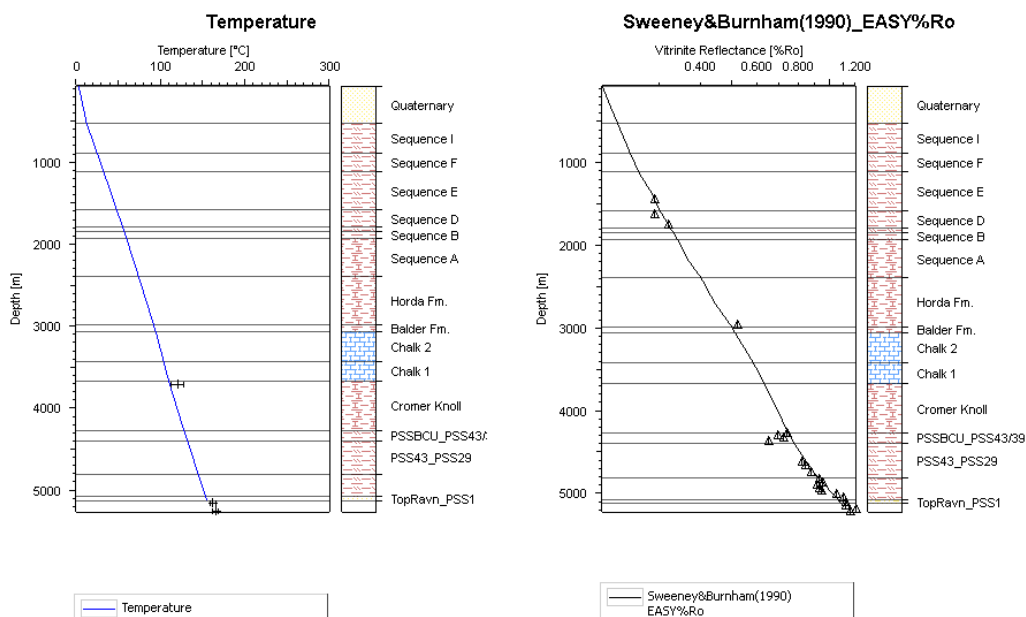
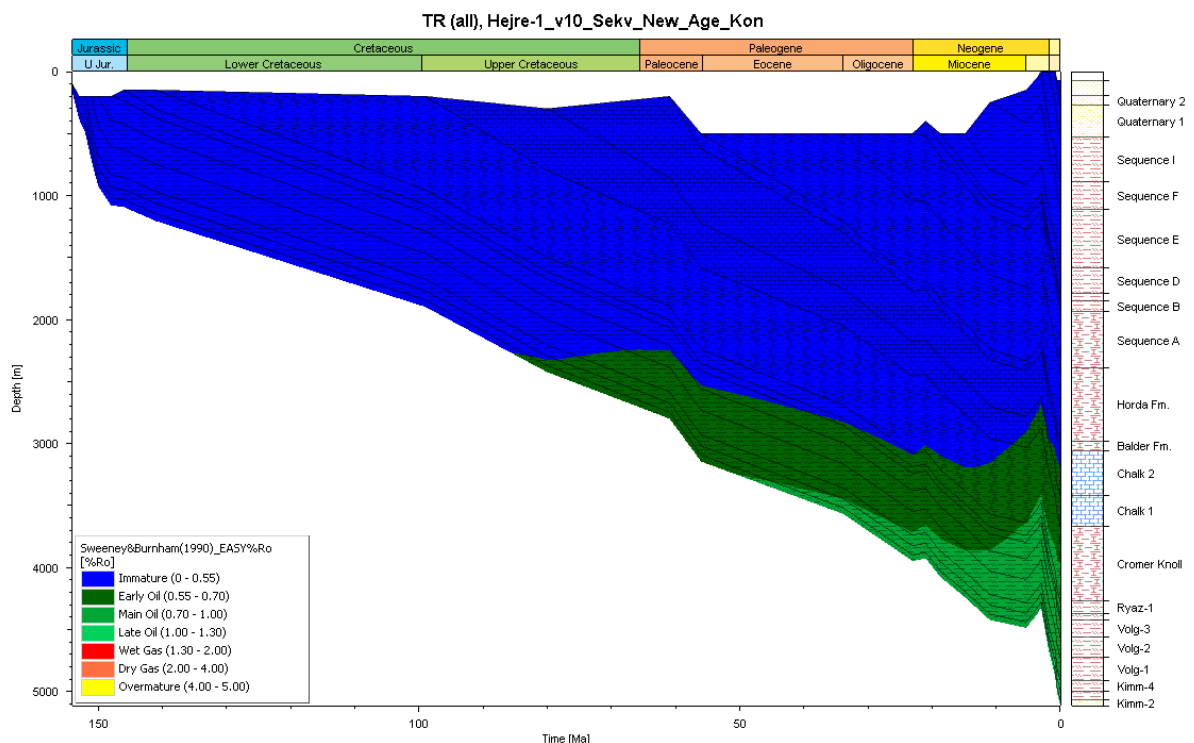


Fig. 7.10: 1D modelling shows a good match between modelled and measured values, hence a seismic based, simplified event-split provides a good frame for the modelling work.

## 7.5 Kinetics

For modelling of hydrocarbon generation history kinetic parameters for type II and III kerogen published by Pepper & Corvi (1995) are applied. An example is presented for the Hejre-1 well (Fig. 7.11), where the hydrocarbon generation history is illustrated in terms of vitrinite reflectance and the corresponding parts of the oil window.



PetroMod

Fig. 7.11: Hydrocarbon generation history at the Hejre-1 well location

## 7.6 Available data for basin modelling

1D event-split of 46 wells and 4 pseudowells (PW1 – 4) are available on the [PETSYS Website](#) under [Modelling](#) and [1D event split](#). Values for the boundary conditions are given for the 17 wells presented in the following and for the PW's. The boundary values can be accessed under [Modelling/Boundary Conditions](#).

In 17 wells (Fig. 7.12) reasonable matches have been found between measured and modelled values of temperature and vitrinite reflectance, and these wells are thus considered useful for regional calibrations:

Well name	Constant HF (mW/m <sup>2</sup> )
Alma-1	58
Cleo-1	55
Elin-1	60
Fasan-1	66
Gert-1	49
Hejre-1	56
Karl-1	52
North Jens-1	62
O-1	62
Olga-1	66
Ophelia-1	60
Rita-1	50
S.E. Igor-1	65
Skjold Flank-1	65
Sten-1	53
Svane-1A	58
Tordenskjold-1	53

*Fig. 7.12: Wells used for regional estimates of heat flow history*

A general decrease of the constant heat flow model is observed from south to north.

In general it has been found difficult to match measured and modelled vitrinite reflectance values in the Post Chalk Group. A possible reason could be a high content of reworked organic matter as observed during biostratigraphic studies, which hampers the possibility of locating autochthonous vitrinite particles suitable for measurements. Main emphasis has been given to obtain a proper match between modelled and measured vitrinite reflectance in the Mesozoic sequence.

For an overview of likely source rock intervals the composite logs provide an overview of the relation between organic rich horizons and sequence stratigraphic and seismic picks (Fig. 7.13).

# OPHELIA-1

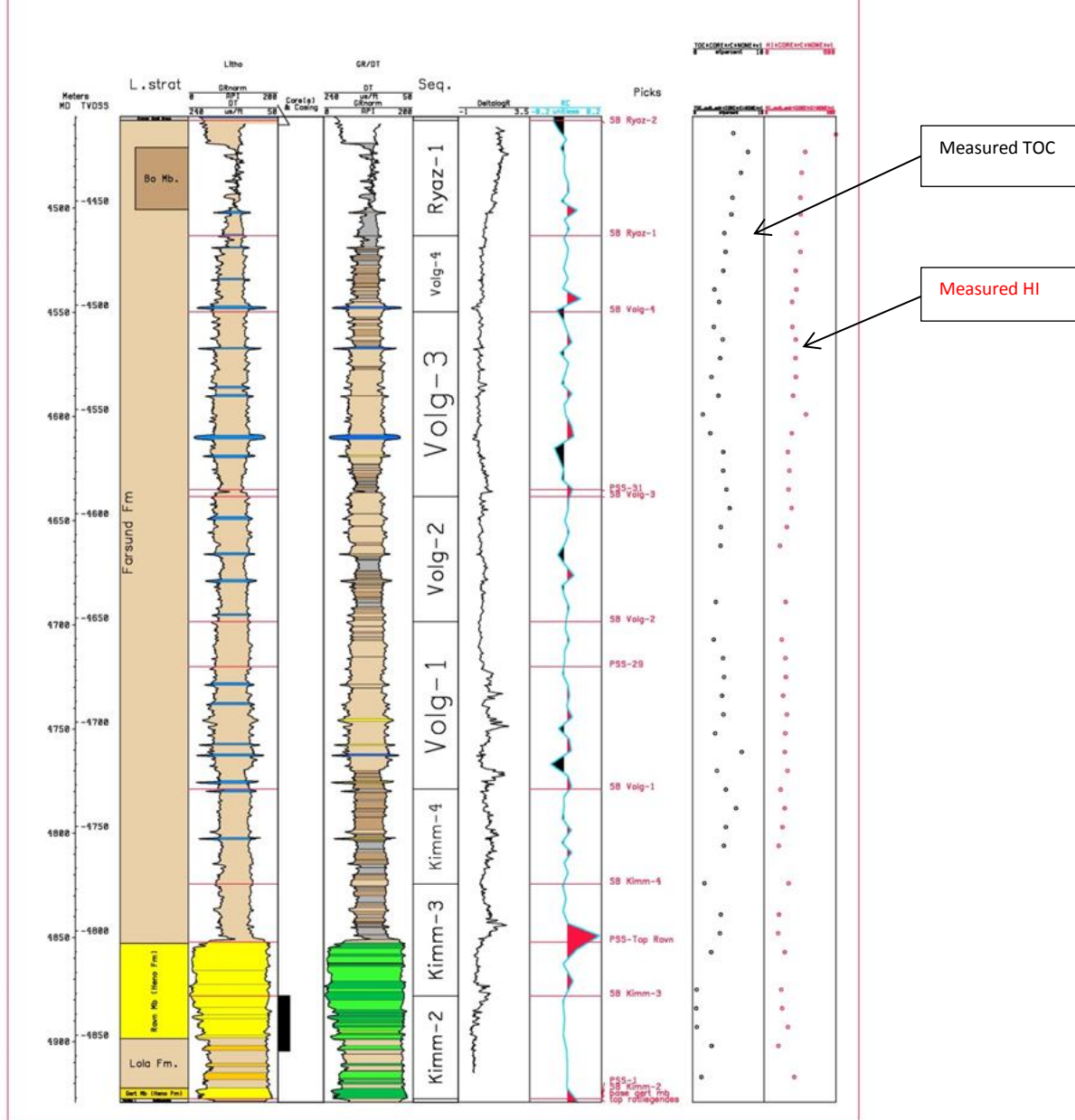


Fig. 7.13: Composite log of Ophelia-1. Note organic rich horizons located in sequences Kimm-3 to Volg-1, which can be mapped seismically as the interval between PSS\_29 and PSS\_15\_TopRavn.

As shown in Fig. 7.13 the organic rich horizons have low Hydrogen Index values, i.e. 140 - 200. Modelling of the transformation ratio and the corresponding vitrinite reflectance for the mid-point of the Kimm-4 sequence shows a transformation ratio of 0.81 and a vitrinite reflectance value of 1.05 %R<sub>o</sub> (Fig. 7.14). Hence the effect of maturation (generation) must be considered. Using programs like PEGIS© for restoration, original HI values of more than 500 have been calculated.

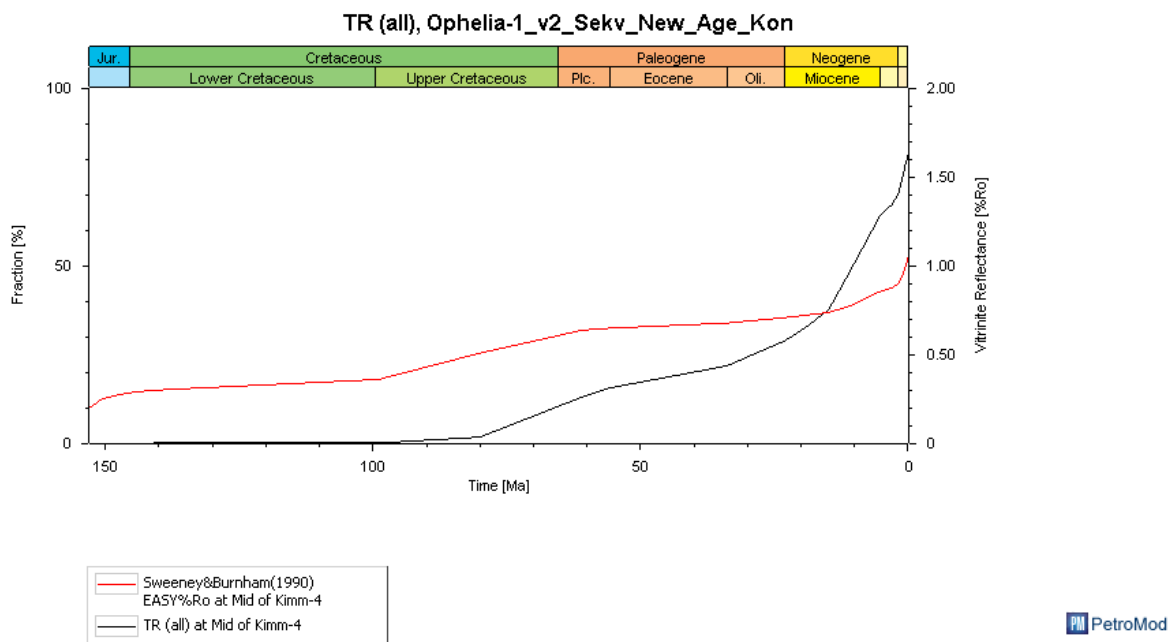


Fig. 7.14: Modelling of transformation ratio (TR) and vitrinite reflectance for the Kimm-4 event in the Ophelia-1 well.

Composite logs are found on the [PETSYS Website](#) under the [Wells](#) button.

Another approach using the [PETSYS Website](#) is the [Map/Map Data/Rock-Eval data](#) facility or the [Lab Datasets/Rock Eval data](#) facility.

## 7.7 2D Basin Modelling

2D Modelling procedures and modelling results will be presented at the final workshop.

## 7.8 References

Gradstein, F.M., Ogg, J.G., Schmitz, M.D., Ogg, G.M., 2012. The geological timescale 2012. Elsevier, Oxford, U.K.

Jensen, R.P. & Dore´, A.G. 1993: A recent Norwegian Shelf heating event – fact or fantasy? – in Dore´ et al. (eds): Basin Modelling: Advances and Applications, NPF Special Publication 3, 85-106.

Pepper, A.S. & Corvi, P.J. 1995: Simple kinetic models of petroleum formation. Part I: oil and gas generation from kerogen. - *Marine and Petroleum Geology*, 12 (3): 291-319.

Rasmussen, E.S., Piasecki, S., Andsbjerg, J., Dybkjær, K., Vejbæk, O.V., Jacobsen, C., Britze, P. & Bryde-Auken, M. 2005: Cenozoic maps of the Danish North Sea area. – GEUS report 2005/33.

Sweeny, R.E. & Burnham, A.K. 1990: Evaluation of a simple model of vitrinite reflectance based on chemical kinetics. – *AAPG Bulletin*, v. 74, 1559 – 1570.

Waples, D.W., Pedersen, M.R. & Kuijpers, P. 2004: Correction of Single Log-Derived Temperatures in the Danish Central Graben, North Sea. – *Natural Resources Research*, Vol. 13, No. 4, December 2004.





## 8 Analysis of oils and source rock extracts using GC-MS and GC-MS-MS

### 8.1 Extraction

Source rocks were extracted using a Soxtec System HT 2 1045 Extraction Unit using dichloromethane/methanol (93:7 vol/vol).

### 8.2 Separation

Oils or extracts were transferred to a pre-weighed vial. After a couple of days, a constant weight was obtained. The residue, which consists of compounds having more than approximately 15 carbon atoms, is called the C15+ fraction. The asphaltenes were removed from oils and extracts by precipitation in at least a 40 fold excess of *n*-pentane. The asphaltene-free oil or extract was fractionated into three fractions (saturated hydrocarbons, aromatic hydrocarbons and polar compounds or NSO) by MPLC (Radke et al., 1980).

### 8.3 Gas chromatography-mass spectrometry (GC-MS and GC-MS-MS)

Gas chromatography-mass spectrometry (GC-MS and GC-MS-MS) was carried out using a Hewlett-Packard 6890N gas chromatograph connected to a Waters (Micromass) Quattro Micro GC tandem quadrupole mass spectrometer (photo). The GC was fitted with an Agilent HP-5 or Phenomenex ZB-5 column (30 m x 0.25 mm i.d., film thickness 0.10  $\mu$ m). The temperature program was 30°C/min from 70 to 100°C and 4°C/min from 100 to 308°C followed by 8 min at 308°C. The samples were dissolved in isooctane, and the concentration was 0.5 mg/100 $\mu$ l (GC-MS) or 1 mg/100 $\mu$ l (GC-MS-MS). Splitless injection was used.

## GC/MS, SIM

*m/z* 71.10 *n*-alkanes

*m/z* 177.16 25-norhopanes

*m/z* 191.18 hopanes

*m/z* 205.20 methylhopanes

*m/z* 217.20 steranes

*m/z* 218.20 steranes

*m/z* 231.21 methylsteranes

*m/z* 253.20 monoaromatic steranes (should be absent in sat. fraction)

*m/z* 355.35 25- and 28-norhopanes

*m/z* 369.35 hopanes

*M/z* 71, 191, 217 and 218 mass chromatograms.

## GC-MS-MS, transitions, MRM

372.38 → 217.20 C<sub>27</sub> steranes

386.39 → 217.20 C<sub>28</sub> steranes

400.41 → 217.20 C<sub>29</sub> steranes

414.42 → 217.20 C<sub>30</sub> steranes

370.36 → 191.18 C<sub>27</sub> hopanes

384.38 → 191.18 C<sub>28</sub> hopanes

398.39 → 191.18 C<sub>29</sub> hopanes

412.41 → 191.18 C<sub>30</sub> hopanes

426.42 → 191.18 C<sub>31</sub> hopanes

440.44 → 191.18 C<sub>32</sub> hopanes

454.45 → 191.18 C<sub>33</sub> hopanes

468.47 → 191.18 C<sub>34</sub> hopanes

482.49 → 191.18 C<sub>35</sub> hopanes

Dwell time: 0.04 sec. /transition. Inter scan delay: 0.07 sec. Inter channel delay: 0.01 sec.

Hopanes and steranes were quantified using GC-MS data ( $m/z$  191 and 217 respectively). Only a few steranes such as the regular C<sub>29</sub> steranes are separated in the  $m/z$  217 mass chromatogram. In order to quantify all C<sub>27</sub> – C<sub>30</sub> diasteranes and steranes ((4 + 4) x 4 = 32), GC-MS-MS data must be used. Only a few sterane ratios can be measured reliably using GC-MS. See also Fowler and Brooks (1989).

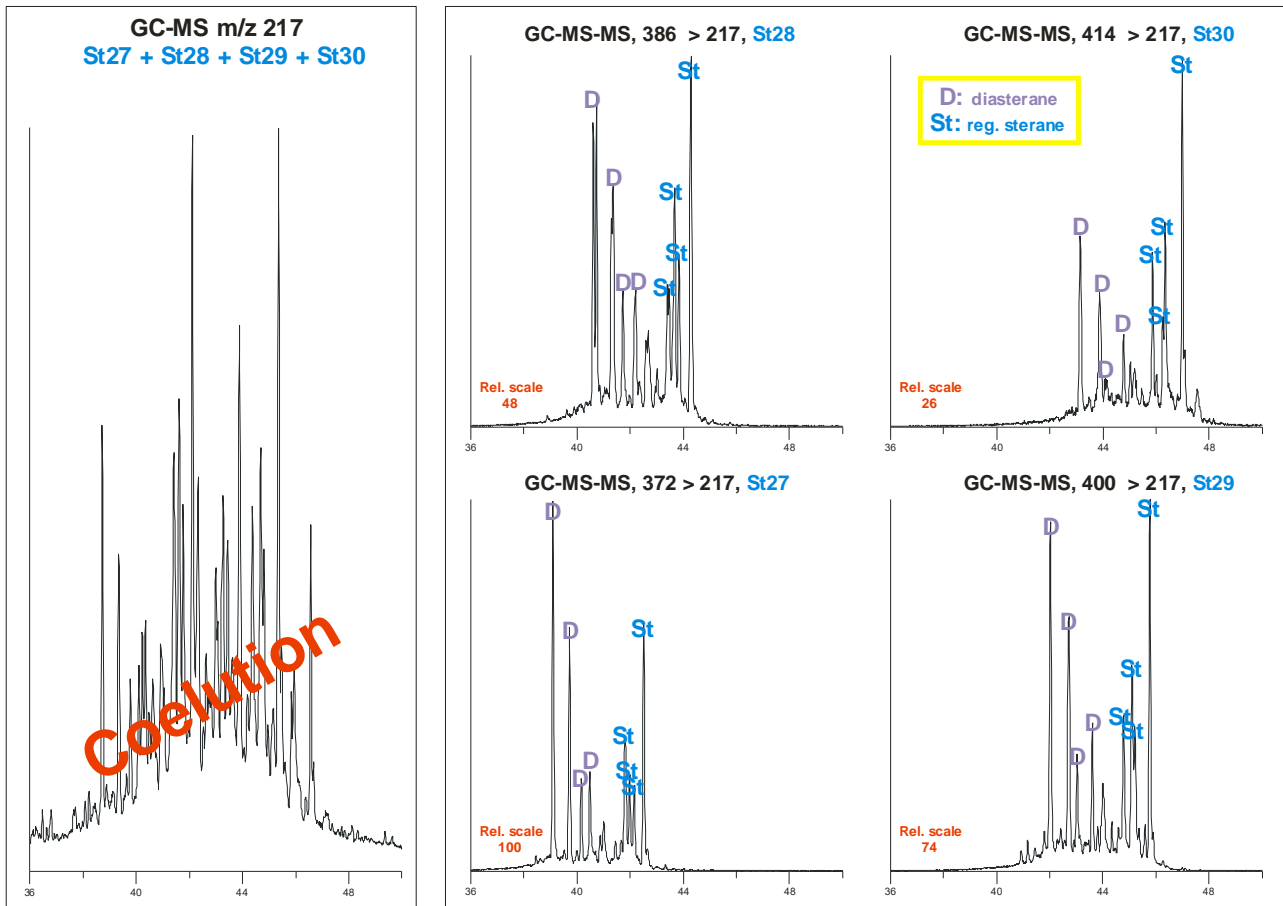


Figure 8.1: Sterane analysis, GC-MS versus GC-MS-MS.

Some hopanes also coelute in the  $m/z$  191 mass chromatogram. A few examples can be mentioned: 28,30-Bisnorhopane (BNH) coelutes with an unidentified  $C_{30}$  hopane and the  $C_{30}$  neohopane (C30Ts) coelutes with a norgammacerane. Common biomarker ratios for each of the oils are presented in single pdf-files which have been uploaded onto the PETSYS Website (hopane ratios: page 1; sterane ratios: page 2). The A-2 oil is shown as an example on pages 7 - 8. GC-MS-MS (MRM) and GC-MS (SIM) may yield slightly different relative response factors for the various compounds. Quantification of compounds is based on peak areas – not peak heights.



*Figure 8.2: GC-MS laboratory.*

## Calculation of hopane ratios

Hopane ratios are self-explanatory with a single exception:

HHI = C<sub>35</sub> Homohopane Index:  $(H35\alpha\beta S + H35\alpha\beta R) / (H31\alpha\beta S + H31\alpha\beta R + H32\alpha\beta S + H32\alpha\beta R + H33\alpha\beta S + H33\alpha\beta R + H34\alpha\beta S + H34\alpha\beta R + H35\alpha\beta S + H35\alpha\beta R)$ .

## Key to steranes (abbreviated sterane names according to NIGOGA, 2000)

### C<sub>27</sub> steranes (372 > 217)

27dβS 13β(H), 17α(H), 20(S)-cholestane (diasterane)

27dβR 13β(H), 17α(H), 20(R)-cholestane (diasterane)

27dαR 13α(H), 17β(H), 20(R)-cholestane (diasterane)

27dαS 13α(H), 17β(H), 20(S)-cholestane (diasterane)

27ααS 5α(H), 14α(H), 17α(H), 20(S)-cholestane

27ββR 5α(H), 14β(H), 17β(H), 20(R)-cholestane

27ββS 5α(H), 14β(H), 17β(H), 20(S)-cholestane

27ααR 5α(H), 14α(H), 17α(H), 20(R)-cholestane

### C<sub>28</sub> steranes (386 > 217)

28dβS 24-methyl-13β(H), 17α(H), 20(S)-cholestane (diasterane)

28dβR 24-methyl-13β(H), 17α(H), 20(R)-cholestane (diasterane)

28dαR 24-methyl-13α(H), 17β(H), 20(R)-cholestane (diasterane)

28dαS 24-methyl-13α(H), 17β(H), 20(S)-cholestane (diasterane)

28ααS 24-methyl-5α(H), 14α(H), 17α(H), 20(S)-cholestane

28ββR 24-methyl-5α(H), 14β(H), 17β(H), 20(R)-cholestane

28ββS 24-methyl-5α(H), 14β(H), 17β(H), 20(S)-cholestane

28ααR 24-methyl-5α(H), 14α(H), 17α(H), 20(R)-cholestane

## C<sub>29</sub> steranes (400 > 217)

29d $\beta$ S	24-ethyl-13 $\beta$ (H), 17 $\alpha$ (H), 20(S)-cholestane (diasterane)
29d $\beta$ R	24-ethyl-13 $\beta$ (H), 17 $\alpha$ (H), 20(R)-cholestane (diasterane)
29d $\alpha$ R	24-ethyl-13 $\alpha$ (H), 17 $\beta$ (H), 20(R)-cholestane (diasterane)
29d $\alpha$ S	24-ethyl-13 $\alpha$ (H), 17 $\beta$ (H), 20(S)-cholestane (diasterane)
29 $\alpha\alpha$ S	24-ethyl-5 $\alpha$ (H), 14 $\alpha$ (H), 17 $\alpha$ (H), 20(S)-cholestane
29 $\beta\beta$ R	24-ethyl-5 $\alpha$ (H), 14 $\beta$ (H), 17 $\beta$ (H), 20(R)-cholestane
29 $\beta\beta$ S	24-ethyl-5 $\alpha$ (H), 14 $\beta$ (H), 17 $\beta$ (H), 20(S)-cholestane
29 $\alpha\alpha$ R	24-ethyl-5 $\alpha$ (H), 14 $\alpha$ (H), 17 $\alpha$ (H), 20(R)-cholestane

## C<sub>30</sub> steranes (414 > 217)

30d $\beta$ S	24- <i>n</i> -propyl-13 $\beta$ (H), 17 $\alpha$ (H), 20(S)-cholestane (diasterane)
30d $\beta$ R	24- <i>n</i> -propyl-13 $\beta$ (H), 17 $\alpha$ (H), 20(R)-cholestane (diasterane)
30d $\alpha$ R	24- <i>n</i> -propyl-13 $\alpha$ (H), 17 $\beta$ (H), 20(R)-cholestane (diasterane)
30d $\alpha$ S	24- <i>n</i> -propyl-13 $\alpha$ (H), 17 $\beta$ (H), 20(S)-cholestane (diasterane)
30 $\alpha\alpha$ S	24- <i>n</i> -propyl-5 $\alpha$ (H), 14 $\alpha$ (H), 17 $\alpha$ (H), 20(S)-cholestane
30 $\beta\beta$ R	24- <i>n</i> -propyl-5 $\alpha$ (H), 14 $\beta$ (H), 17 $\beta$ (H), 20(R)-cholestane
30 $\beta\beta$ S	24- <i>n</i> -propyl-5 $\alpha$ (H), 14 $\beta$ (H), 17 $\beta$ (H), 20(S)-cholestane
30 $\alpha\alpha$ R	24- <i>n</i> -propyl-5 $\alpha$ (H), 14 $\alpha$ (H), 17 $\alpha$ (H), 20(R)-cholestane

## Sterane ratios

Diasteranes (Dia) vs. regular steranes (Reg) for C<sub>27</sub>, C<sub>28</sub> & C<sub>29</sub> steranes.

Sterane isomerisation, 20S/(20S + 20R) for C<sub>27</sub>, C<sub>28</sub> & C<sub>29</sub> steranes.

5 $\alpha$ (H),14 $\beta$ (H),17 $\beta$ (H)-steranes ( $\beta\beta$ ) vs. 5 $\alpha$ (H),14 $\alpha$ (H),17 $\alpha$ (H)-steranes ( $\alpha\alpha$ ) for C<sub>27</sub>, C<sub>28</sub> & C<sub>29</sub>.

% C<sub>27</sub>, C<sub>28</sub> & C<sub>29</sub> steranes (C<sub>27</sub> + C<sub>28</sub> + C<sub>29</sub> = 100).

% C<sub>30</sub> steranes (C<sub>27</sub> + C<sub>28</sub> + C<sub>29</sub> + C<sub>30</sub> = 100).

Sterane ratio	MRM transition, (pdf)	Definition
C27 Dia/(Dia + Reg)	372 → 217 (St27)	(27d $\beta$ S+27d $\beta$ R+27d $\alpha$ R+27d $\alpha$ S)/ (27d $\beta$ S+27d $\beta$ R+27d $\alpha$ R+27d $\alpha$ S+27 $\alpha\alpha$ S+27 $\beta\beta$ R+27 $\beta\beta$ S+27 $\alpha\alpha$ R)
C28 Dia/(Dia + Reg)	386 → 217 (St28)	(28d $\beta$ S+28d $\beta$ R+28d $\alpha$ R+28d $\alpha$ S)/ (28d $\beta$ S+28d $\beta$ R+28d $\alpha$ R+28d $\alpha$ S+28 $\alpha\alpha$ S+28 $\beta\beta$ R+28 $\beta\beta$ S+28 $\alpha\alpha$ R)
C29 Dia/(Dia + Reg)	400 → 217 (St29)	(29d $\beta$ S+29d $\beta$ R+29d $\alpha$ R+29d $\alpha$ S)/ (29d $\beta$ S+29d $\beta$ R+29d $\alpha$ R+29d $\alpha$ S+29 $\alpha\alpha$ S+29 $\beta\beta$ R+29 $\beta\beta$ S+29 $\alpha\alpha$ R)
C27 20S/(20S + 20R)	372 → 217 (St27)	27 $\alpha\alpha$ S/(27 $\alpha\alpha$ S+27 $\alpha\alpha$ R)
C28 20S/(20S + 20R)	386 → 217 (St28)	28 $\alpha\alpha$ S/(28 $\alpha\alpha$ S+28 $\alpha\alpha$ R)
C29 20S/(20S + 20R)	400 → 217 (St29)	29 $\alpha\alpha$ S/(29 $\alpha\alpha$ S+29 $\alpha\alpha$ R)



C27 $\beta\beta/(\alpha\alpha+\beta\beta)$	372 → 217 (St27)	$(27\beta\beta R+27\beta\beta S)/(27\alpha\alpha S+27\beta\beta R+27\beta\beta S+27\alpha\alpha R)$
C28 $\beta\beta/(\alpha\alpha+\beta\beta)$	386 → 217 (St28)	$(28\beta\beta R+28\beta\beta S)/(28\alpha\alpha S+28\beta\beta R+28\beta\beta S+28\alpha\alpha R)$
C29 $\beta\beta/(\alpha\alpha+\beta\beta)$	400 → 217 (St29)	$(29\beta\beta R+29\beta\beta S)/(29\alpha\alpha S+29\beta\beta R+29\beta\beta S+29\alpha\alpha R)$

% C27 sterane 372, 386, 400 → 217  
(St27, St28, St29)

$$100(27d\beta S+27d\beta R+27d\alpha R+27d\alpha S+27\alpha\alpha S+27\beta\beta R+27\beta\beta S+27\alpha\alpha R)/$$

$$(27d\beta S+27d\beta R+27d\alpha R+27d\alpha S+27\alpha\alpha S+27\beta\beta R+27\beta\beta S+27\alpha\alpha R+$$

$$28d\beta S+28d\beta R+28d\alpha R+28d\alpha S+28\alpha\alpha S+28\beta\beta R+28\beta\beta S+28\alpha\alpha R+$$

$$29d\beta S+29d\beta R+29d\alpha R+29d\alpha S+29\alpha\alpha S+29\beta\beta R+29\beta\beta S+29\alpha\alpha R)$$

% C28 sterane 372, 386, 400 → 217  
(St27, St28, St29)

$$100(28d\beta S+28d\beta R+28d\alpha R+28d\alpha S+28\alpha\alpha S+28\beta\beta R+28\beta\beta S+28\alpha\alpha R)/$$

$$(27d\beta S+27d\beta R+27d\alpha R+27d\alpha S+27\alpha\alpha S+27\beta\beta R+27\beta\beta S+27\alpha\alpha R+$$

$$28d\beta S+28d\beta R+28d\alpha R+28d\alpha S+28\alpha\alpha S+28\beta\beta R+28\beta\beta S+28\alpha\alpha R+$$

$$29d\beta S+29d\beta R+29d\alpha R+29d\alpha S+29\alpha\alpha S+29\beta\beta R+29\beta\beta S+29\alpha\alpha R)$$

% C29 sterane 372, 386, 400 → 217  
(St27, St28, St29)

$$100(29d\beta S+29d\beta R+29d\alpha R+29d\alpha S+29\alpha\alpha S+29\beta\beta R+29\beta\beta S+29\alpha\alpha R)/$$

$$(27d\beta S+27d\beta R+27d\alpha R+27d\alpha S+27\alpha\alpha S+27\beta\beta R+27\beta\beta S+27\alpha\alpha R+$$

$$28d\beta S+28d\beta R+28d\alpha R+28d\alpha S+28\alpha\alpha S+28\beta\beta R+28\beta\beta S+28\alpha\alpha R+$$

$$29d\beta S+29d\beta R+29d\alpha R+29d\alpha S+29\alpha\alpha S+29\beta\beta R+29\beta\beta S+29\alpha\alpha R)$$

% C30 sterane 372, 386, 400, 414 → 217  
(St27, St28, St29, St30)

$$100(30d\beta S+30d\beta R+30d\alpha R+30d\alpha S+30\alpha\alpha S+30\beta\beta R+30\beta\beta S+30\alpha\alpha R)/$$

$$(27d\beta S+27d\beta R+27d\alpha R+27d\alpha S+27\alpha\alpha S+27\beta\beta R+27\beta\beta S+27\alpha\alpha R+$$

$$28d\beta S+28d\beta R+28d\alpha R+28d\alpha S+28\alpha\alpha S+28\beta\beta R+28\beta\beta S+28\alpha\alpha R+$$

$$29d\beta S+29d\beta R+29d\alpha R+29d\alpha S+29\alpha\alpha S+29\beta\beta R+29\beta\beta S+29\alpha\alpha R+$$

$$30d\beta S+30d\beta R+30d\alpha R+30d\alpha S+30\alpha\alpha S+30\beta\beta R+30\beta\beta S+30\alpha\alpha R)$$

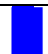
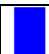
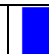
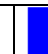
















A-2 oil, DST 8, 30-01-1978

Source age: Jurassic

GEUS no. 2010023-18491

## Hopane ratios








Ratio	MRM transition	Value	SIM	Value
C27 Ts/(Ts+Tm)	370 → 191	0.652	191	0.60
C29 Ts/(Ts+H29αβ)	398 → 191	0.357	191	0.31
C30Ts/H30αβ	412 → 191	0.054	n.a.	n.a.
E30/H30αβ	412 → 191	0.027	191	n.a.
D30/H30αβ	412 → 191	0.086	191	0.07
D31/H30αβ	426 → 191, 412 → 191	0.026 + 0.024	n.a.	n.a.
H30β <sub>α</sub> /H30αβ	412 → 191	0.063	191	0.12
BNH/H30αβ	384 → 191, 412 → 191	0.135	191	0.13
H29αβ/30αβ	398 → 191, 412 → 191	0.471	191	0.46
H31αβ/H30αβ	426 → 191, 412 → 191	0.383 + 0.290	191	0.39 + 0.29
H32αβ/H30αβ	440 → 191, 412 → 191	0.237 + 0.173	191	0.26 + 0.20
H33αβ/H30αβ	454 → 191, 412 → 191	0.149 + 0.107	191	0.17 + 0.13
H34αβ/H30αβ	468 → 191, 412 → 191	0.075 + 0.055	191	0.09 + 0.06
H35αβ/H30αβ	482 → 191, 412 → 191	0.052 + 0.039	191	0.06 + 0.05
H31αβ	426 → 191	0.569	191	0.57
H32αβ	440 → 191	0.578	191	0.56
H35/H34	482 → 191, 468 → 191	0.71	191	0.74
HHI	426 – 482 → 191	0.059	191	0.07
Gammacerane/H30	412 → 191	< 0.01	191	n.a.

																				
H27	H28	H29	H30	H31	H32	H33	H34	H35		m/z 71	m/z 177	m/z 191L	m/z 191S	191	m/z 205	m/z 355				

## Sterane ratios

Ratio	MRM transition	Value	SIM	Value
C27	372 → 217	0.544	n.a.	n.a.
C28	386 → 217	0.521	n.a.	n.a.
C29	400 → 217	0.494	n.a.	n.a.
C27	372 → 217	0.417	n.a.	n.a.
C28	386 → 217	0.353	n.a.	n.a.
C29	400 → 217	0.320	217	0.36
C27	372 → 217	0.296	n.a.	n.a.
C28	386 → 217	0.409	n.a.	n.a.
C29	400 → 217	0.419	217	0.40
% C27 sterane	372, 386, 400 → 217	34.94	n.a.	n.a.
% C28 sterane	372, 386, 400 → 217	30.16	n.a.	n.a.
% C29 sterane	372, 386, 400 → 217	34.91	n.a.	n.a.
% C30 sterane	372, 386, 400, 414 → 217	7.58	n.a.	n.a.

Sterane/hopane	$\Sigma M^+ \rightarrow 217 / \Sigma M^+ \rightarrow 191$	2.48	n.a.	n.a.
----------------	---	------	------	------

																		
St27	St28	St29	St30		m/z	m/z	217											

These data sheets will be found in the wells/biomarker folder as well as in the Lab datasets/Biomarker folder. Clicking on the blue or red icons below the tables will show individual

integrated chromatograms (will only work on pdf-files downloaded to Adobe Acrobat - not here).  
The data will also be available in an Excel spreadsheet.

All A-2 oil chromatograms with identification of the major and minor compounds are shown on pages 9 - 24.

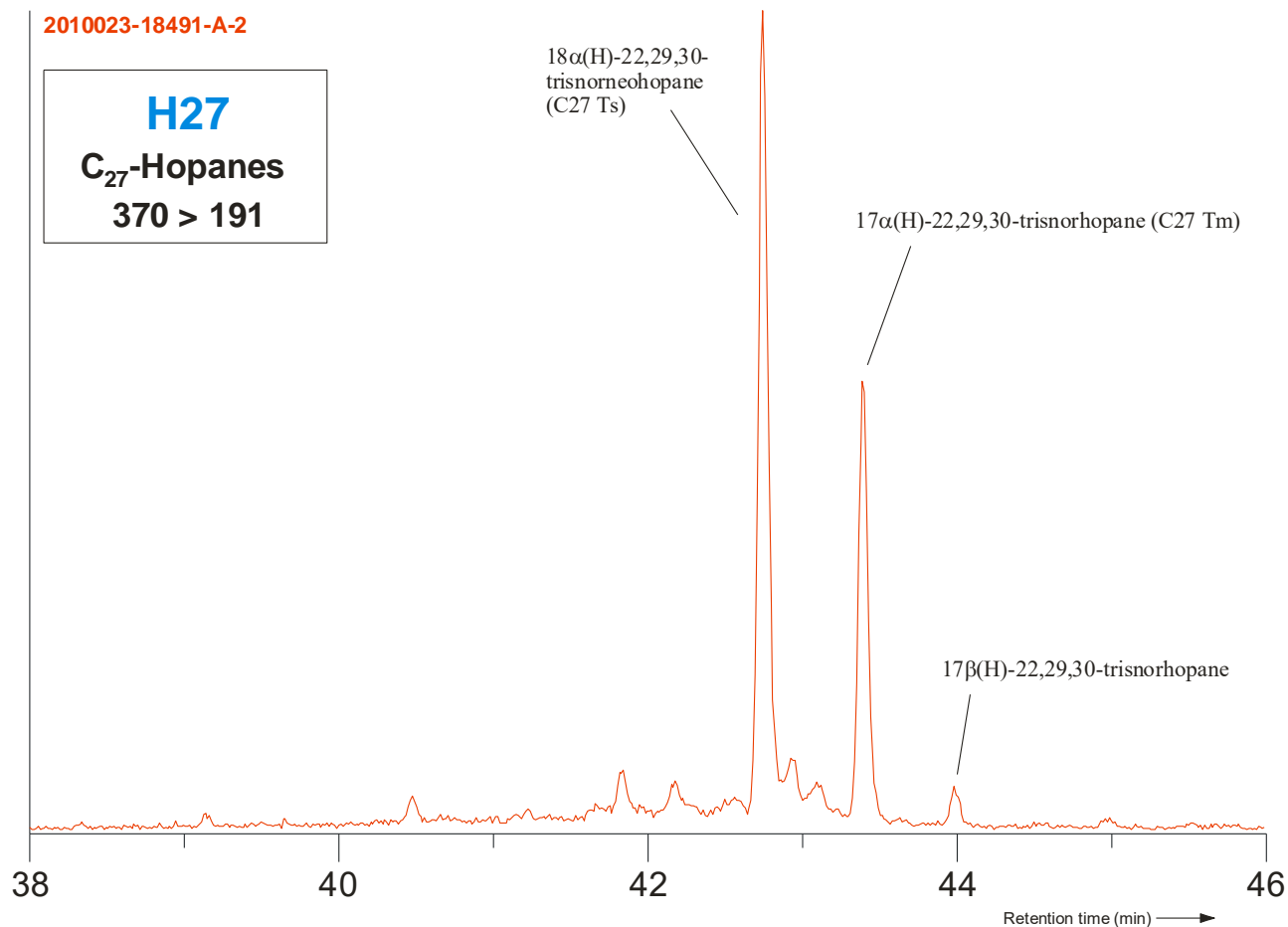


Figure 8.3: C<sub>27</sub> hopanes, GC-MS-MS, 370 → 191.

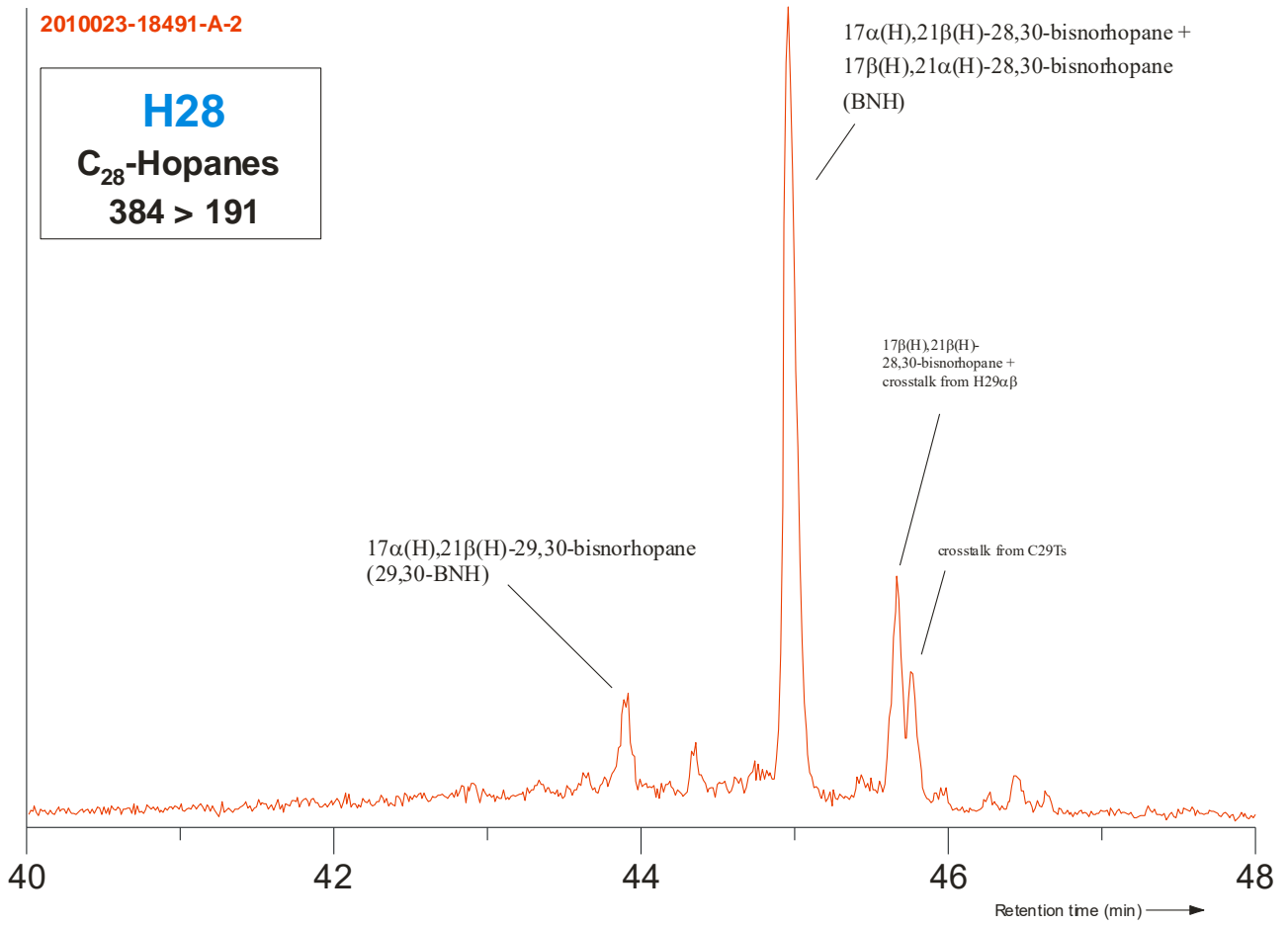


Figure 8.4: C<sub>28</sub> hopanes, GC-MS-MS, 384 → 191.

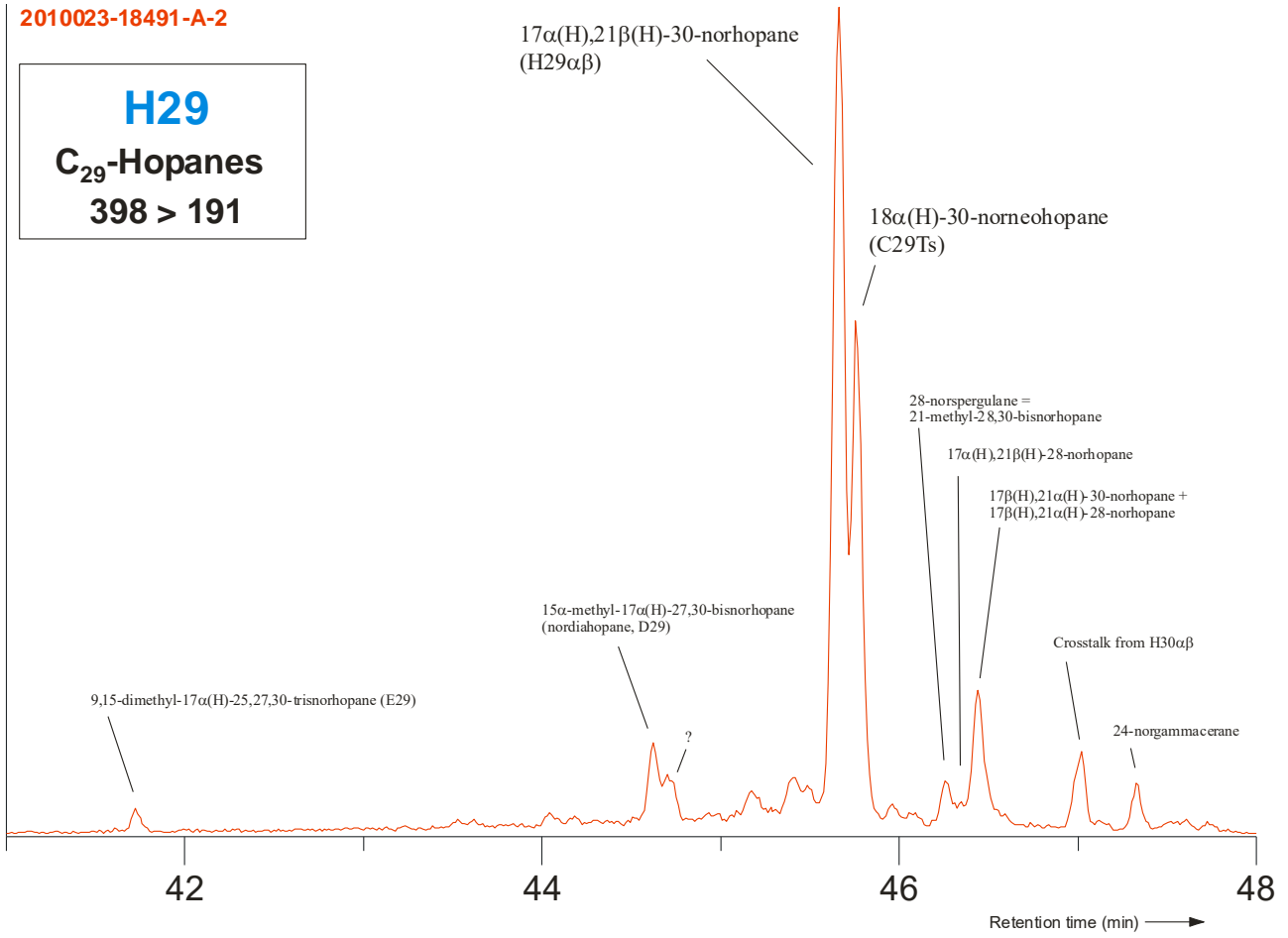


Figure 8.5: C<sub>29</sub> hopanes, GC-MS-MS, 398 → 191.

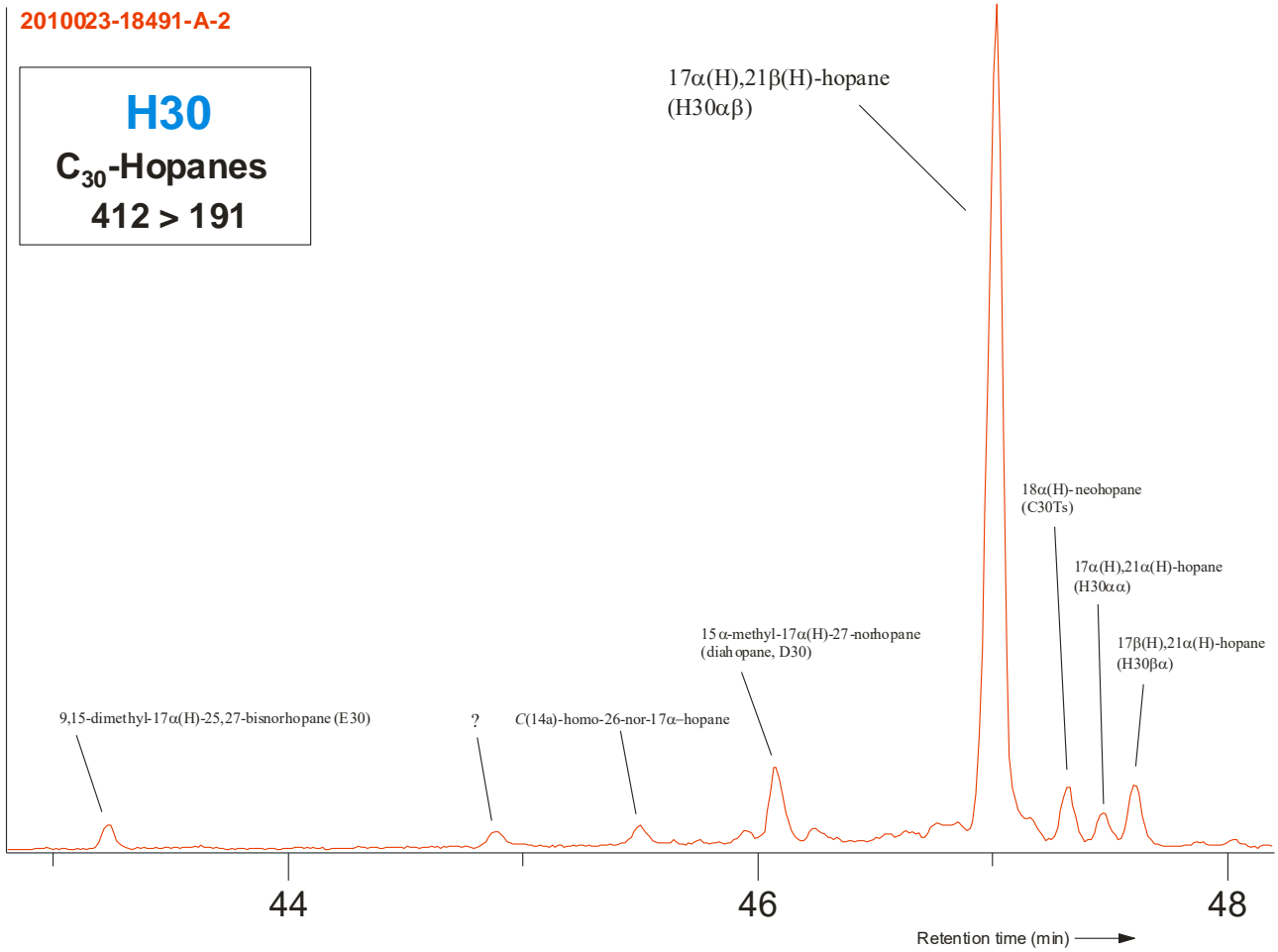


Figure 8.6: C<sub>30</sub> hopanes, GC-MS-MS, 412 → 191.

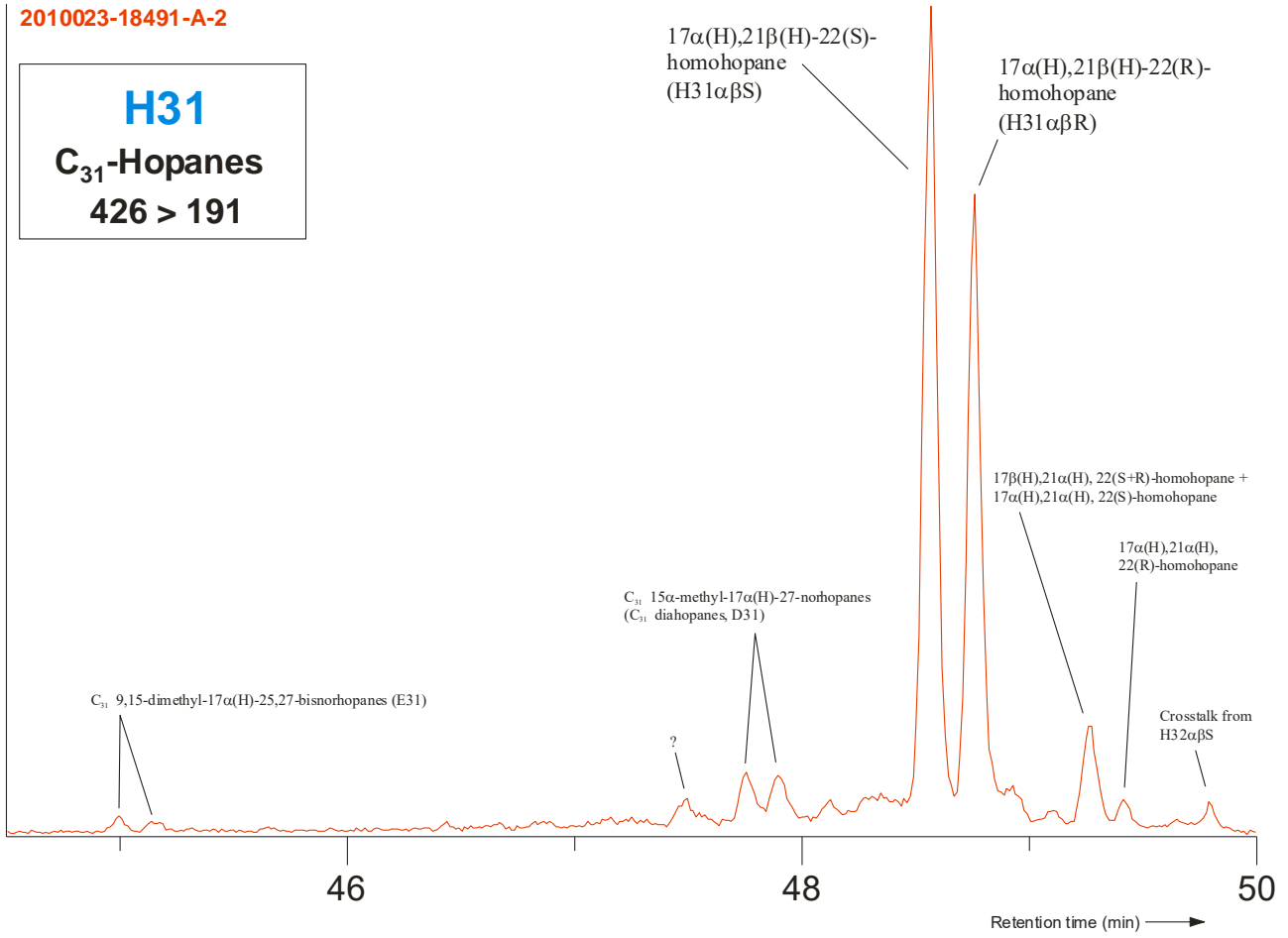


Figure 8.7: C<sub>31</sub> hopanes, GC-MS-MS, 426 → 191.



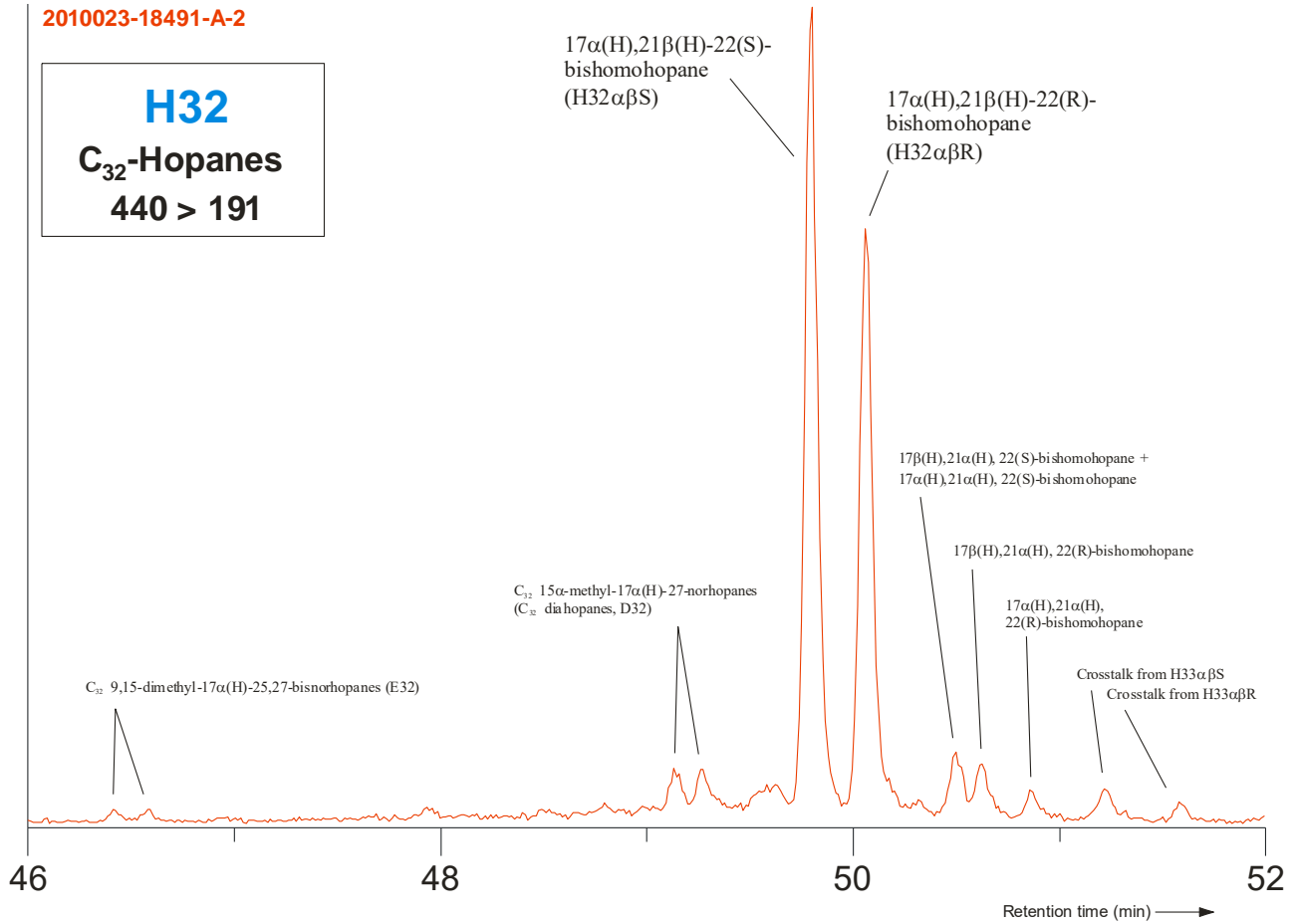


Figure 8.8: C<sub>32</sub> hopanes, GC-MS-MS, 440 → 191.

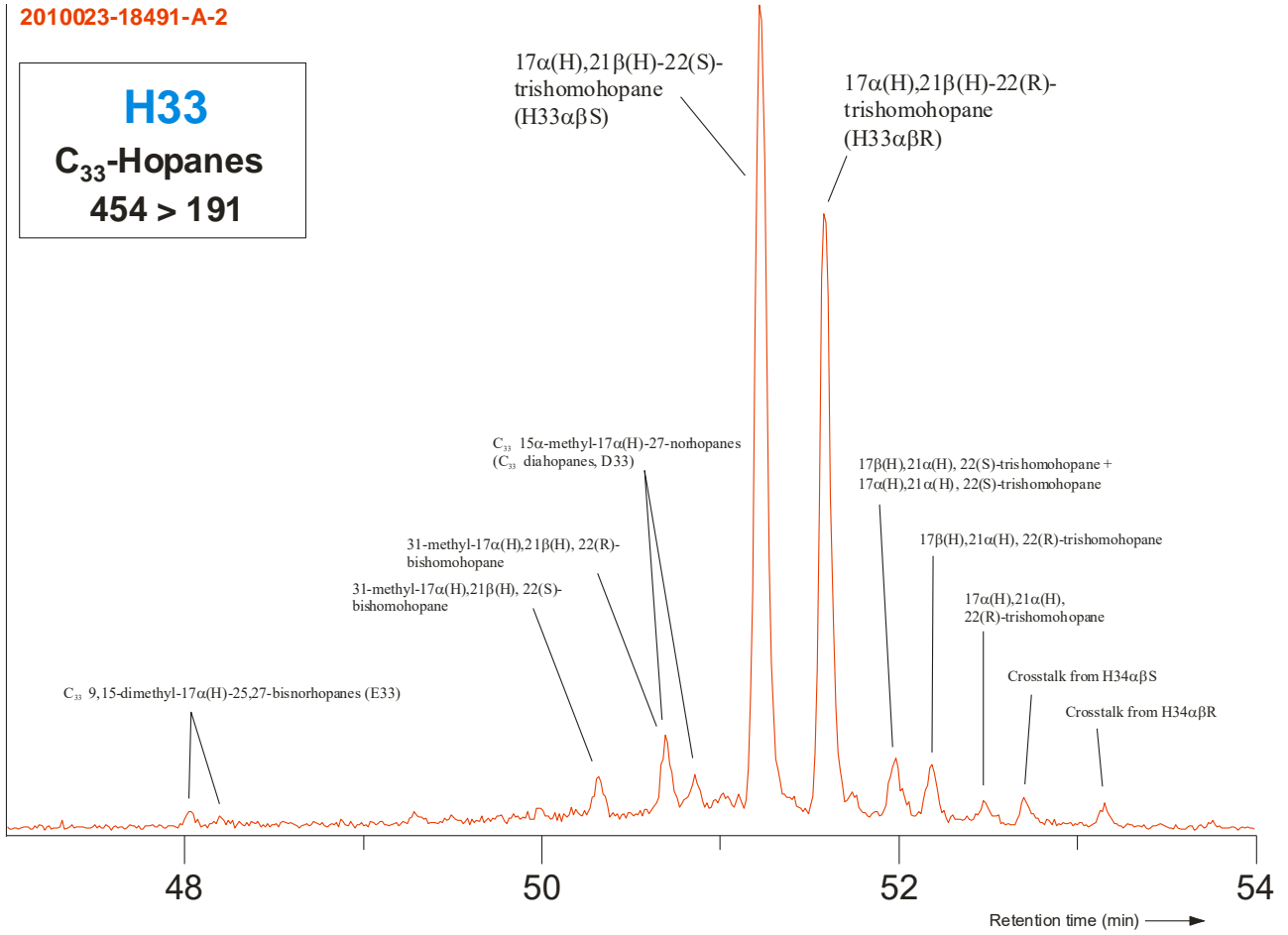


Figure 8.9: C<sub>33</sub> hopanes, GC-MS-MS, 454 → 191.

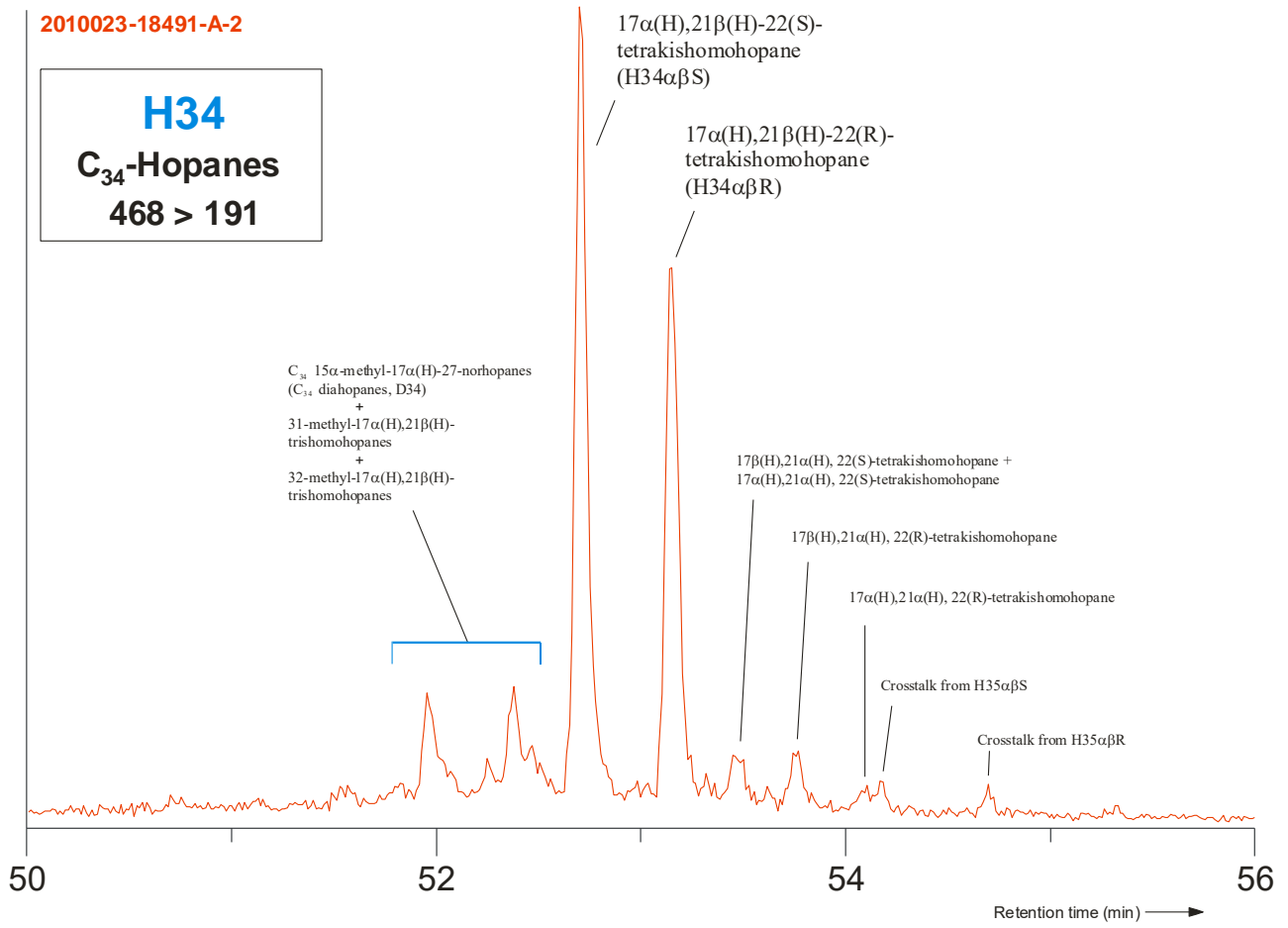


Figure 8.10: C<sub>34</sub> hopanes, GC-MS-MS, 468 → 191.

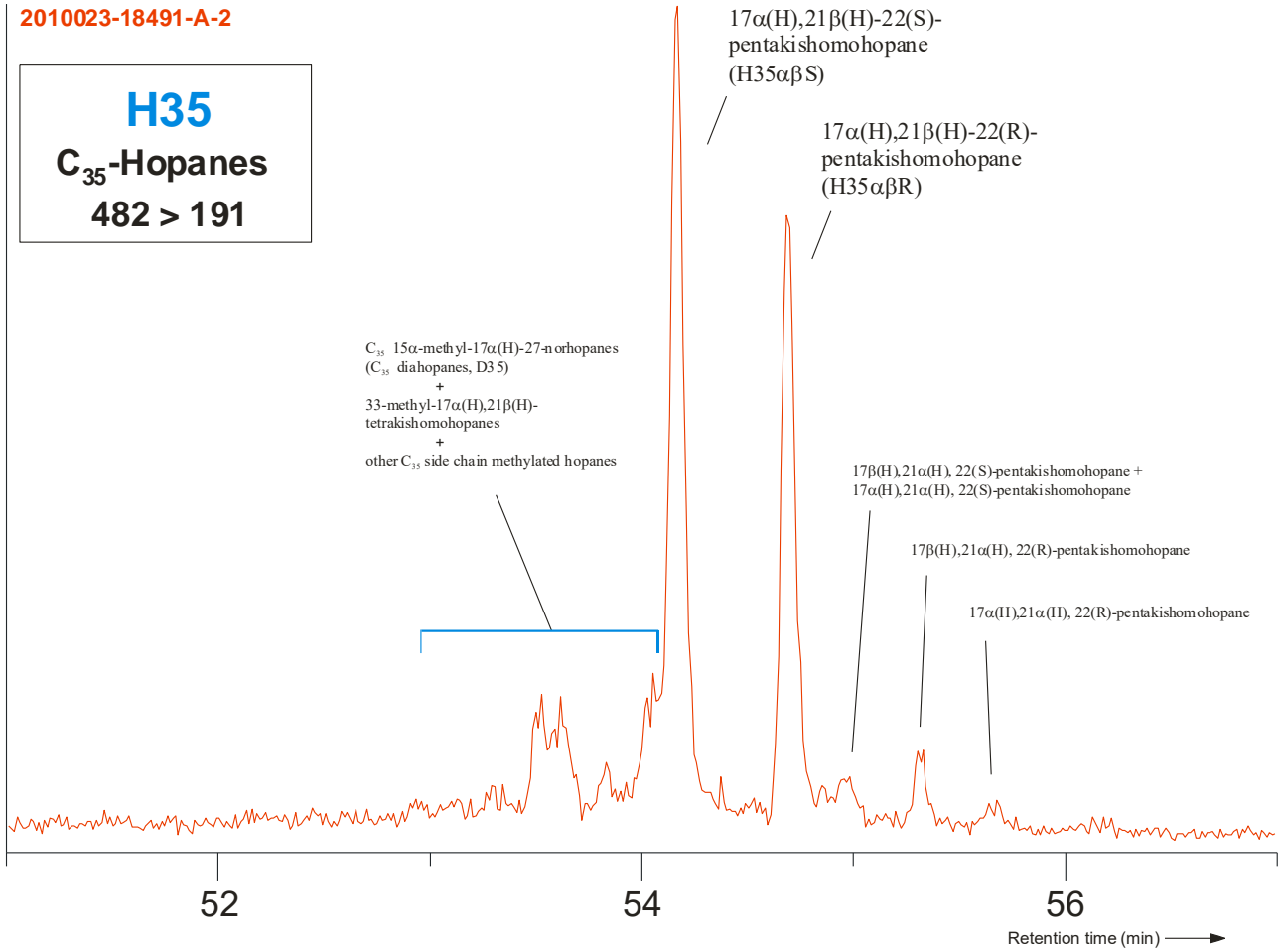


Figure 8.11: C<sub>35</sub> hopanes, GC-MS-MS, 482 → 191.

2010023-18491-A-2

Hopanes + tri- and  
tetracyclic terpanes  
m/z 191

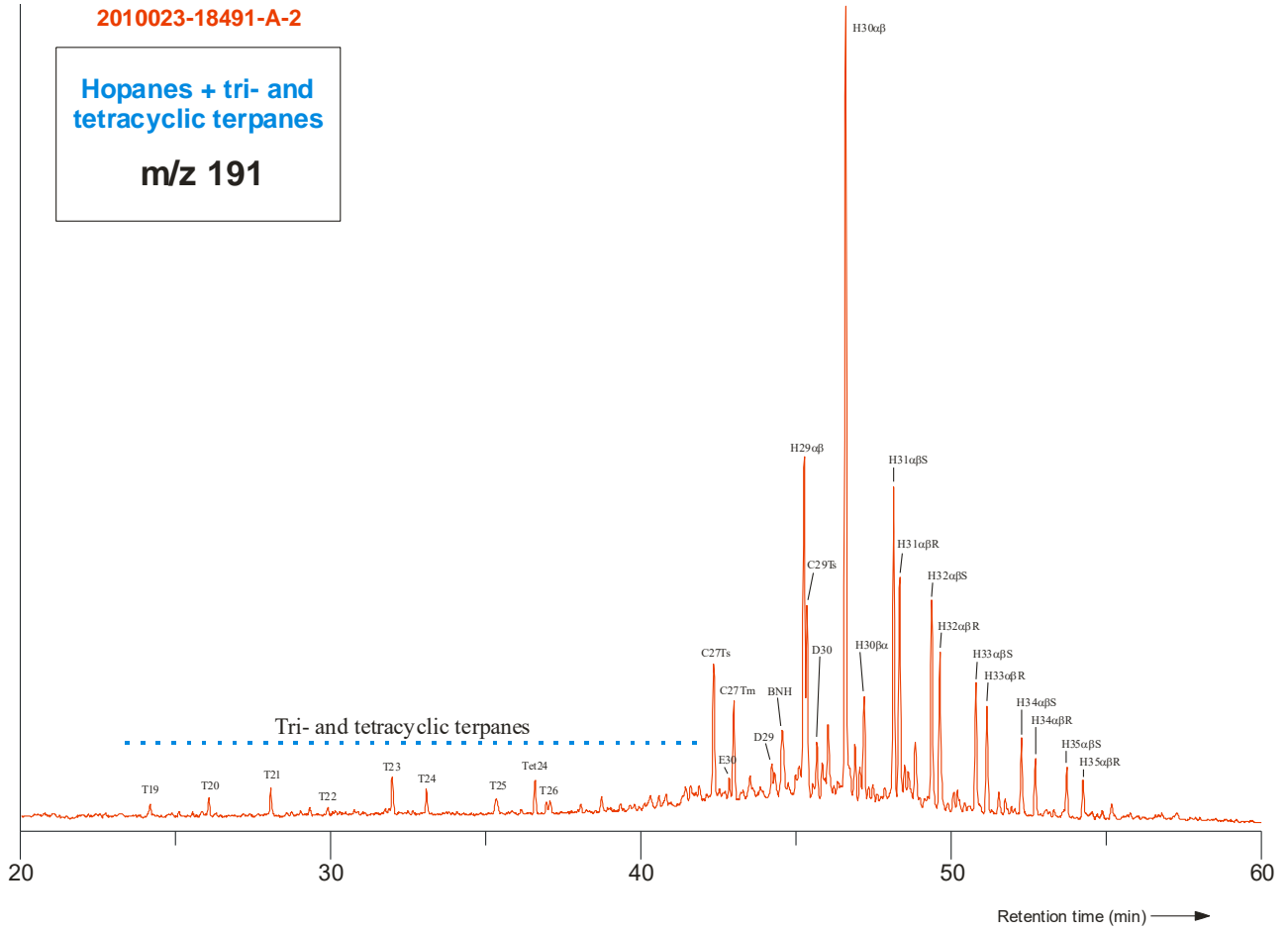


Figure 8.12: Hopanes, tri- and tetracyclic terpanes, GC-MS, m/z 191.

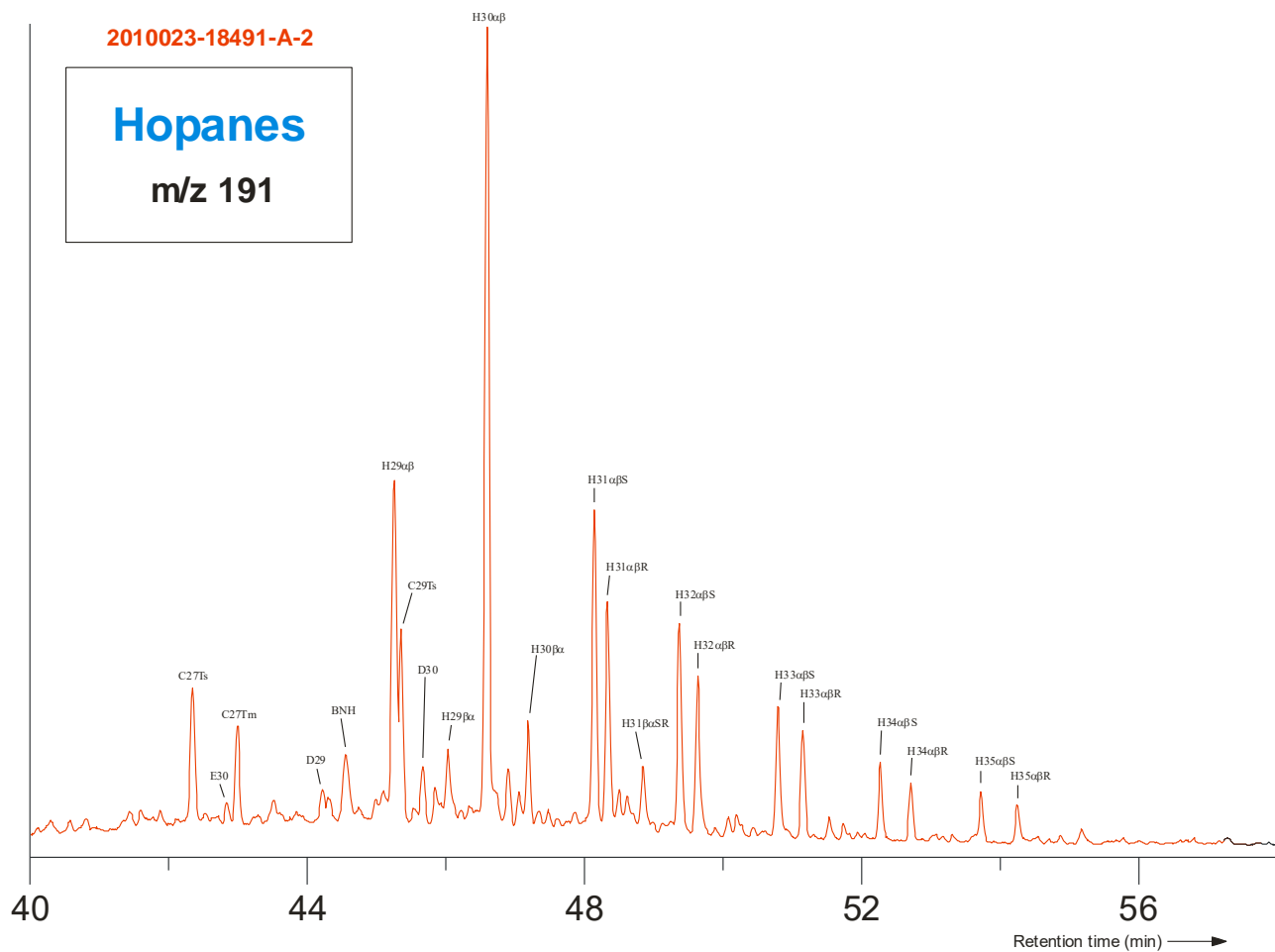


Figure 8.13: Hopanes, GC-MS, m/z 191.

2010023-18491-A-2

28 Norhopanes  
+ C<sub>27</sub> hopanes  
m/z 355

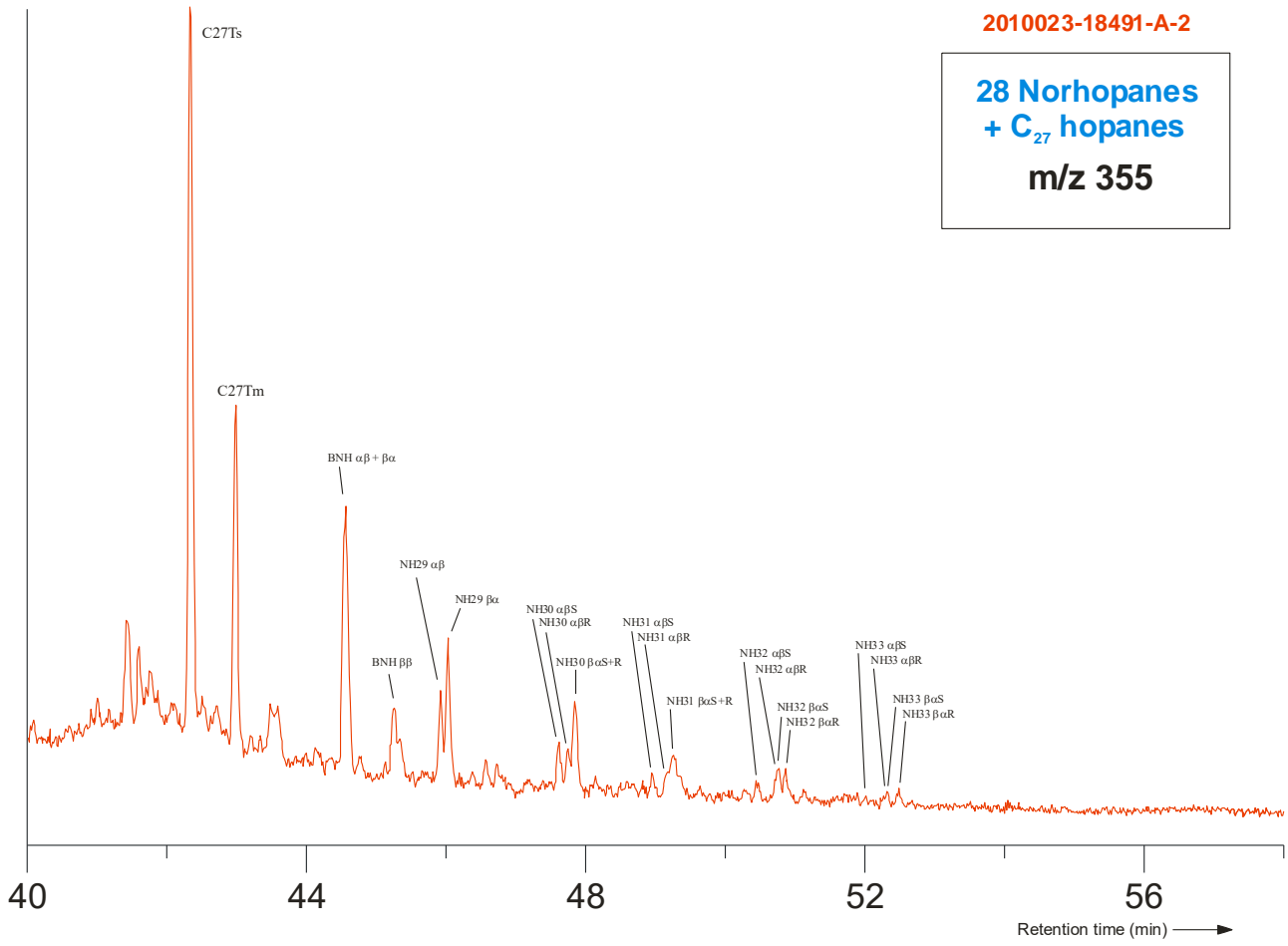


Figure 8.14: 28-Norhopanes and C<sub>27</sub> hopanes, GC-MS, m/z 355.

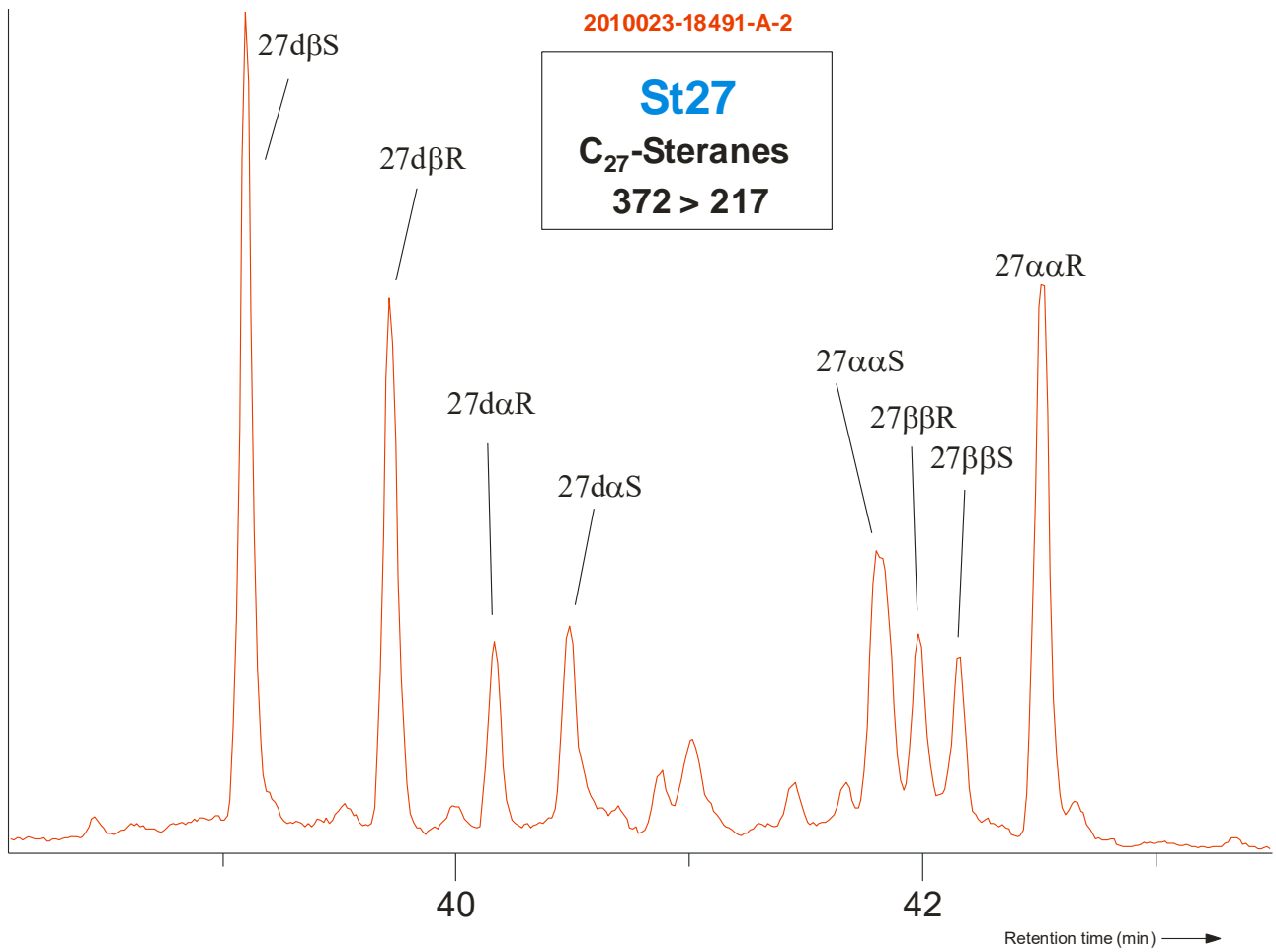


Figure 8.15: C<sub>27</sub> steranes, GC-MS-MS, 372 → 217.



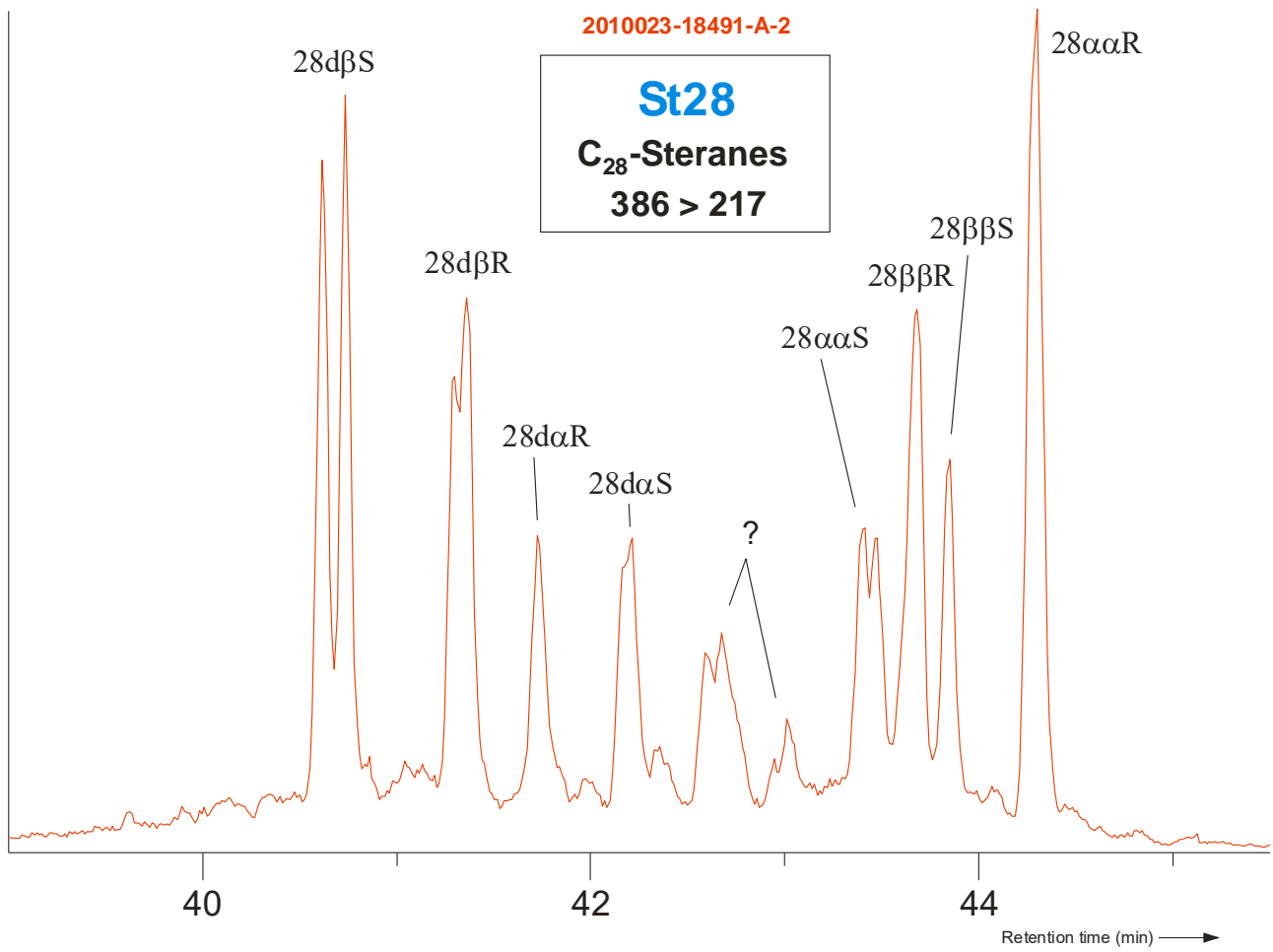


Figure 8.16: C<sub>28</sub> steranes, GC-MS-MS, 386 → 217.

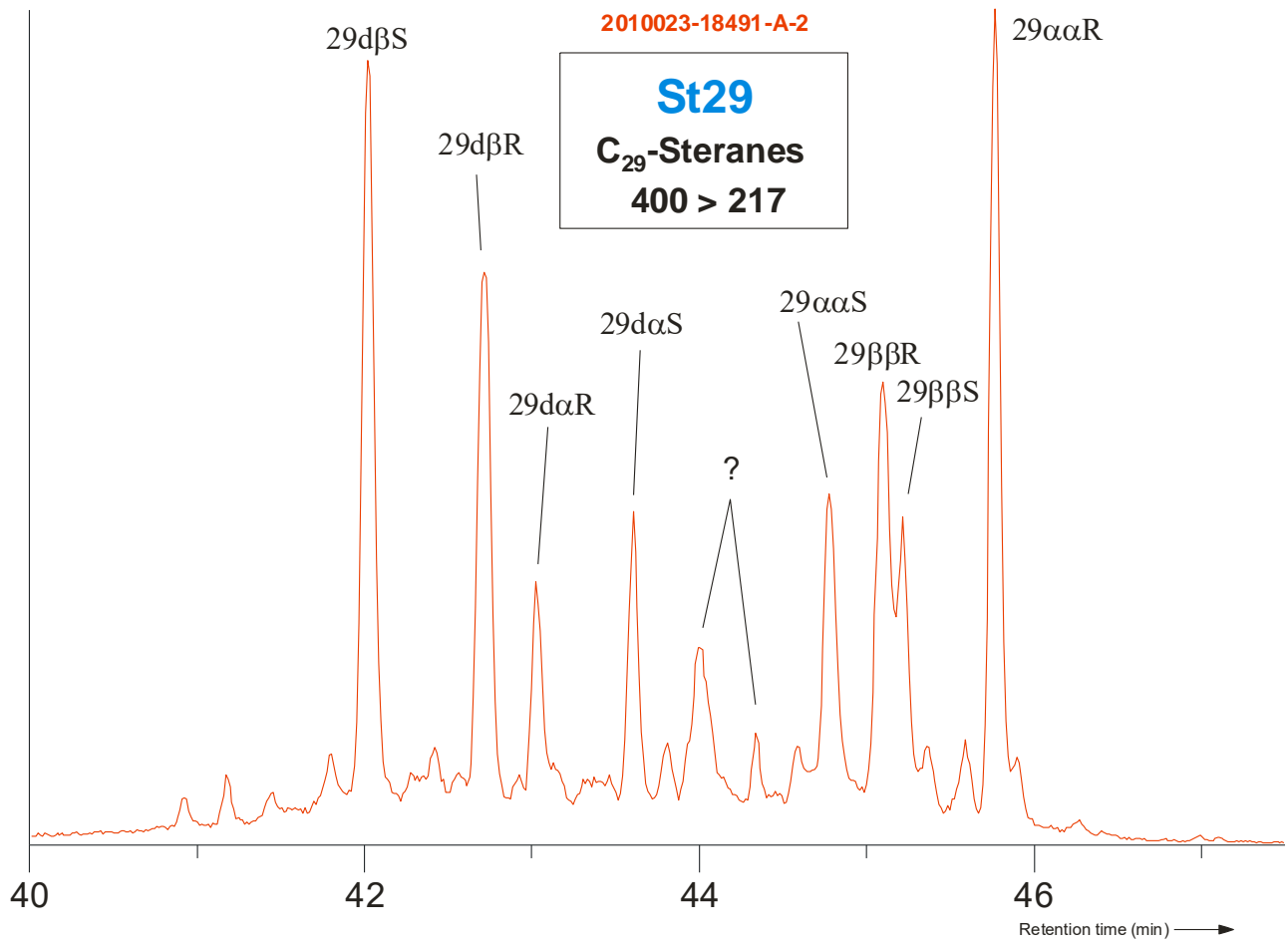


Figure 8.17: C<sub>29</sub> steranes, GC-MS-MS, 400 → 217.

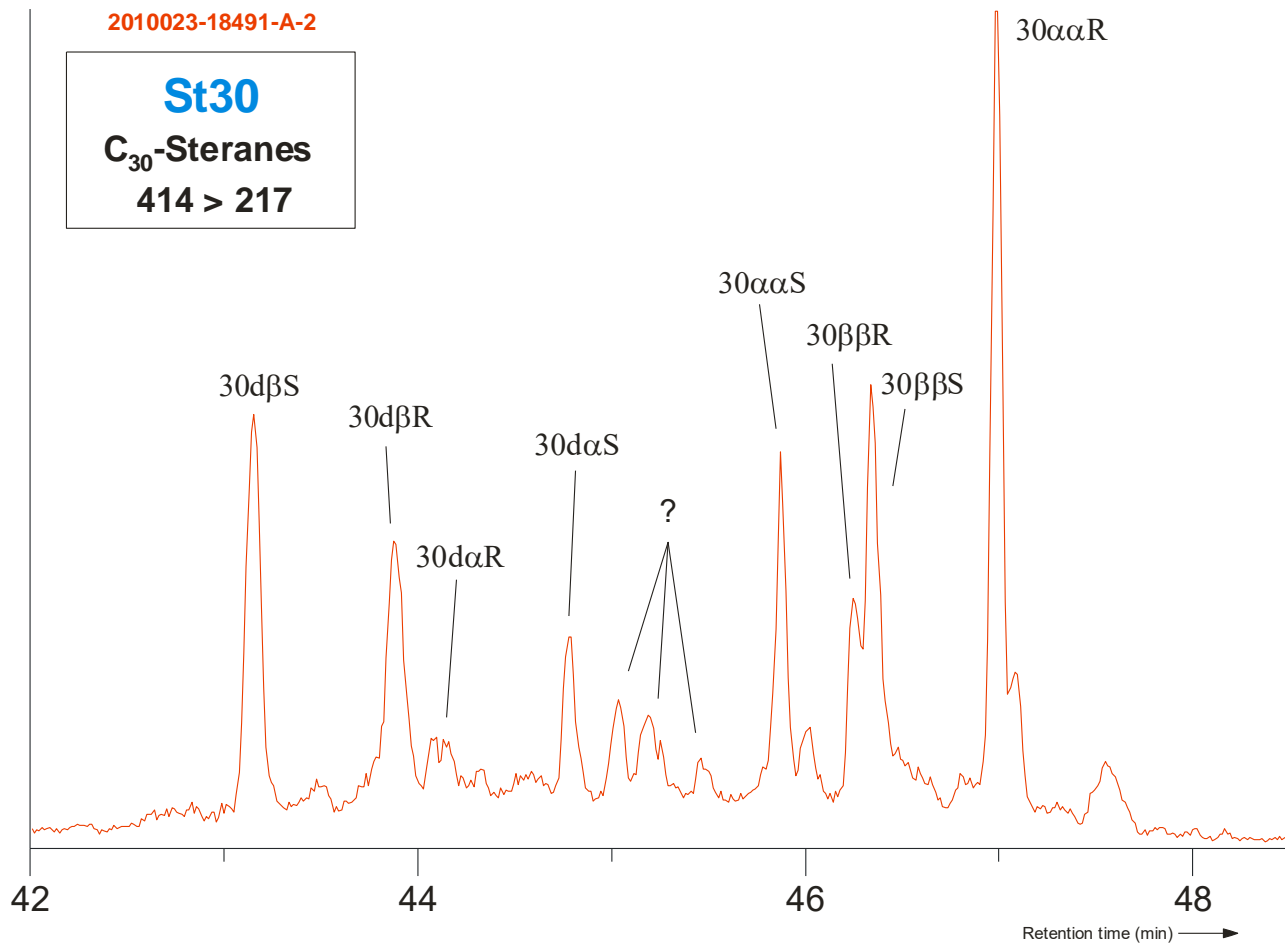
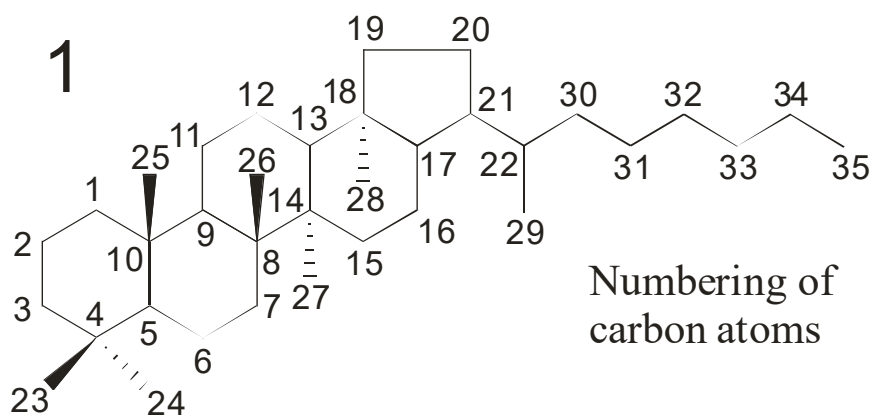
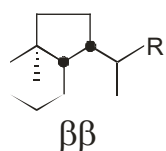


Figure 8.18: C<sub>30</sub> steranes, GC-MS-MS, 414 → 217.

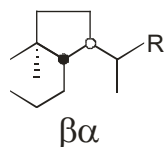
# Hopanes



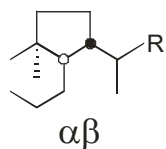
Stereochemistry at C-17 and C-21



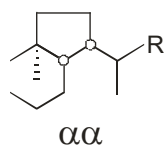
$\beta\beta$ -hopanes



$\beta\alpha$ -hopanes



$\alpha\beta$ -hopanes

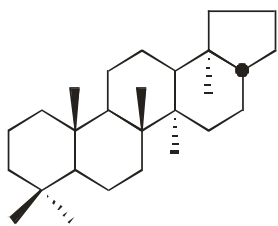


$\alpha\alpha$ -hopanes

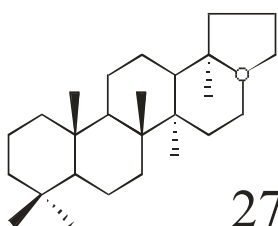
$C_{29}$  : R = H  
 $C_{30}$  : R =  $CH_3$   
 $C_{31}$  : R =  $C_2H_5$   
 $C_{32}$  : R =  $n-C_3H_7$   
 $C_{33}$  : R =  $n-C_4H_9$   
 $C_{34}$  : R =  $n-C_5H_{11}$   
 $C_{35}$  : R =  $n-C_6H_{13}$

Figure 8.19: Structure and stereochemistry of regular hopanes (Rohmer et al., 1992; Nytoft et al., 2001 and references therein).

# C<sub>27</sub> hopanes

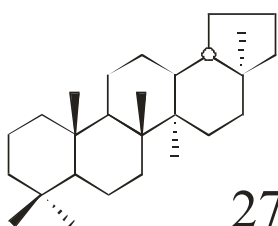


17β(H)-22,29,30-trisnorhopane



27Tm

17α(H)-22,29,30-trisnorhopane

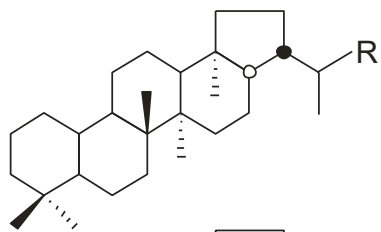


27Ts

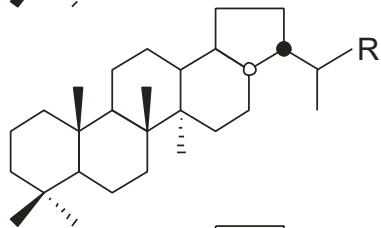
18α(H)-22,29,30-trisnorneohopane

Figure 8.20: Structure of C<sub>27</sub> hopanes.

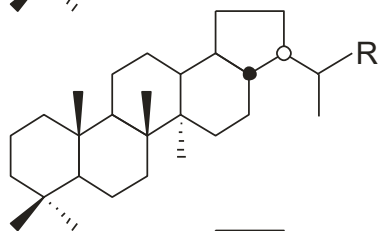
## Demethylated hopanes



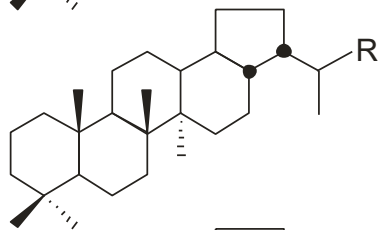
25-norhopanes



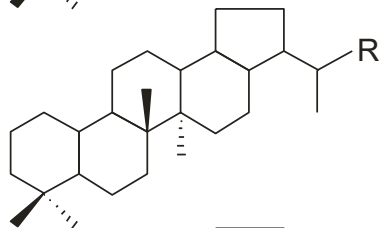
$\alpha\beta$ -28-norhopanes



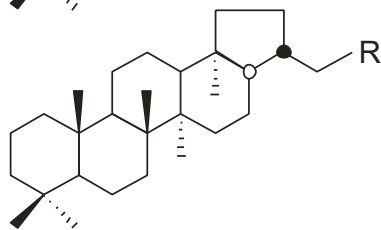
$\beta\alpha$ -28-norhopanes



$\beta\beta$ -28-norhopanes



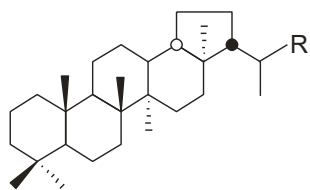
25,28-bisnorhopanes



30-norhopanes

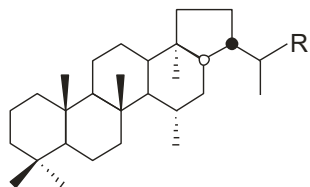
Figure 8.21: Structure of some norhopanes. Only 28-Norhopanes (Grantham et al., 1980; Moldowan et al., 1984; Nytoft et al, 2000) are present in the "PETSYS oils".

## Rearranged hopanes



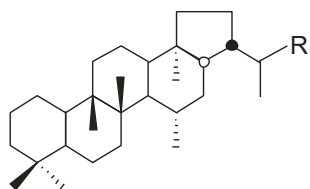
### 18 $\alpha$ -neohopanes

29Ts: R = H, 30Ts: R = CH<sub>3</sub>



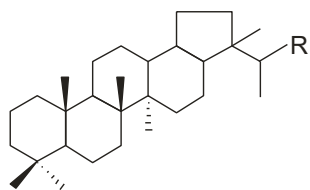
### 17 $\alpha$ -diahopanes

D30: R = CH<sub>3</sub>, D31: R = C<sub>2</sub>H<sub>5</sub>



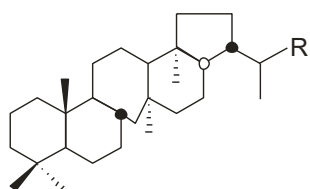
### 9,15-dimethyl- 25,27-dinorhopanes "Early eluting series"

E30: R = CH<sub>3</sub>



### 21-methyl-28-norhopanes

Not quantified



### C(14a)-homo-26-nor-17 $\alpha$ -hopanes

Not quantified

Figure 8.22: Structure of some rearranged hopanes (Moldowan et al., 1991; Trendel et al., 1993; Farrimond and Telnæs, 1996; Nytoft et al., 2006).

## Tri- and tetracyclic terpanes

not quantified

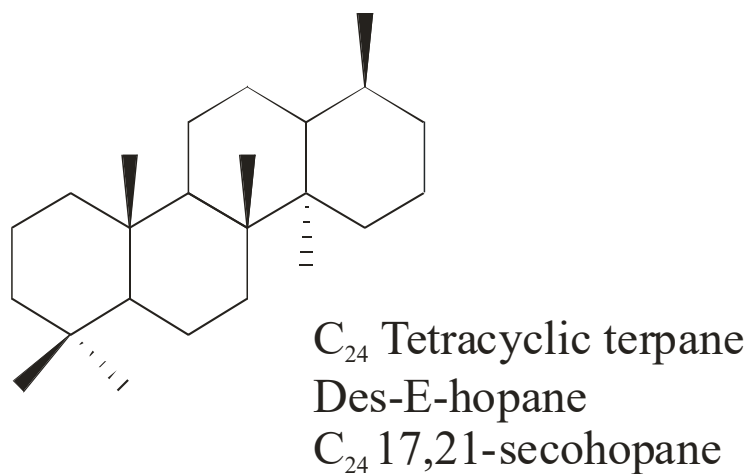
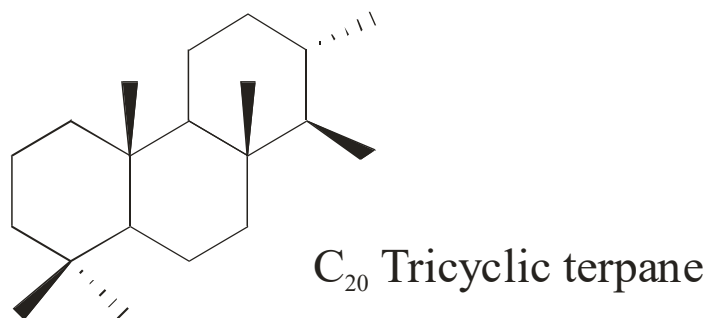
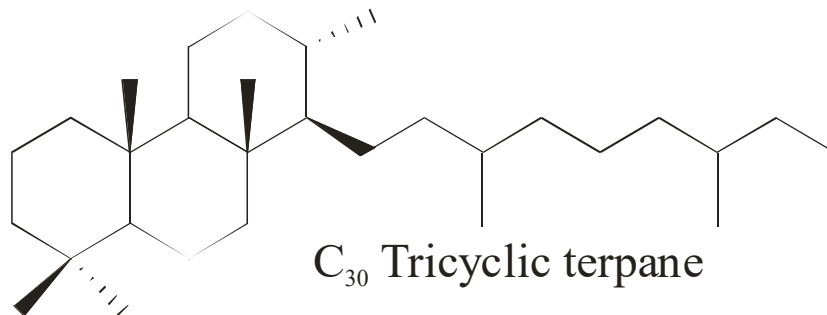


Figure 8.23: Structure of some tri- and tetracyclic terpanes.



## 8.4 References

- Farrimond, P., Telnæs, N., 1996. Three series of rearranged hopanes in Toarcian sediments (northern Italy). *Organic Geochemistry* 25, 165-177.
- Fowler, M.G., Brooks, P.W., 1989. Organic geochemistry as an aid in the interpretation of the history of oil migration into different reservoirs at the Hibernia K-18 and Ben Nevis I-45 wells, Jeanne d'Arc Basin, offshore eastern Canada. *Organic Geochemistry* 16, 461-475.
- Grantham, P. J., Posthuma, J., De Groot, K., 1980. Variation and significance of the C<sub>27</sub> and C<sub>28</sub> triterpane content of a North Sea core and various North Sea crude oils. In *Advances in Organic Geochemistry, 1979*, Eds. A. G. Douglas and J. R. Maxwell, pp. 29-38. Pergamon Press, Oxford
- Moldowan, J.M., Seifert, W.K., Arnold, E., Clardy, J., 1984. Structure proof and significance of stereoisomeric 28,30-bisnorhopanes in petroleum and petroleum source rocks. *Geochimica et Cosmochimica Acta* 48. 1651-1661.
- Moldowan J. M., Fago F. J., Carlson R. M. K., Young D. C., van Duyne G., Clardy J., Schoell M., Pillinger C. T and Watt D. S., 1991. Rearranged hopanes in sediments and petroleum. *Geochimica et Cosmochimica Acta* 55, 3333-3353.
- NIGOGA, The Norwegian Industry Guide to Organic Geochemical Analyses, Edition 4.0, 30 May 2000.
- Nytoft, H.P., Bojesen-Koefoed, J.A., Christiansen, F.G., 2000. C<sub>26</sub> and C<sub>28</sub>-C<sub>34</sub> 28-norhopanes in sediments and petroleum. *Organic Geochemistry* 31, 25-39.
- Nytoft, H.P., Bojesen-Koefoed, J.A., 2001. 17 $\alpha$ (H),21 $\alpha$ (H)-hopanes: natural and synthetic. *Organic Geochemistry* 32, 841-856.
- Nytoft, H.P., Lutnæs, B.F., Johansen, J.E., 2006. 28-Nor-spergulanenes, a novel series of rearranged hopanes. *Organic Geochemistry* 37, 772-786.
- Radke, M., Willsch, H., Welte, D.H., 1980. Preparative hydrocarbon group determination by automated Medium Pressure Liquid Chromatography. *Analytical Chemistry* 52, 406-411.
- Rohmer, M., Bissere, P., Neunlist, S., 1992. The hopanoids, procaryotic triterpenoids and precursors of ubiquitous molecular fossils. In: Moldowan, J.M., Albrecht. P., Philp, R.P (Eds.).

Biological Markers in Sediments and Petroleum. Prentice Hall, Englewood Cliffs, New Jersey. pp. 1-17.

Trendel, J.-M., Graff, R., Wehrung, P., Albrecht, P., Dessort, D., Connan, J., 1993. C(14a)-Homo-26-nor-17 $\alpha$ -hopanes, a novel and unexpected series of molecular fossils in biodegraded petroleum. Journal of the Chemical Society, Chemical Communications 5, 461-463.

## 9 Provenance of Upper Jurassic sandstones in the Danish North Sea

### 9.1 Introduction

One of the factors determining the reservoir properties of sandstone is the mineralogical composition which is a result of the character of the source area and the sediment dispersal system conveying the sediment to the sink. The aim of provenance analysis is to fingerprint the detrital minerals composing the sediment and tie these fingerprints to potential source areas and to project areas with specific sediment composition characteristics into unknown areas based on knowledge of the sediment dispersal system.

The aim of this technical note is to briefly describe the work that has been done (zircon) and a test of rutile and quartz analysis as provenance tools in the North Sea.

### 9.2 Zircon provenance

Traditional provenance analysis focuses on the heavy mineral component of the sediment because they contain a large range of chemical characteristics that tie them to their source. The most prominent mineral used for this is zircon which combine robustness with ability conserve the age of formation in the source. Studies of detrital zircon in Heno Formation sandstones in Hejre-2, Gert-2, Gert-4, Jeppe-1 and Diamant-1 were conducted by Weibel & Knudsen (2007).

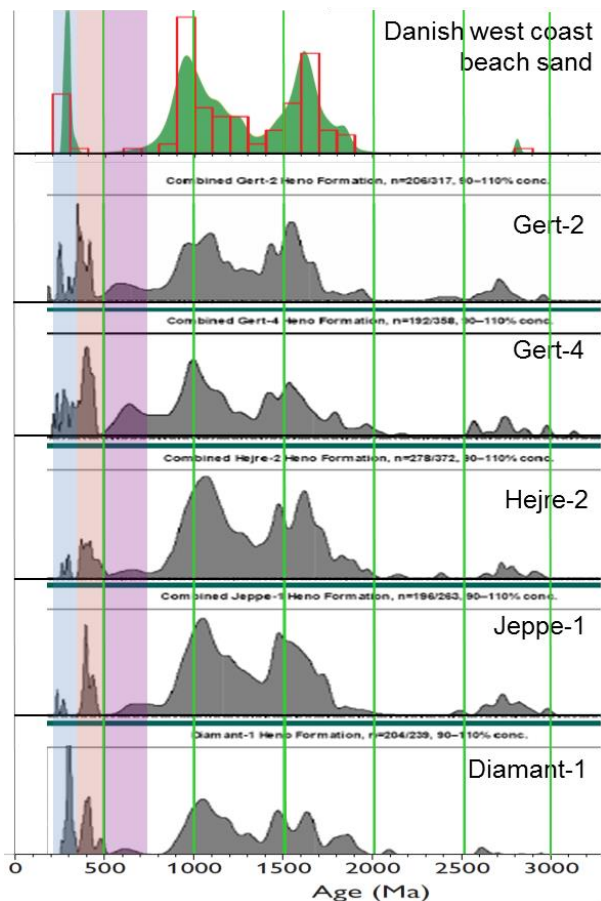


*Fig. 9.1: Detrital zircon age distribution patterns based from Heno Formation compared to recent beach on the west coast of Jutland. Ca. 300 zircons were analyzed from each well (Weibel & Knudsen, 2007). The majority of the detrital zircons (85 – 90 %) have ages in the range 2.000 to 800 Ma (Figure 9.1) and the main source area is likely to be the Scandinavian Shield. This is similar to what composes Danish beaches mainly derived from the Scandinavian Shield. Minor zircon population components have ages in the range 800-500 Ma derived from the British Isles (“Avalonian”), The 450-400 Ma population is Caledonian (Scotland & Norway) and the 360-300 Ma population is from the Variscan Orogeny (Central Europe).*

Gert-2 and Gert-4 have slightly higher content of “Avalonian” and Caledonian ages as compared to the other wells suggesting a higher contribution from the west. Diamant-1 that is situated south of the other wells has a slightly higher contribution of “Variscan” zircons.

The very high stability of zircon means that if the sediment is recycled many times zircon will stay, and the provenance signature in the different wells were fairly similar suggesting that at least the very stable detrital minerals were homogenized to some degree during their way from the source to the present position.

### **9.3 Rutile chemistry**

Rutile is a titanium mineral almost entirely composed of  $\text{TiO}_2$ . However, the composition varies depending on a number of factors e.g. the metamorphic temperature of formation ( $\text{ZrO}_2$  content) and the geochemical environment in which it was formed ( $\text{Cr}_2\text{O}_3$ ,  $\text{Nb}_2\text{O}_5$ ). Accordingly, the composition of rutile can be used to fingerprint the provenance of the sediment (Zack et al 2004).

The chemical composition of rutile in 5 samples was analyzed using the Electron MicroProbe at University of Copenhagen (Figure 9.2).

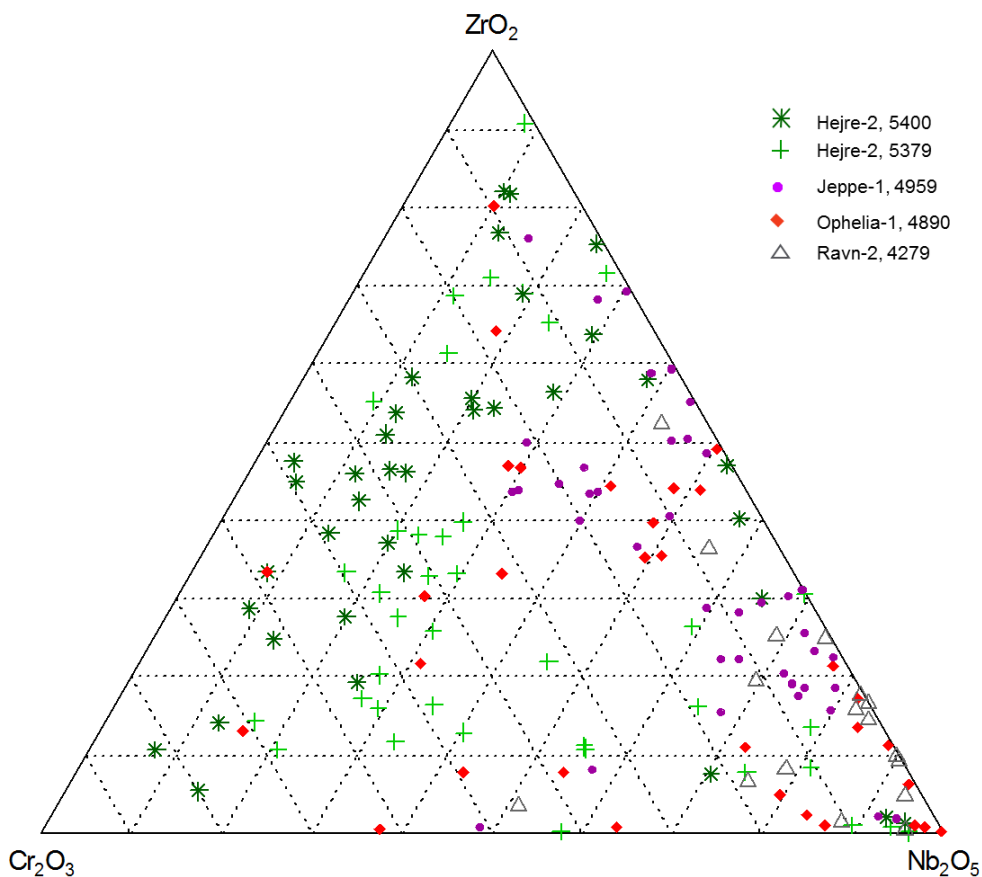


Fig. 9.2: Distribution of  $\text{Cr}_2\text{O}_3$ ,  $\text{Nb}_2\text{O}_5$  and  $\text{ZrO}_2$  in rutile from the Heno Formation.

The composition of rutile varies among the different wells (Figure 9.2). The Ravn-2 sample has a fairly restricted range of compositions compared to the other samples and Jeppe-1 has a slightly larger range. Ophelia-1 has yet a larger range of compositions and the two samples from Hejre-2 has the largest range of compositions and relatively lower contents of  $\text{Nb}_2\text{O}_5$  as compared to the other samples.

How these compositions are tied to their source areas is not known as there is no database of source characteristics to compare with. The compositions can at this stage only be used as a fingerprinting tool aiming at comparing how much the rutile content in different wells are likely to share a common source of sediment.

In this case, the two samples from Hejre-2 share (not surprisingly) source characteristics. They also have similarities with Ophelia-1. On the other hand, the source for Ravn-2 and Jeppe-1 are more like each other as compared to Hejre-2.

## 9.4 Quartz chemistry

Quartz is almost pure  $\text{SiO}_2$ . However, advances in analytical techniques have made it possible to analyze the small amounts of impurities that are in quartz. Trace elements that may fit in to the atomic lattice structure of quartz includes Al, B, Ba, Be, Ca, Cr, Cu, Fe, Ge, H, K, Li, Mg, Mn, Na, P, Pb, Rb, Sr, Ti and U (Larsen et al 2004). The content of trace elements varies with the

geochemical environment and the geological processes responsible for the formation of the quartz. This suggests that the quartz will contain a fingerprint of the source area. However, this has not been tested as a provenance tool yet and it is difficult to find descriptions of this in the literature.

To test the method 5 samples from Hejre-2 (5379 and 5400 m respectively), Jeppe-1, Ophelia-1 and N 3-7/7 (Norwegian sector) was crushed, sieved and sand-grains  $> 100\mu$  was mounted in epoxy and the sample was polished. The trace element content was analyzed at Institute of Geology AS CR, Prague, Czech Republic using an Element-2 ICP-MS equipped with a 213 nm Laser ablation system. The following elements were analyzed: Al, B, Ba, Cr, Fe, Ge, Li, Mn, P, Pb, Rb, Sn, Sr and Ti.

Some of the results are shown in Figures 9.3, 9.4 and 9.5.

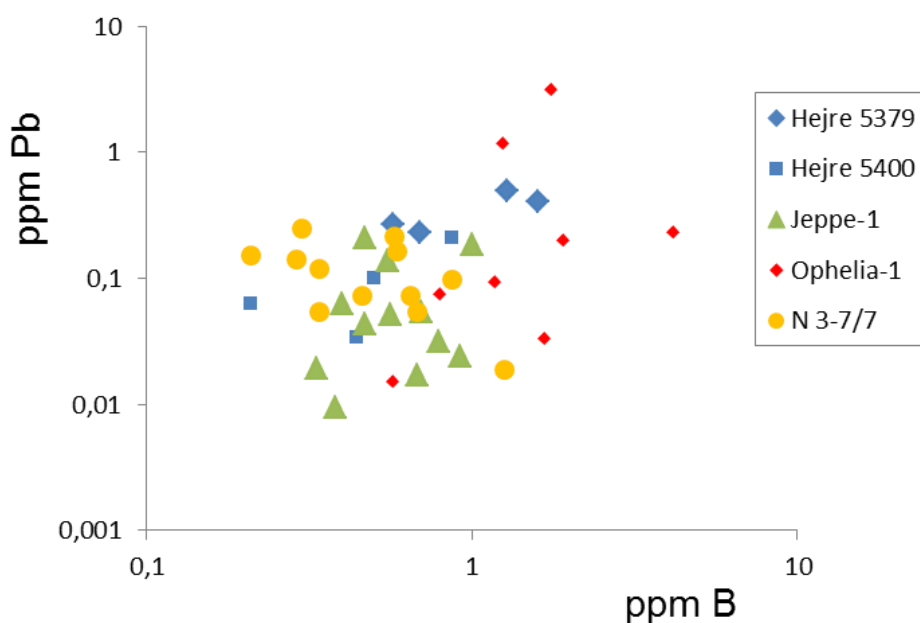


Fig. 9.3: ppm B versus ppm Pb in quartz from samples from the Heno Formation.

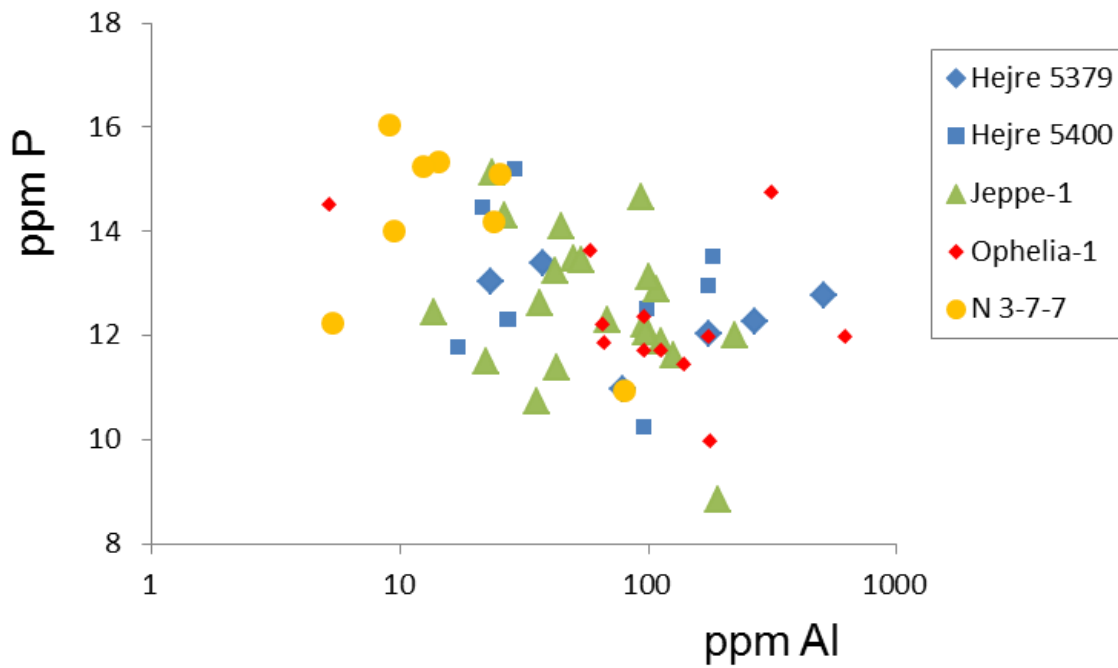


Fig. 9.4: ppm Al versus ppm P in quartz from samples from the Heno Formation.

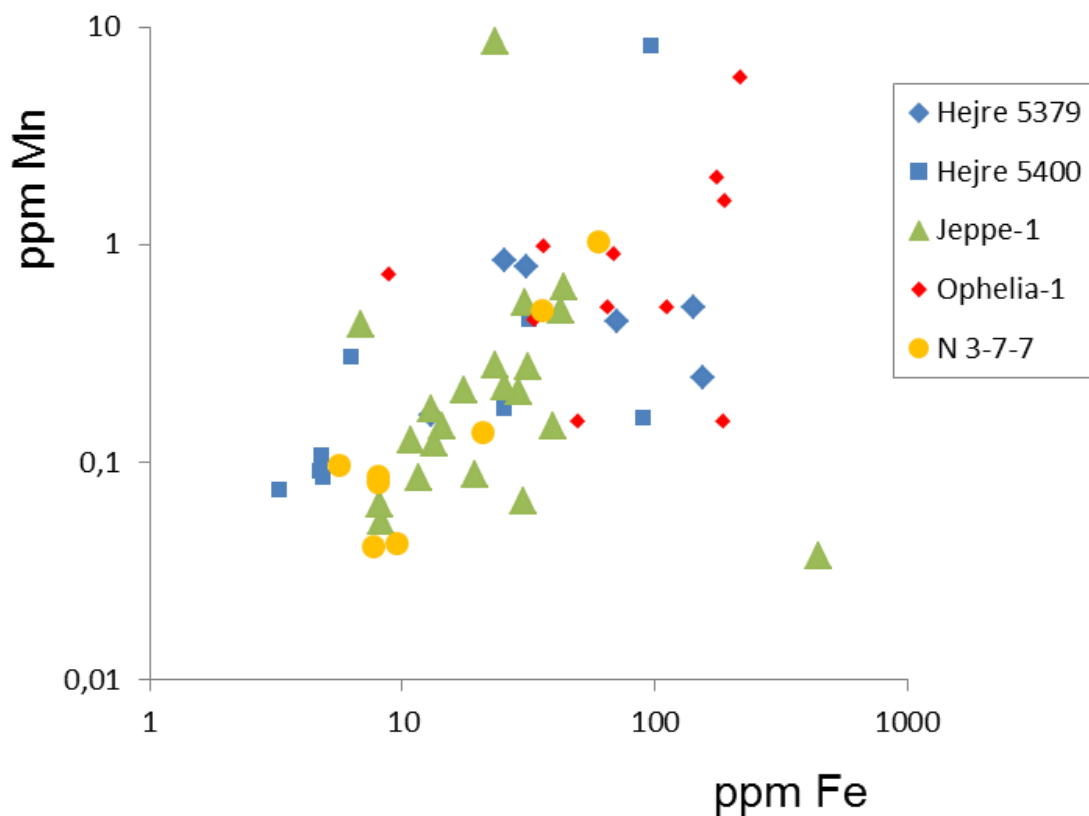


Fig. 9.5: ppm Fe versus ppm Mn in quartz from samples from the Heno Formation.

Based on the distribution of quartz grain compositions in Figures 9.3, 9.4 and 9.5 it is not possible to point out which sandstones share the same source regions. However, there are some differences

in the distributions that may be useful when trying to establish similarities and differences among the sandstone units.

A considerably larger database of compositions from the different wells would be needed to be able to use such data. Further, it would be necessary to obtain information concerning the textural relationships of the individual grains analyzed to avoid possible contribution from diagenetic features.

## 9.5 References

Larsen, R.B., Henderson, I., Ihlen, P.M. and Jacamon, F. 2004: Distribution and petrogenetic behaviour of trace elements in granitic quartz from South Norway. *Contributions to Mineralogy and Petrology*, 147, 615-628.

Weibel, R. & Knudsen, C. 2007: Chemostratigraphy and mineral chemical fingerprinting: Heno Formation, Danish North Sea. *Danmarks og Grønlands Geologiske Undersøgelse Rapport 2007/42*. 165 pp.

Zack, T., von Eynatten, H. & Kronz, A. 2004: Rutile geochemistry and its potential use in quantitative provenance studies. *Sediment Geol.* 171:37-58



## 10 Variation in chemical composition, Ar/Ar ages and Pb/Pb isotope signature of K-feldspar in Heno Formation sandstones in selected wells

### 10.1 Summary

The content of detrital K-feldspar is high in wells like Hejre-1, Hejre-2, Ophelia-1 and N 3-7/6. The same wells show a broad range of K-feldspar chemical compositions. One interpretation of this could be that the high content of K-feldspar in these wells is a result of reworking of alkaline volcanic material.

In situ UV laser ablation analysis of Ar/Ar K-feldspars in 6 samples produced a range of dates. The youngest ages are Tertiary and can either be interpreted as representing the timing of K-feldspar overgrowth or interpreted as the result of resetting of the age due to a thermal event. Jurassic as well as Permian ages are not uncommon; these may be primary, but can also be a result of a “mixture age” lying between the event generating new K-feldspar age and an older age caused by  $^{40}\text{Ar}$  that has become decoupled from parent potassium in the detrital K-feldspar. Caledonian and Precambrian ages are also common showing A) that the primary Ar/Ar age of the detrital K-feldspar can survive in this environment and B) that K-feldspar has been sourced from terrains with these ages.

Pb/Pb isotopic characterization of K-feldspar has been conducted in 5 samples and the isotopic fingerprints of the K-feldspar can be tied to source terrains.

The entire study has only been focused on very few samples and very few grains in each sample. It is as such a pilot study to test if these methods potentially can yield valuable information.

### 10.2 Introduction

The content of detrital K-feldspar is high in wells like Hejre-1, Hejre-2, Ophelia-1 and 3-7/6 (Norwegian sector). Secondary porosity tied to dissolution of K-feldspar is described e.g. in Hejre-2, Jeppe-1 and Gert-1 (Weibel et al., 2010) and the reason for these high K-feldspar contents is of importance for the understanding of reservoir properties in the Heno Formation.

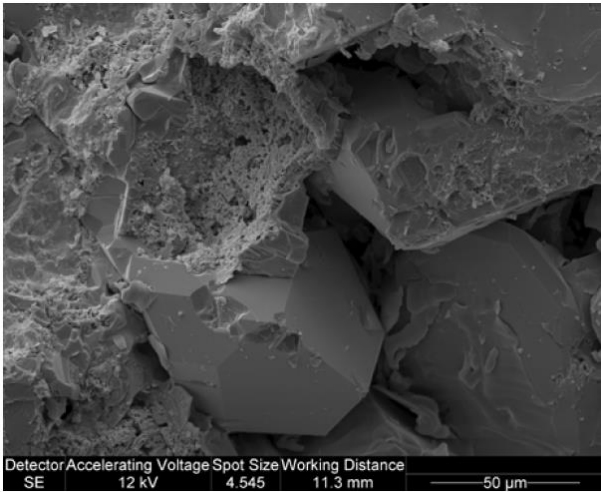


Fig. 10.1: Quartz overgrowth on detrital quartz and partly in secondary porosity after dissolved feldspar grain (scanning electron micrograph).

The content of detrital K-feldspar is variable and locally very high in the Heno Formation. In Hejre-2, and 3-7/6 in the Norwegian sector the content of K-feldspar is high, which can be seen by the very high ratio between  $K_2O$  and  $Al_2O_3$  on Figure 10.2. Elevated  $K_2O/Al_2O_3$  are also observed in Hejre-1 and Ophelia-1. A volcanic source supplying K-feldspar may be responsible for the high  $K_2O/Al_2O_3$  observed in both the Gert and Ravn members (Weibel et al. 2010).

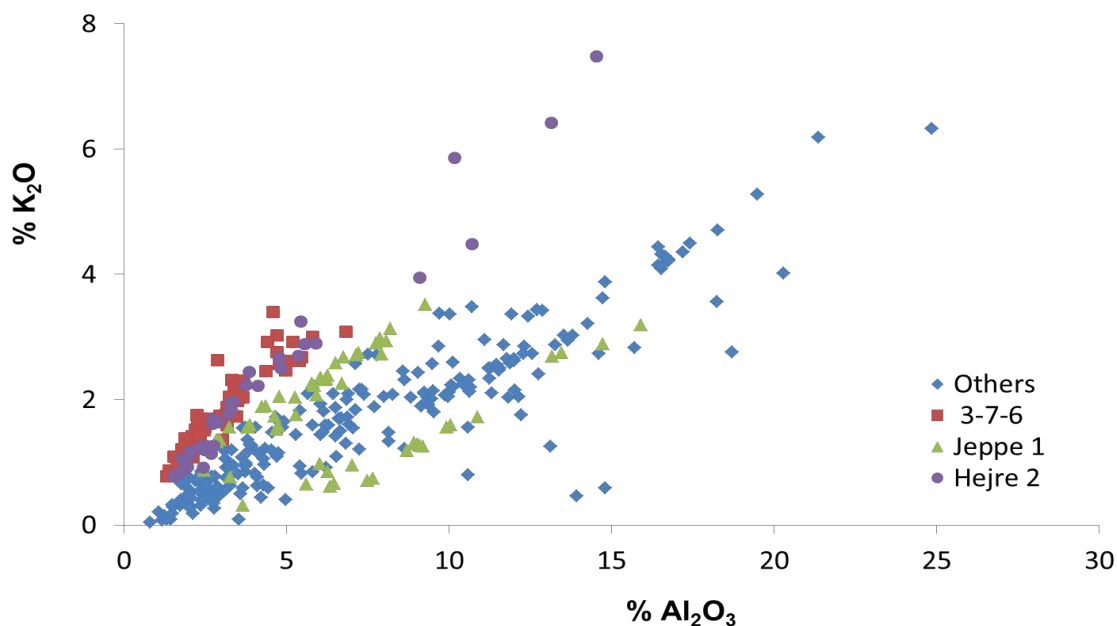


Fig. 10.2:  $K_2O$  versus  $Al_2O_3$  in bulk rock geochemical analysis of Upper Jurassic sandstones. The samples from Jeppe-1 with high  $K_2O/Al_2O_3$  ratio are from Ravn Mb. whereas the low ratios are from the sands in the Farsund Fm.

The most prominent alkaline volcanic suite in the North Sea is of Permian age (Hereemans et al 2004) and the volcanic rocks as well as volcanoclastic units are described as the Karl Formation, Rotliegend Group (Stemmerik et al., 2000). Volcanic rocks with alkaline composition and Jurassic age are also known from the North Sea (Fall et al 1982, Smith & Richie, 1993). In Hejre-2, the K-feldspar-rich intervals were deposited on top of volcanics and contain abundant volcanic fragments.

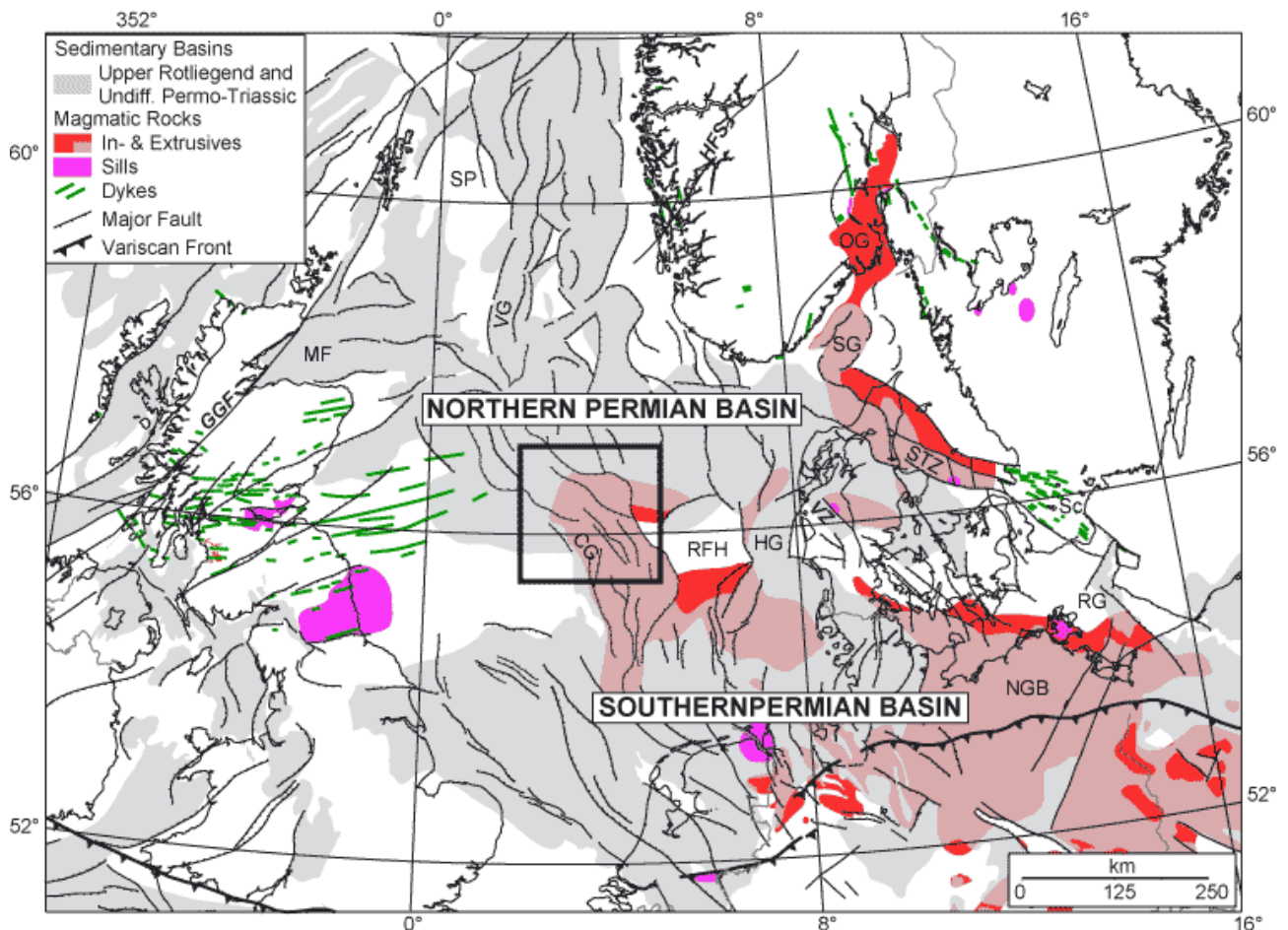


Fig. 10.3: Occurrence of Permian volcanic rocks in the North Sea and surroundings (from Hereemans et al 2004)

This note describes the findings of a pilot study of the K-feldspar, focused on the chemical composition, Pb/Pb isotope signature and Ar/Ar ages. The aim of the study is to contribute to the understanding of the K-feldspar provenance and history in the reservoir sandstones of the Heno Formation.

### 10.3 Microprobe analysis

Electron MicroProbe Analysis (EMPA) of the chemical composition of K-feldspar from 6 samples from Hejre-2, Jeppe-1, Gwen-1, Ophelia-1, Eg-1 and Ravn-2 was conducted using the JEOL JXA-8200 Superprobe at the Institute for Geosciences and Natural Resource Management, University of Copenhagen.

The aim was to test if compositional differences in the source regions could be recognized in the K-feldspar.

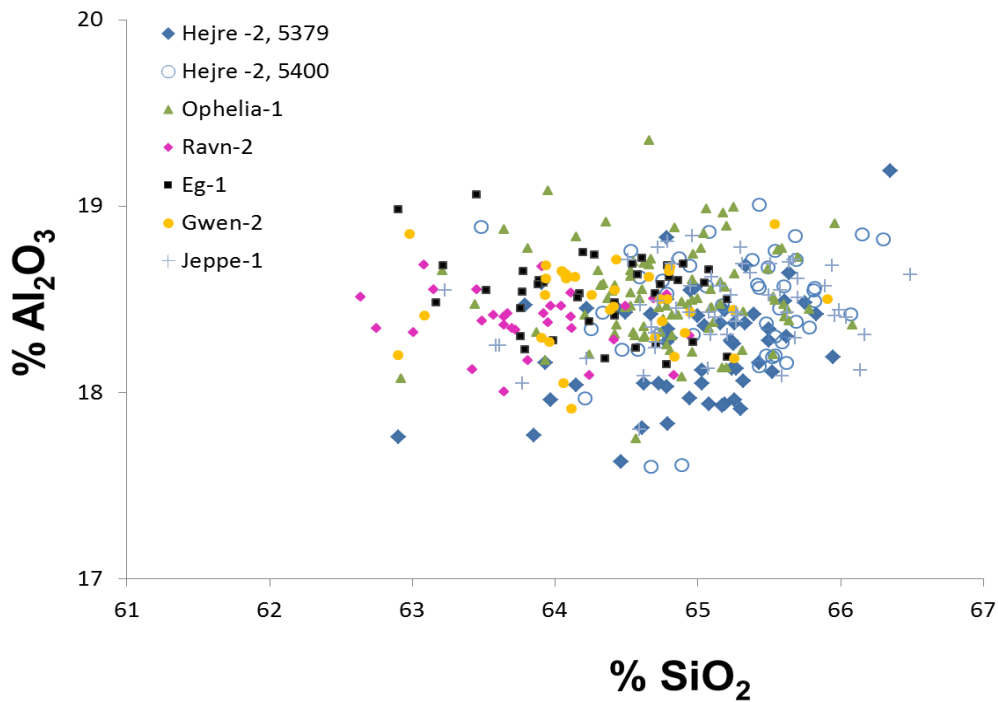


Fig. 10.4:  $\text{SiO}_2$  versus  $\text{Al}_2\text{O}_3$  by EMPA of K-feldspar from Hejre-2, Jeppe-1, Gwen-1, Ophelia-1, Eg-1 and Ravn-2.

There is a range of compositions of the K-feldspar in each sample (Figure 10.4) and the different samples cover different compositional fields with Ravn-2, Gwen-1 and Eg-1 having lower  $\text{SiO}_2$  compared to e.g. Hejre-2, Jeppe-1 and Ophelia-1.

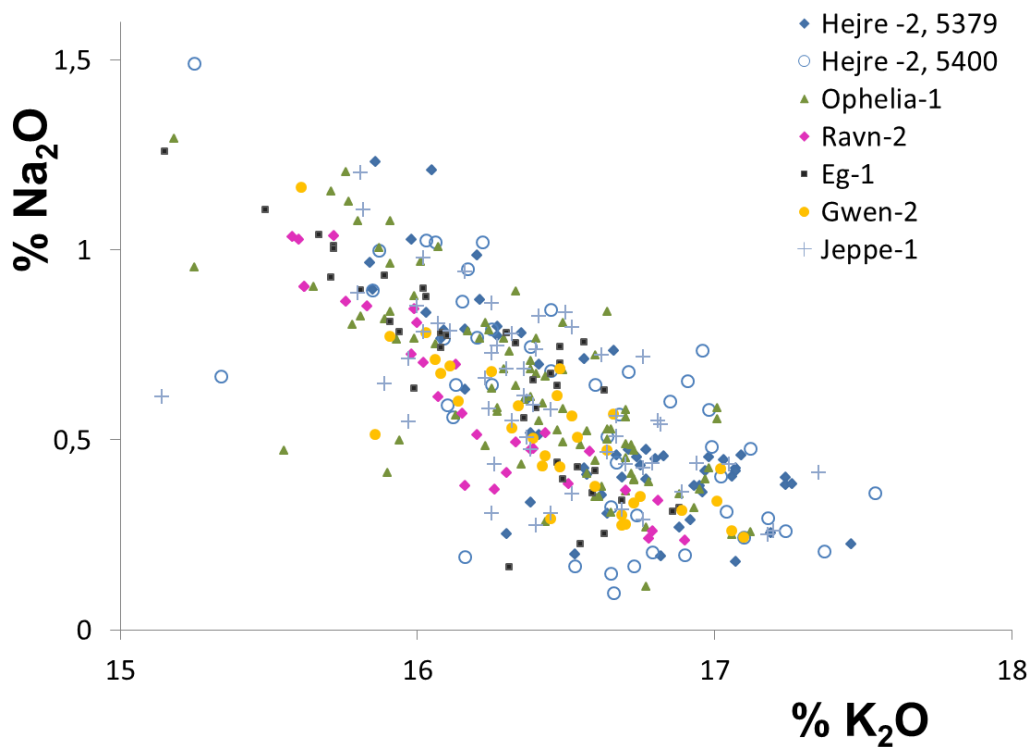


Fig. 10.5:  $\text{Na}_2\text{O}$  versus  $\text{K}_2\text{O}$  in K-feldspar (EMPA) from Hejre-2, Jeppe-1, Gwen-1, Ophelia-1, Eg-1 and Ravn-2.

As was the case in Figure 10.4 there is compositional variation among the samples in the Na<sub>2</sub>O versus K<sub>2</sub>O cross plot (Figure 10.5) and the compositional fields of e.g. Ravn-2, Gwen-2 and Eg-1 are more restricted and average lower contents as compared to Hejre-2, Jeppe-1 and Ophelia-1. These three wells are also wells characterized by high K<sub>2</sub>O/Al<sub>2</sub>O<sub>3</sub> ratios in the bulk geochemical analysis (e.g. Figure 10.2) indicating high contents of K-feldspar may be caused by redeposition of volcanics. The larger range of compositions in Hejre-2, Jeppe-1 and Ophelia-1 may be caused by these wells containing K-feldspar from basement as well as reworked volcanics, whereas the other wells with more restricted compositional variation only contain K-feldspar from the basement.

## 10.4 Ar/Ar dating

6 samples were dated at the Argon and Noble Gas Research Laboratory, The Open University, UK: Two from Hejre-2 (depth 5397,37 and 5400,37 m respectively), Ravn-2 (4279.47 m) Jeppe-1 (4959.91 m), Ophelia-1 (4890.5 m) and the Norwegian well 3-7/7 (3794 m).

The main aim of this study was to test if volcanogenic K-feldspar from e.g. Permian or Jurassic deposits could be detected using this technique and if they can be differentiated from detrital K-feldspar from the basement. A subordinate aim was to test if it was possible to obtain information about the timing of diagenetic events involving authigenic growth of K-feldspar.

### Ar/Ar dating methodology

The 6 samples were prepared for analysis by making polished slabs, 100 µm in thickness. Samples were irradiated at the McMaster Nuclear Reactor (McMaster University, Canada) for 100 hours. For in situ analysis the samples were loaded into the ultra-high vacuum system and a 213nm wavelength UV laser was used to ablate 30µm spots in the sample. Analyses were carried out on the cores feldspar grains where possible to reduce mixed ages from different material. A Nu Instruments Noblesse mass spectrometer was used for measurement.

### Ar/Ar results

18 analyses from Hejre-2 5379,37 m, produced ages ranging between 49 and 1205 Ma (Figure 10.6).

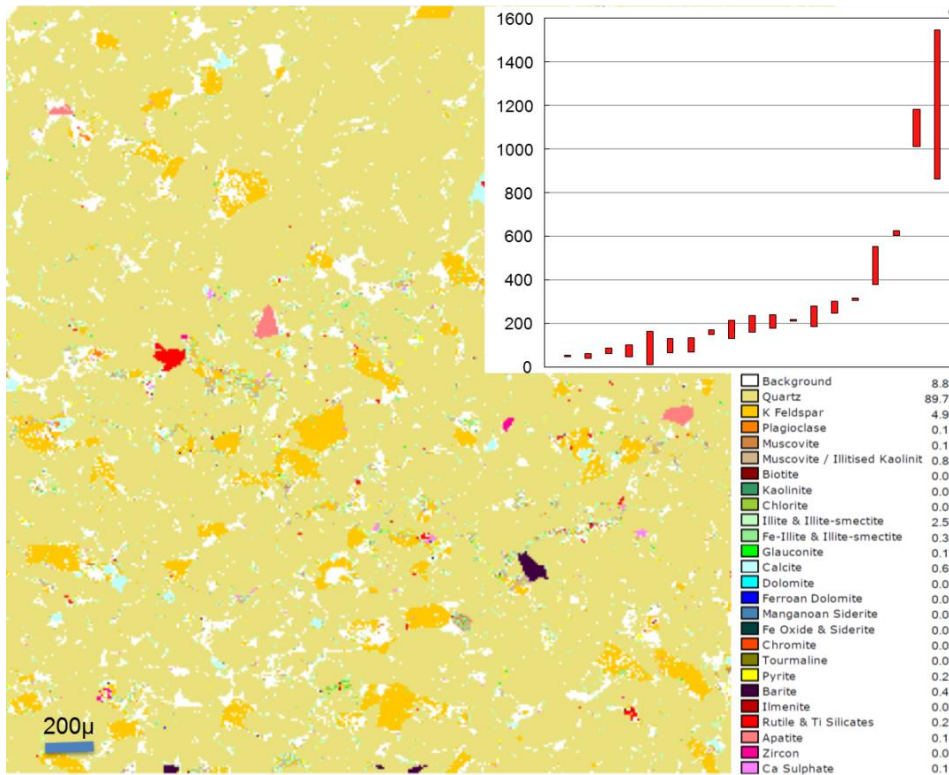


Fig. 10.6: Qemscan image of the sample Hejre-2 5379.37 m. Gert Mb. Ar/Ar ages, upper right, data in million years (Ma,  $2\sigma$  error bars). The youngest 7 dates (103 - 49 Ma) are younger than the depositional age and reflect either the timing of overgrowth or resetting of the Ar/Ar age by a thermal episode.

There are three Jurassic ages in the sample that may represent re-deposited volcanic material. The oldest 4 ages (1205 - 464 Ma) probably represent detritus from Caledonian and Precambrian terrains.

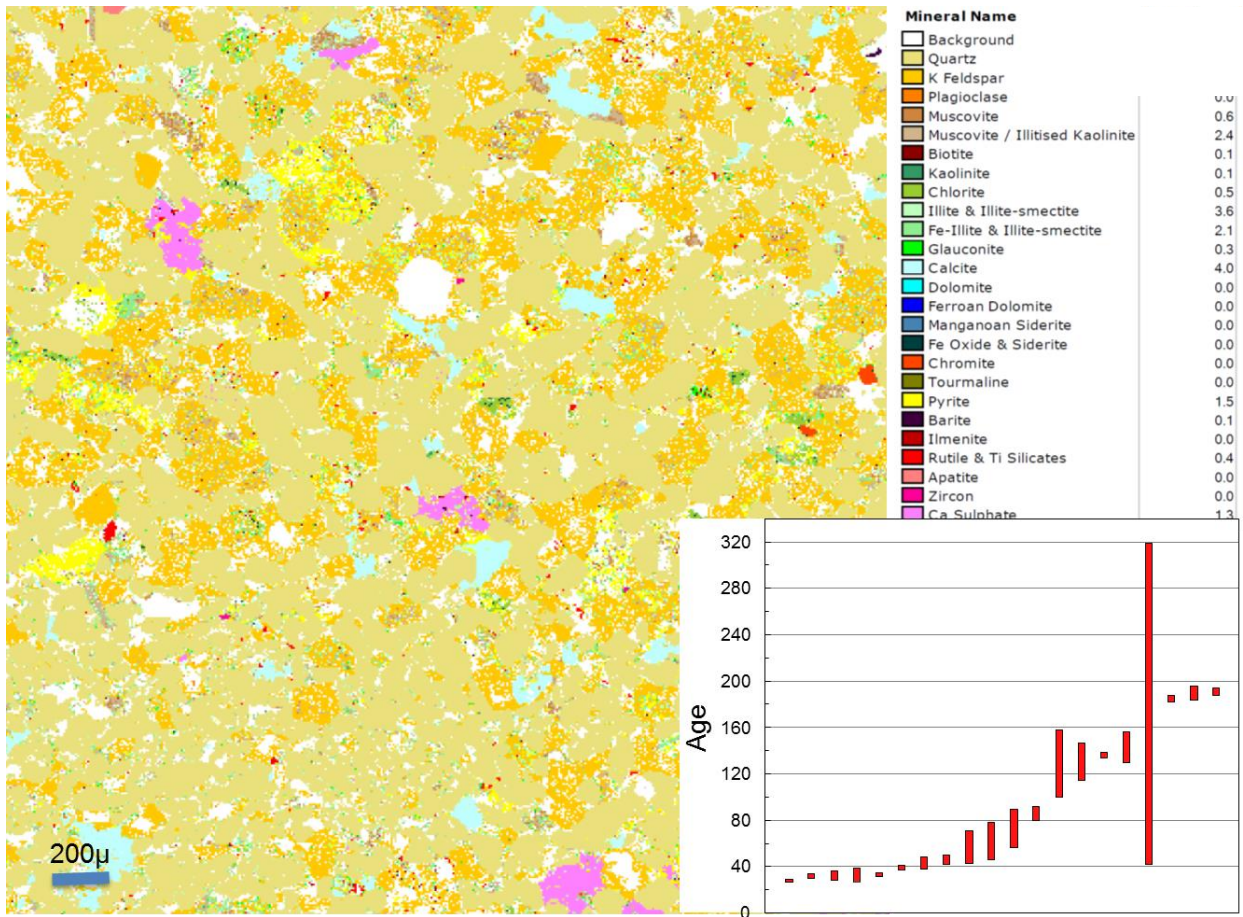


Fig. 10.7: Qemscan image of sample Hejre-2 5400,37 m. Gert Mb. In situ Ar/Ar age data (2σ error bars) lower right.

The sample is very rich in K-feldspar (Figure 10.7) and the K-feldspar is rather coarse-grained, porous and with many inclusions.

The 20 in situ ages are from 191 Ma to 28 Ma. The youngest 8 dates have a weighted mean of  $32.1 \pm 4.2$  Ma. This could reflect the timing of overgrowth or resetting of the age by a thermal episode.

The remainder of the ages forms a continuum from 191.2 to 57.2 Ma. Most of these ages are younger than the depositional age and are likely to represent areas that comprise both detrital and authigenic K-feldspar in close proximity and unresolvable with the laser.

The sample from the Ravn-2 well (Figure 10.8) is finer grained compared to the samples from Hejre-2.

The 20 Ar/Ar ages from Ravn-2 range from 220 to 853 Ma (Figure 10.8). 15 of the dates are between 220 and 310 Ma with a weighted mean of  $259 \pm 15$  Ma. These ages may represent Permian volcanics. However, overgrowth of K-feldspar may produce apparent ages in between original age of the detrital grain and the overgrowth.

The five grains with older ages of between 427 and 853 Ma are likely to represent ages of the detrital minerals.

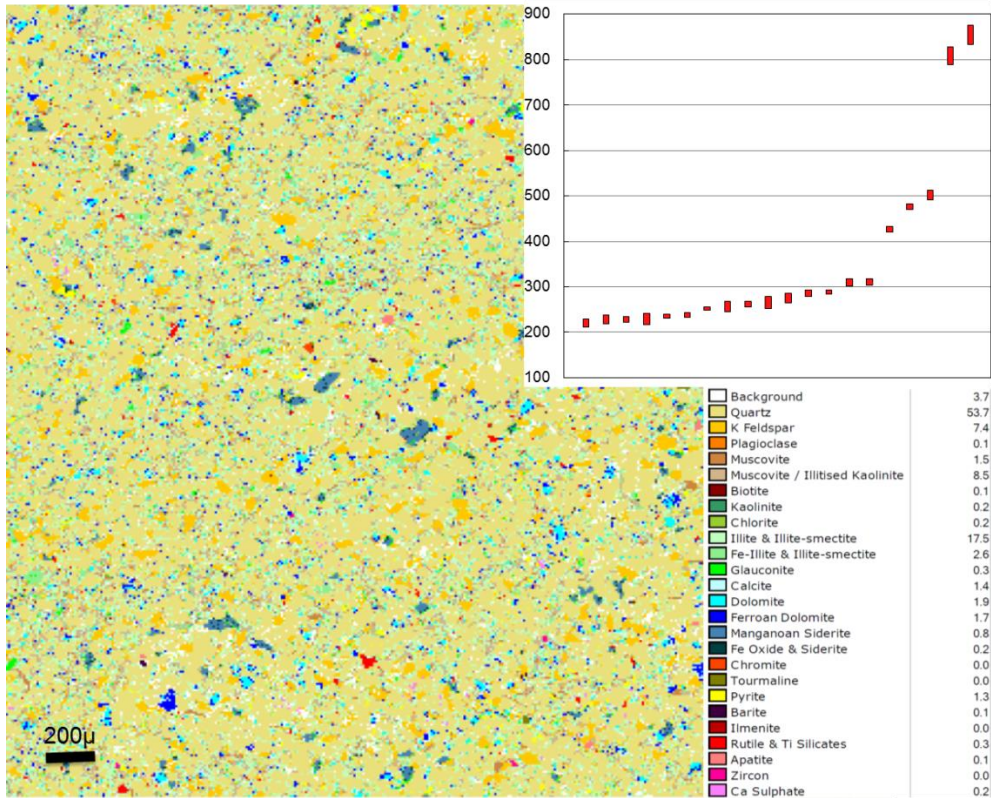


Fig. 10.8: Qemscan image of Ravn-2 (4279,47 m Ravn Mb). In situ Ar/Ar age data upper right.

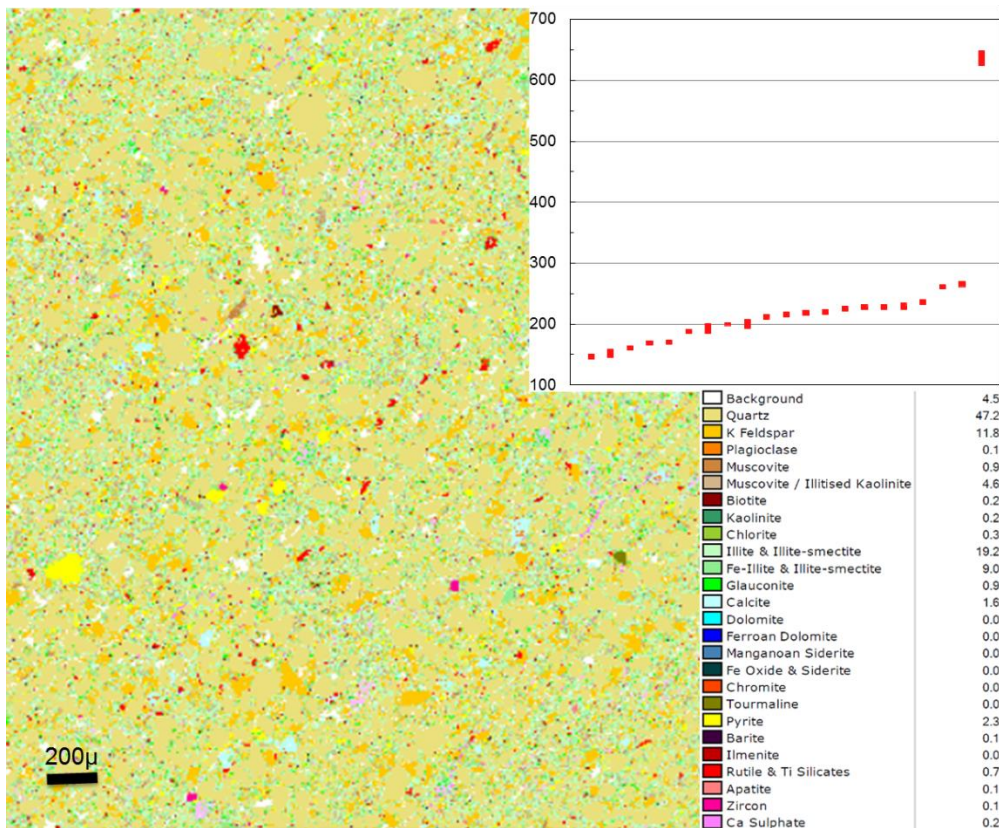


Fig. 10.9: Qemscan image of Ophelia-1 (4890,5 m, Ravn Mb.) Ar/Ar age data upper right.

21 analyses from Ophelia-1 produced ages of between 146 and 636 Ma. 20 of the dates are <265 Ma and may be interpreted as Permian, some of which are affected by overgrowth.



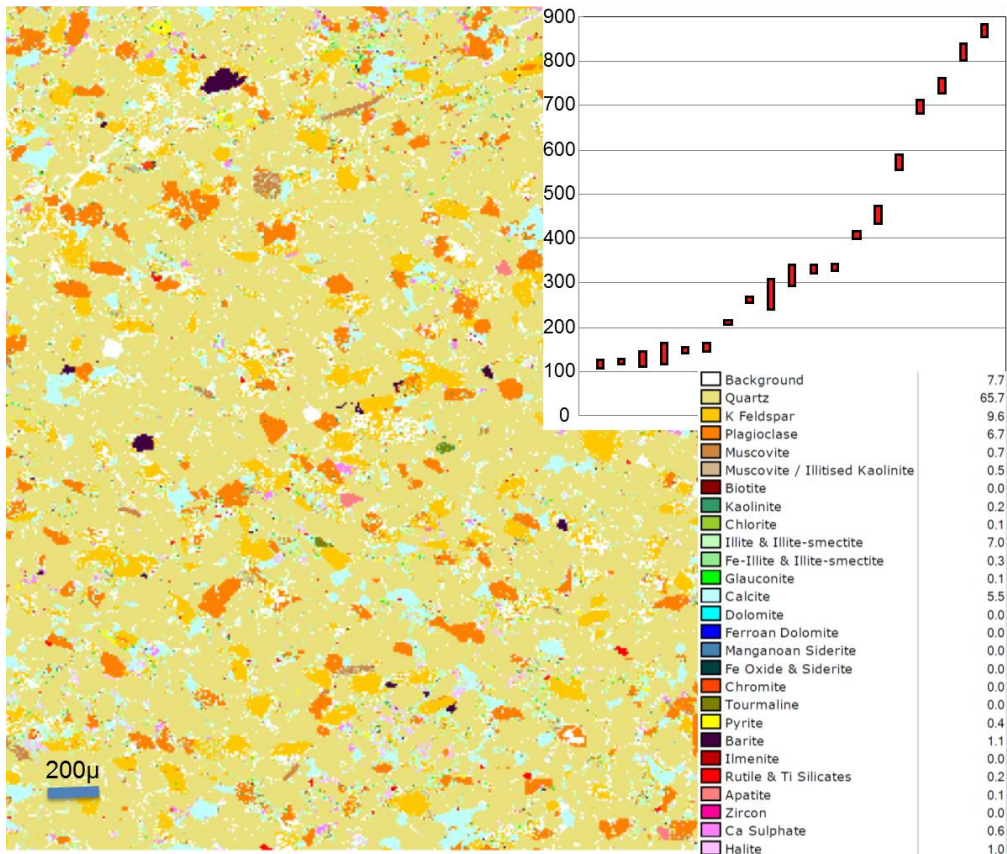


Fig. 10.10: Qemscan image of Jeppe-1 (4959.91 Ravn Mb.): In situ Ar/Ar age data upper right.

This sample has a high content of K-feldspar as well as albite (Figure 10.10). 19 analyses gave ages between 163 and 870 Ma (Figure 10.10). The 6 youngest ages have a Jurassic weighted mean age of  $182 \pm 15$  Ma and the 13 oldest ages (252 to 870 Ma) may reflect the age of detrital minerals sourced from Permian volcanics, Caledonian granites and Precambrian basement.

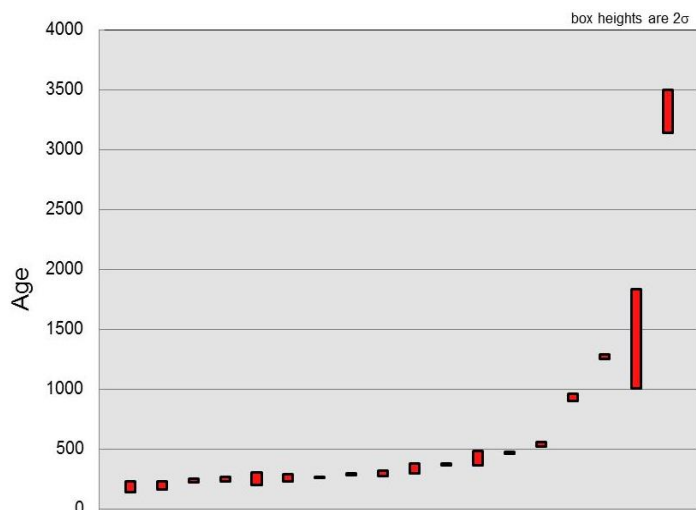


Fig. 10.11: Sample 3-7-7 (3794 m): In situ Ar/Ar age data ( $2\sigma$  error bars). 20 analyses produced ages between 193 and 3325 Ma. The youngest 8 dates are between 193 and 298 Ma. The weighted mean of these analyses is  $269 \pm 15$  Ma (Permian). The next 5 ages may be Caledonian and the remaining 5 are of Precambrian age.

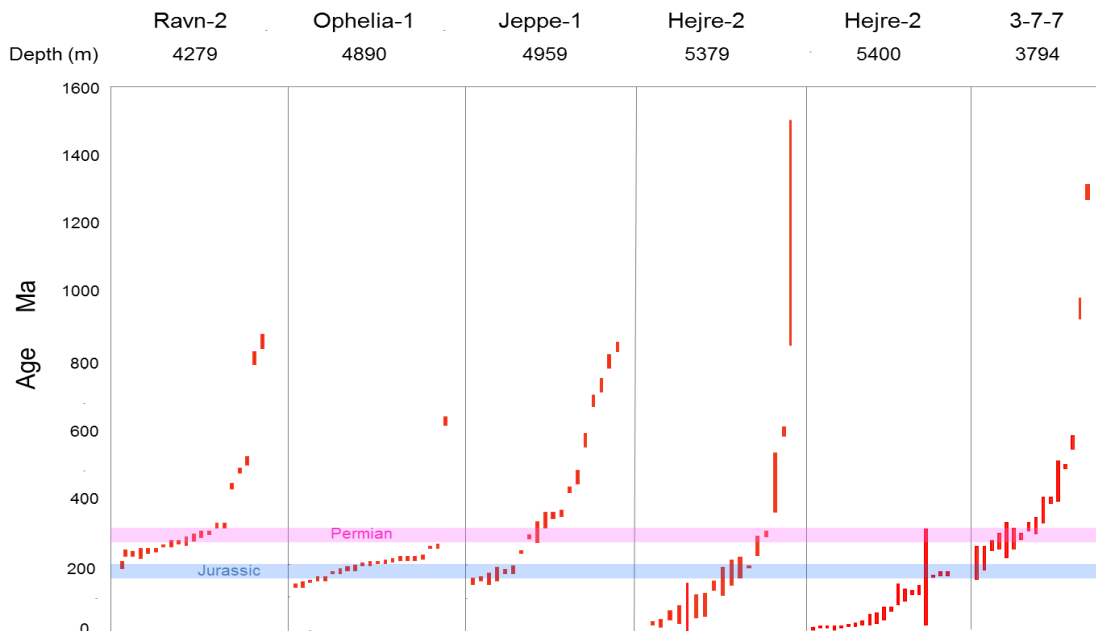


Fig. 10.12: Compilation of the Ar/Ar ages.

### Discussion of the Ar/Ar results

The K-feldspar in Hejre-2 has a different signature compared to the other wells. The youngest Ar/Ar dates found in Hejre-2 are Tertiary and much younger than the depositional age. There are two possible explanations for such young ages:

1. Overgrowth, or growth of new authigenic K-feldspar
2. Resetting of the K-feldspar Ar/Ar age

Overgrowth on detrital K-feldspar by authigenic K-feldspar is a common feature described from Hejre-2, but this is mainly tied to the rim of the K-feldspar grains (Weibel et al, 2010) and the laser ablation spots that produced the Ar/Ar ages were located in the cores of grains. However, the sample where the youngest ages are found is also the sample with the most inhomogeneous and inclusion-rich K-feldspar (Figure 10.7). The range of ages from Oligocene towards older ages could be interpreted as the result of mixing of the age of the overgrowth with  $^{40}\text{Ar}$  from the preexisting/clastic grains. Minerals may be affected by the presence of excess argon,  $^{40}\text{Ar}$  that has become decoupled from parent potassium and is artificially elevating the age of the sample to produce the older apparent age; this is common in water mediated minerals of various types (e.g. Sherlock et al. 2008), and could also be the explanation for the older apparent ages and the large and variable spread of ages produced from these samples.

A thermal episode exceeding the Ar-closing temperature of K-feldspar could reset the Ar/Ar clock of the K-feldspar. The Ar/Ar closing temperature is in the range 210-260°C (Kelley 2002), but if there is a fine sub-grain network the closure temperature may be even lower (Mark et al 2008). The range of ages seen in the Hejre-2 samples could be caused by different abilities to preserve their original age.

Finally it should be noted that the presentday temperature at 5,400 m in Hejre-2 is approximately 165°C which is not far below the Ar/Ar closure temperature of K-feldspar.

Unravelling the different possible causes of this spread and distribution of ages would require more detailed investigation including petrology of detrital grains.

## 10.5 Pb/Pb isotopes in the K-feldspar

The aim of Pb/Pb isotope characterization of K-feldspar is to test the possibility to discriminate the different source areas of the K-feldspar. A total of 22 grains in 5 samples were analyzed at the Geological Survey of Finland.

### LAMCICPMS methodology

A Cameca SX 100 ElectronMicroProbe has been used to produce a mosaic of the thin sections. The biggest K-feldspars was selected and their chemical composition checked using EDS. Each grain was photographed and the coordinates of four recoordination marks for each thin section and all the grains were recorded. Pb-Pb isotope analyses were performed using a Nu Plasma HR multicollector ICPMS combined with a Photon Machine Analyte G2 laser microprobe. The MC-ICP-MS was equipped with 9 Faraday detectors and amplifiers.

### Pb/Pb isotope results

The results of the analyses are shown on Figure 10.13.

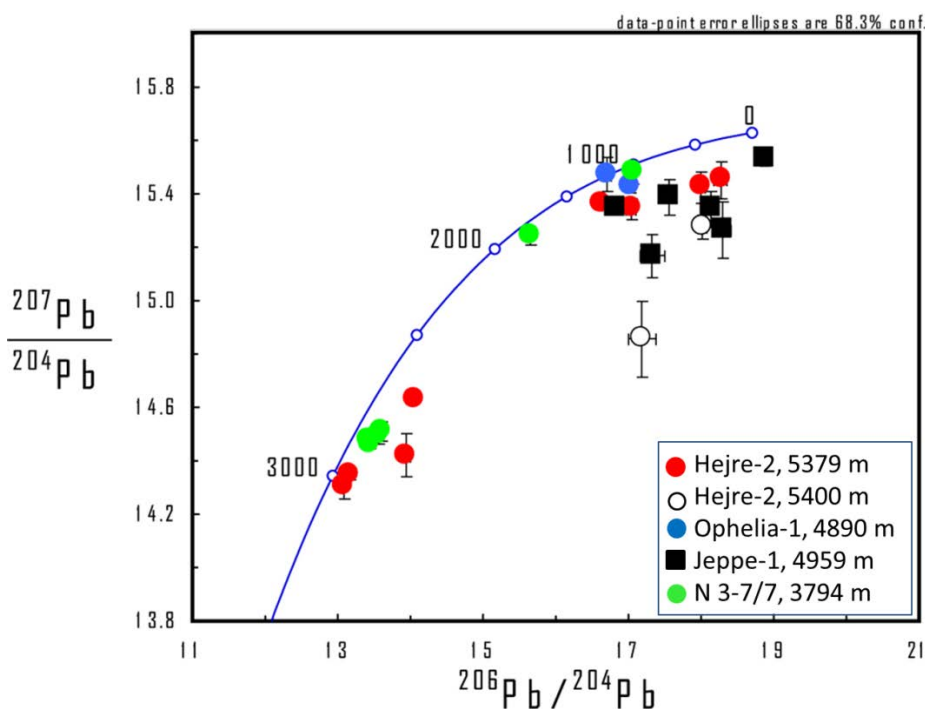


Fig. 10.13:  $^{206}\text{Pb}/^{204}\text{Pb}$  -  $^{207}\text{Pb}/^{204}\text{Pb}$  diagram. The blue line is the growth curve with the numbers representing typical isotopic compositions of material extracted from the earth's mantle at that time (Ma).

The Pb/Pb isotope data on Figure 10.13 show that it is possible to obtain isotopic fingerprints of the K-feldspar in the Jurassic sandstone samples from the North Sea.

In Hejre-2 (5379 m) 50% of the K-feldspar crystals (4) have a signature suggesting an Archean source, which is also seen in N 3-7/7. The number of analyses is too small to yield a good impression of the relative distribution of source terrains for the individual samples/wells, but it is surprising that Archean grains are represented, as the potential source terrains are fairly remote (Scotland or Finland). It was not possible to obtain good data from the underlying Hejre-2 sample (5400 m) which may be due to high degree of recrystallization as also indicated by the Ar/Ar data. The K-feldspar from Jeppe-1 have been derived from sources with ages ranging from Sveco-Norwegian (Ca 1.000 Ma) to Mesozoic – which is in fairly good agreement with the findings in the Ar/Ar dating study.

## 10.6 References

- Fall, H. G, Gibb, F. G. F. & Kanaris-Sotiriou, R. 1982: Jurassic volcanic rocks of the northern North Sea. *Journal of the Geological Society, London*, 139, 277-292,
- Heeremans, M., Timmerman, M.J., Kirstein, J.I., and Faleide, J.I. 2004. New constraints on the timing of late Carboniferous - early Permian volcanism in the central North Sea. In: Wilson, M., Neumann, E.-R., Davies, G.R., Timmerman, M.J., Heeremans, M., and Larsen, B.T. (eds) *Permo-Carboniferous Magmatism and Rifting in Europe*. Geological Society, London, Special Publications, 223, 177-194.
- Kelley, S., 2002. Excess argon in K-Ar and Ar-Ar geochronology. *Chem. Geol.*, 188, 1–22.
- Mark, D.F., Kelley, S.P., Lee, M.R., Parnell, J., Sherlock, S.C. & Brown D.J. 2008: Ar–Ar dating of authigenic K-feldspar: quantitative modelling of radiogenic argon-loss through subgrain boundary networks. *Geochimica et Cosmochimica Acta*, 72. 2695–2710
- Sherlock, S.C., Zalasiewicz, J., Kelley, S.P. and Evans, J. 2008. Excess argon ( $^{40}\text{Ar}_E$ ) uptake during slate formation: A  $^{40}\text{Ar}/^{39}\text{Ar}$  UV laserprobe study of muscovite strain-fringes from the Palaeozoic Welsh Basin, UK: *Chemical Geology*, v.257, p.206-220.
- Smith, K & Ritchie, J.D. 1993: Jurassic volcanic centres in the Central North Sea. Geological Society, London, *Petroleum Geology Conference series*. 4, 519-531.
- Stemmerik, L., Ineson, J.R. & Mitchell, J.G. 2000. Stratigraphy of the Rotliegend Group in the Danish part of the Northern Permian Basin, North Sea. *Journal of the Geological Society of London*, 157, 1127-1136.
- Weibel, R. Johannessen, P.N. Dybkjær, K., Rosenberg, P. & Knudsen, C. 2010: Chemostratigraphy of upper Jurassic reservoir sandstones, Danish Central Graben, North Sea. *Marine and Petroleum Geology*. 27. 1572-1594.